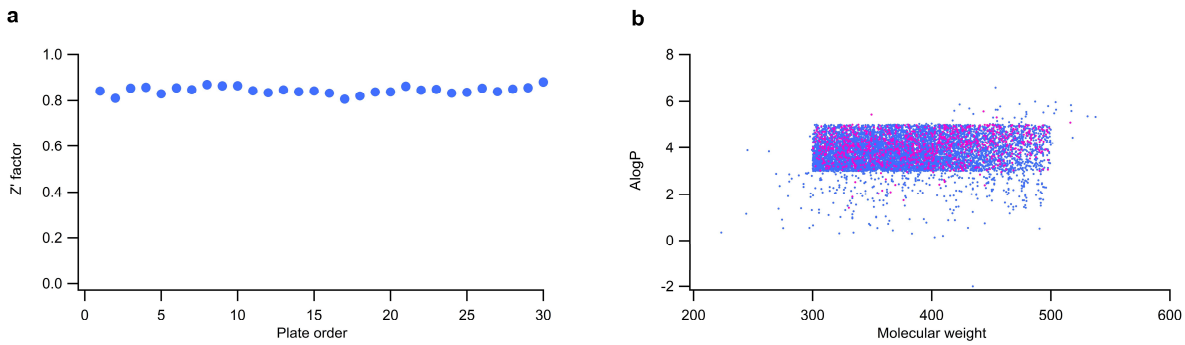
Supplementary information

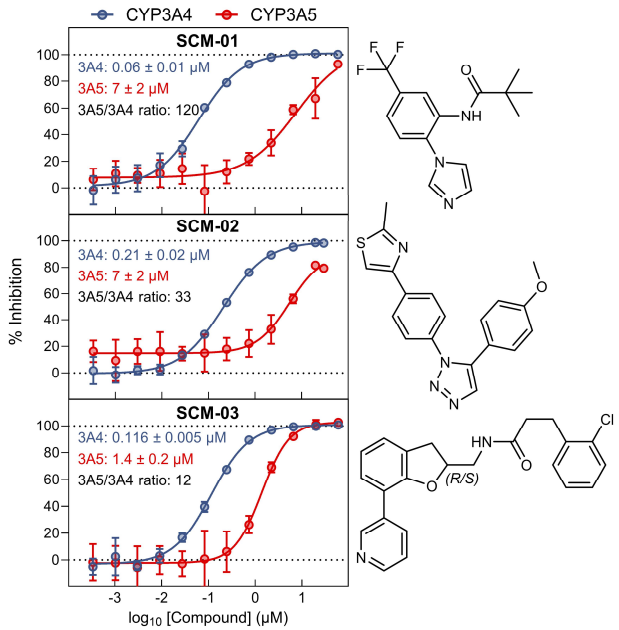
Decoding the Selective Chemical Modulation of CYP3A4

Jingheng Wang[1,†], Stanley Nithianantham[1,†], Sergio C. Chai[1,†], Young-Hwan Jung[1,†], Lei Yang[1], Han Wee Ong[1], Yong Li[1], Yifan Zhang[1], Darcie J. Miller[2], Taosheng Chen[1,*]

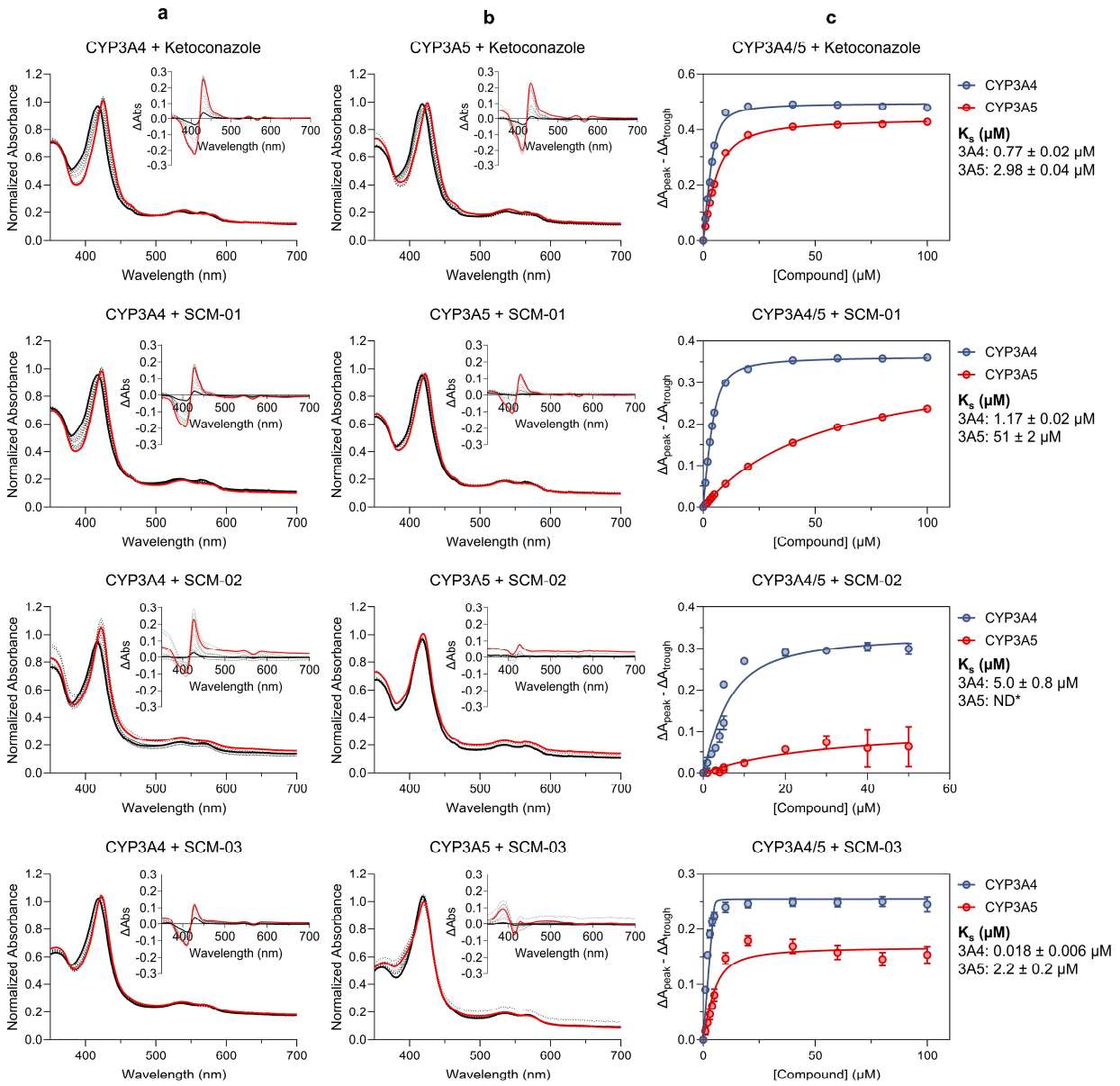
[1]Department of Chemical Biology and Therapeutics, St. Jude Children's Research Hospital, 262 Danny Thomas Place, Memphis, TN, 38105, USA.
[2]Department of Structural Biology, St. Jude Children's Research Hospital, 262 Danny Thomas Place, Memphis, TN, 38105, USA.
[†]These authors contributed equally to this work: Jingheng Wang, Stanley Nithianantham, Sergio C. Chai, Young-Hwan Jung
*Corresponding author address: 262 Danny Thomas Place, MS 1000, Memphis, TN, 38105; e-mail: taosheng.chen@stjude.org; phone: (901) 595-5937



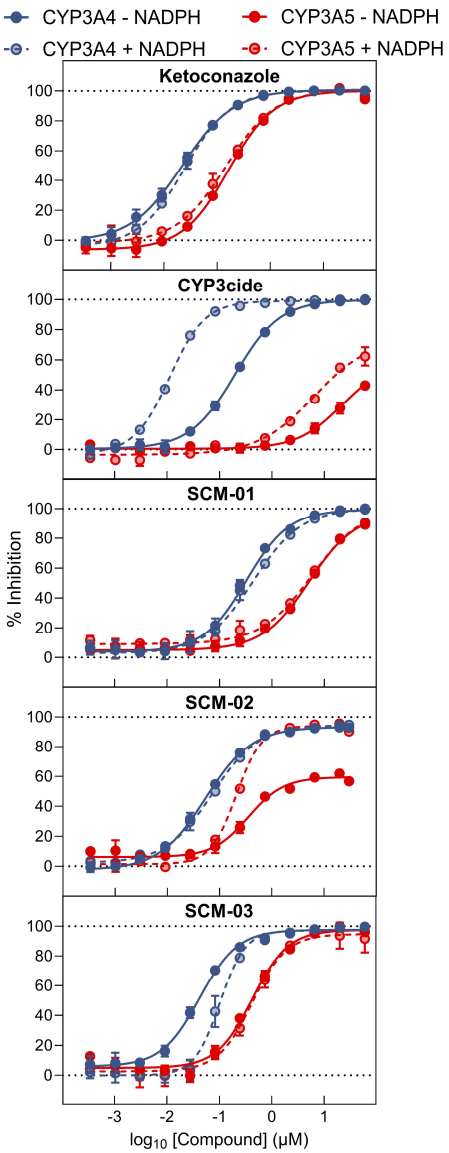
Supplementary Fig. 1 | HTS assay robustness and screened compound drug-like properties. (a) Assessment of assay robustness in the primary screen as indicated by Z' factor values. Each data point represents values from an assay plate based on the positive (ritonavir) and negative (DMSO) controls. (b) Most of the screened compounds (blue) have physicochemical properties typical of a drug-like chemical space as reflected by AlogP and molecular weight. Hits from the primary screen are colored in pink. Source data for (a) are provided as a Source Data file.



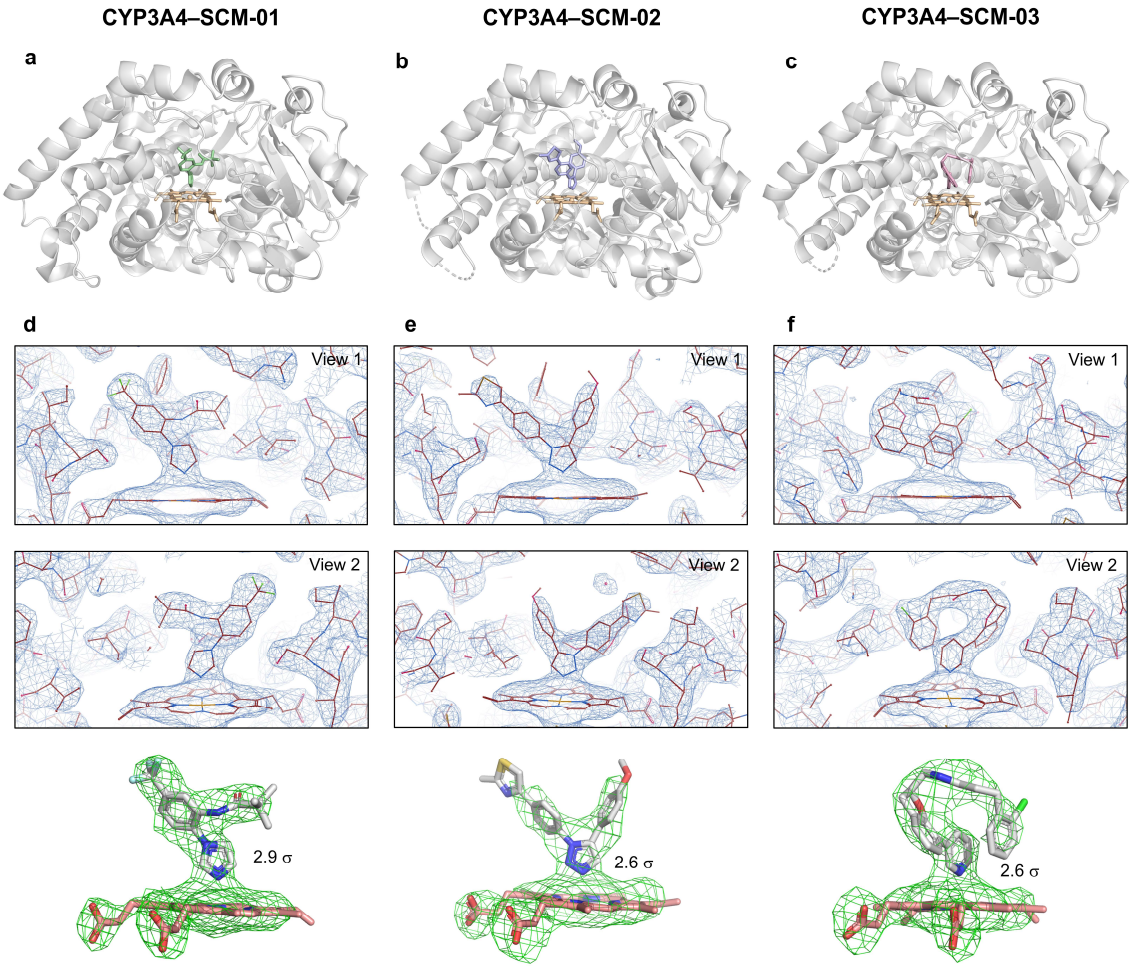
Supplementary Fig. 2 | SCM-01, SCM-02, and SCM-03 are selective CYP3A4 inhibitors in the cellular context. Dose–response curves showing concentration-dependent inhibition of CYP3A4 and CYP3A5 by each compound as measured using the cell-based P450-Glo assay. Percentage inhibition data were normalized against DMSO controls (as 0% inhibition) and 30 μM ketoconazole controls (as 100% inhibition). The reported numerical values are the means and standard deviations of the IC_{50} values calculated from triplicate experiments (n = 3). The chemical structures of SCM-01, SCM-02, and SCM-03 are shown to the right of the plots for those compounds. Source data are provided as a Source Data file.



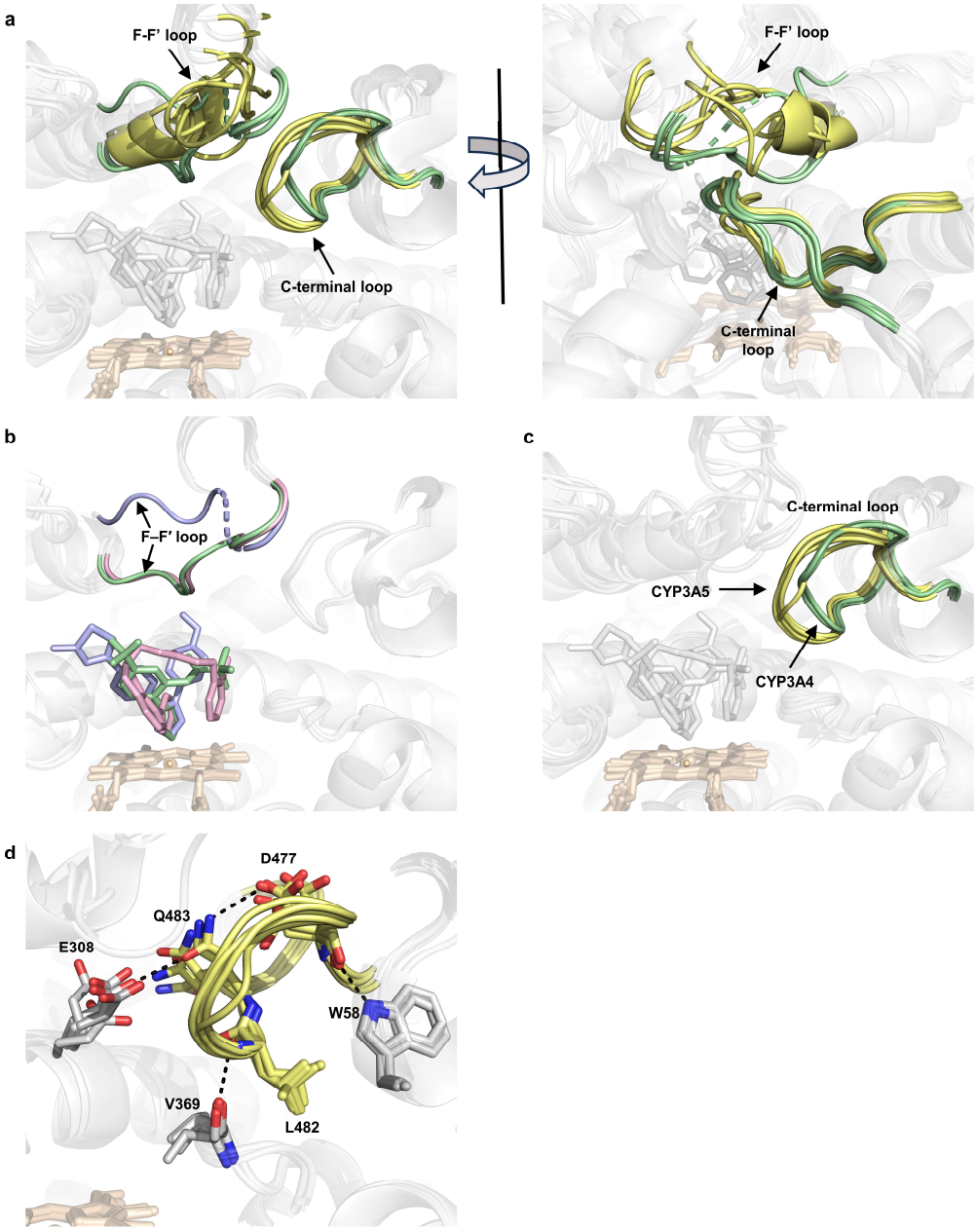
Supplementary Fig. 3 | Selective inhibitors bind preferentially to CYP3A4. (a,b) Normalized UV-vis spectra of CYP3A4/5 showing spectral changes upon binding of selective inhibitor. The insets are difference spectra calculated by subtracting the spectrum of ligand-free CYP3A4/5 from that for each of the ligand-bound states. Spectra of the ligand-free state are shown as the black solid lines, and spectra at the highest ligand concentration are shown as red solid lines. (c) $\Delta A_{peak} - \Delta A_{trough}$ vs. compound concentration plots, showing the effect of selective inhibitor binding on CYP3A4/5 spectral signals. The reported numerical values are the means and standard deviations of K_s values derived from triplicate experiments ($n = 3$). Source data are provided as a Source Data file.



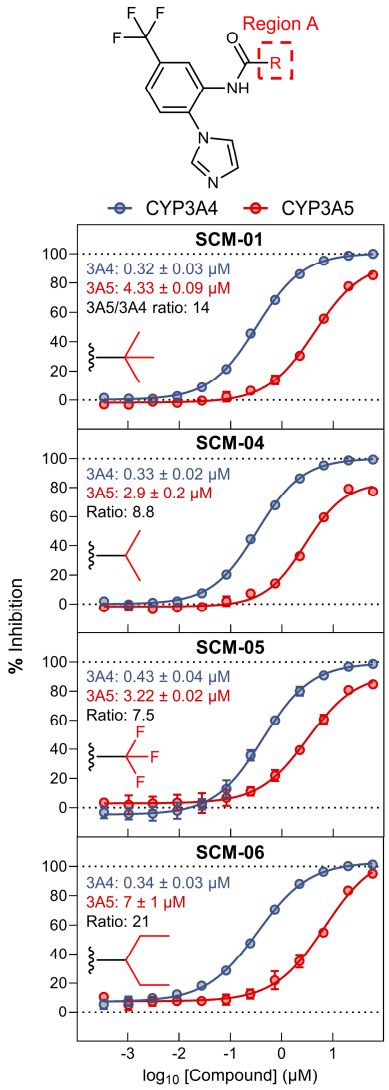
Supplementary Fig. 4 | SCM-01 is a non-suicide CYP3A4/5 inhibitor. Dose–response curves showing time-dependent inhibition of CYP3A4/5 by selective inhibitors. Percentage inhibition data were normalized against DMSO controls (as 0% inhibition) and 30 μM ketoconazole controls (as 100% inhibition). The IC_{50} values calculated from triplicate experiments (n = 3) are reported in Supplementary Table 5. Source data are provided as a Source Data file.



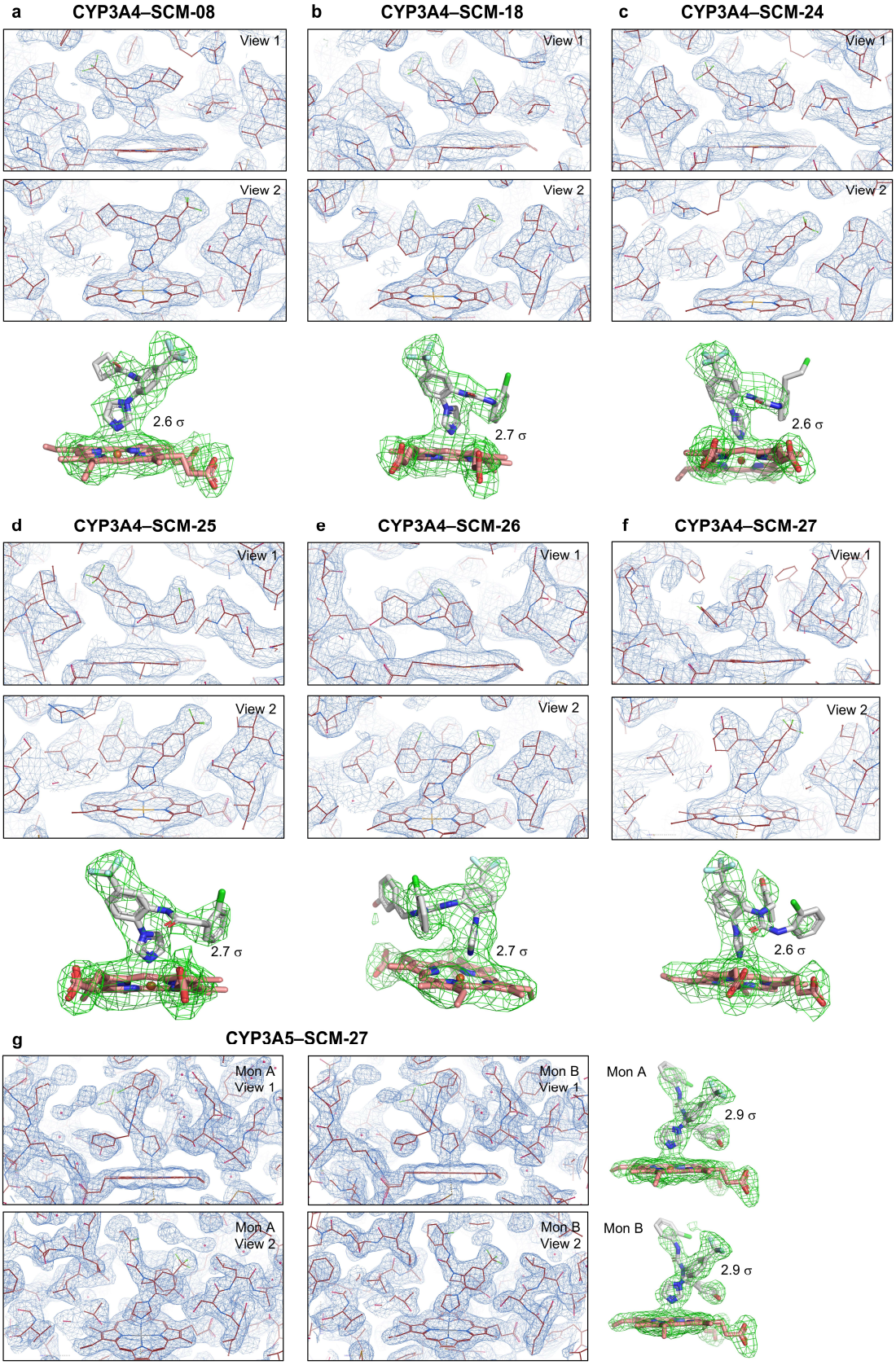
Supplementary Fig. 5 | SCM-01, SCM-02, SCM-03 co-crystallized with CYP3A4. (a–c) Crystal structures of CYP3A4 in complex with (a) SCM-01, (b) SCM-02, (c) SCM-03. The heme group is colored wheat, and the selective inhibitors are colored green, blue, and pink, respectively. (d-f) Crystal structure models (sticks) and electron density maps (meshes) of (d) SCM-01, (e) SCM-02, (f) SCM-03, and the heme group. The original figure-of-merit–weighted $2F_o–F_c$ map is contoured in blue at 1.0 standard deviation. The $F_o–F_c$ omit maps of the heme group and selective inhibitors are shown in green at 2.6-2.9 standard deviations.



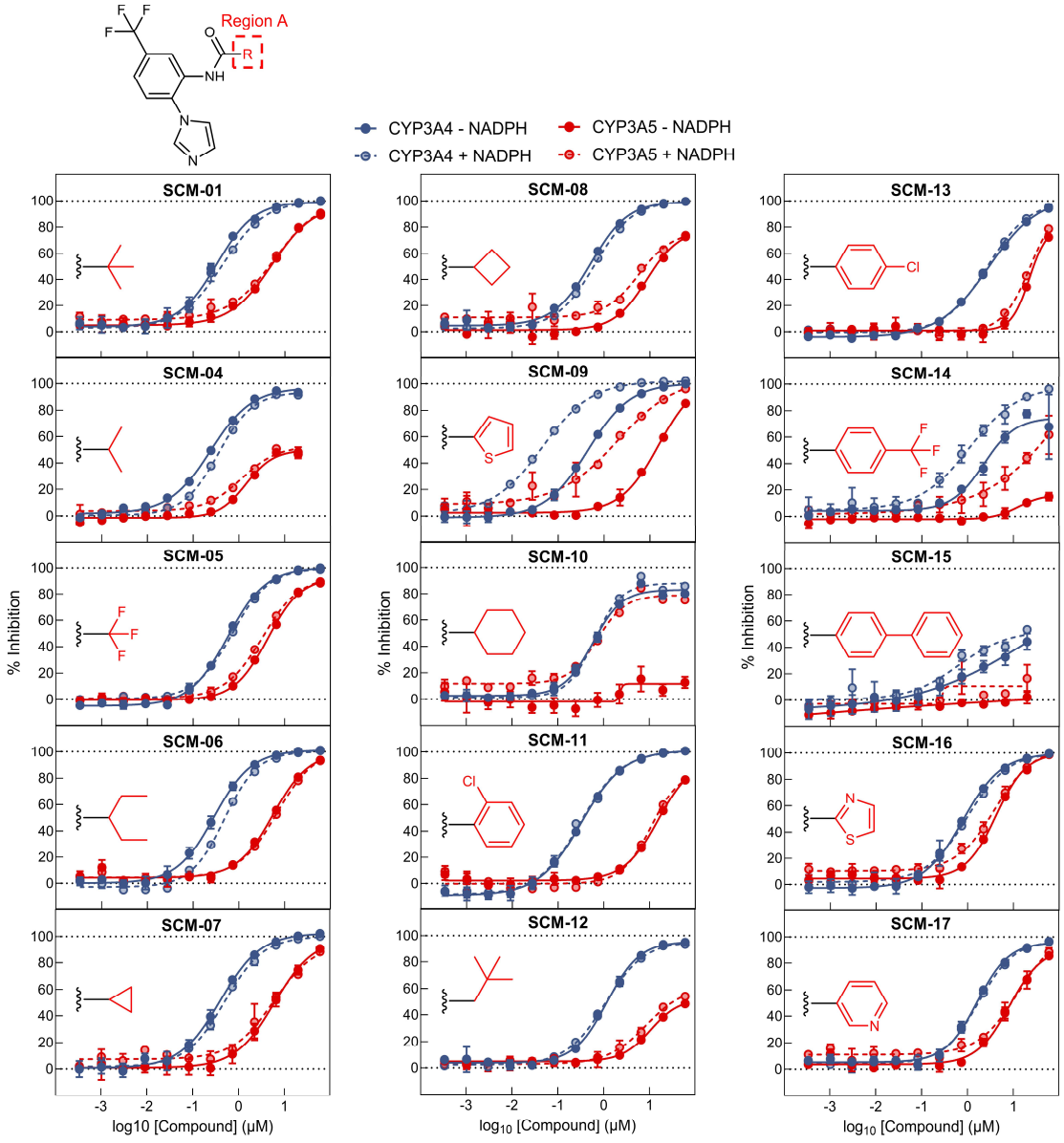
Supplementary Fig. 6 | Analysis of CYP3A4 crystal structures bound to SCM-01, SCM-02 and SCM-03 suggests the differential positioning of the C-terminal loop is important for selective inhibition. (a) Overlay of the three selective inhibitor–bound CYP3A4 structures (green) and all CYP3A5 structures (yellow) showing that the F–F′ and C-terminal loops have different conformations between CYP3A4 and CYP3A5. (b) Overlay of the selective inhibitor–bound CYP3A4 (green, blue, pink) crystal structures showing that the F–F′ loop in CYP3A4-SCM-02 (blue) is displaced by the ligand and does not interact with it. (c) Overlay of the three selective inhibitor–bound CYP3A4 structures (green) and all CYP3A5 structures (yellow) showing that the C-terminal loop conformation is conserved within selected CYP3A4 and CYP3A5 structures, respectively. (d) Overlay of CYP3A5 crystal structures showing that the H-bonds that stabilize the conformation of the C-terminal loop (yellow) are conserved in CYP3A5.



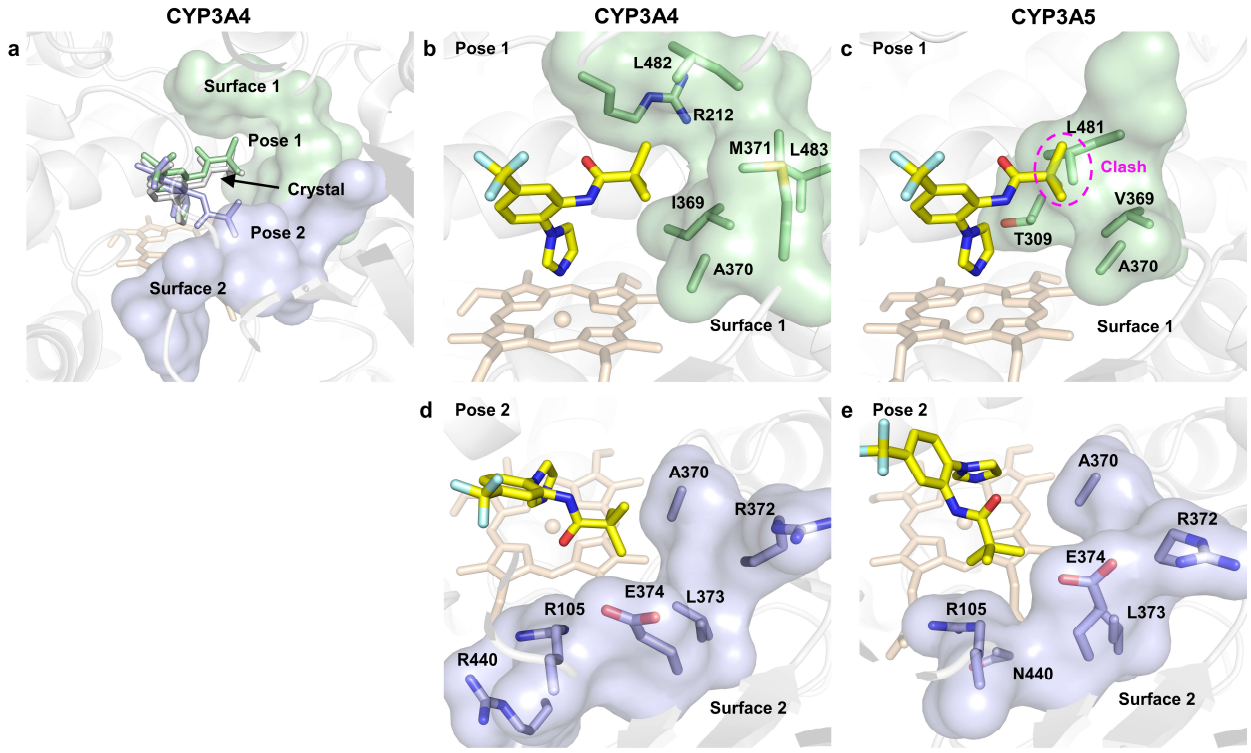
Supplementary Fig. 7 | Region A groups similar to the tert-butyl group in size did not affect CYP3A4/5 inhibition or selectivity. Dose–response curves showing concentration-dependent inhibition of CYP3A4 and CYP3A5 by SCM-01 and analogs with similar sized region A groups. Percentage inhibition data were normalized against their DMSO controls (as 0% inhibition) and 30 μM ketoconazole controls (as 100% inhibition). The reported numerical values are the means and standard deviations of the IC_{50} values derived from triplicate experiments ($n = 3$). The chemical scaffold of SCM-01 analogs is shown on top, and the structure of the region A group for each compound is shown in the inset. Source data are provided as a Source Data file.


a
CYP3A4–SCM-08
View 1
View 2
2.6 σ
b
CYP3A4–SCM-18
View 1
View 2
2.7 σ
c
CYP3A4–SCM-24
View 1
View 2
2.6 σ
d
CYP3A4–SCM-25
View 1
View 2
2.7 σ
e
CYP3A4–SCM-26
View 1
View 2
2.7 σ
f
CYP3A4–SCM-27
View 1
View 2
2.6 σ
g
CYP3A5–SCM-27
Mon A
View 1
Mon A
View 2
Mon B
View 1
Mon B
View 2
Mon A
2.9 σ
Mon B
2.9 σ

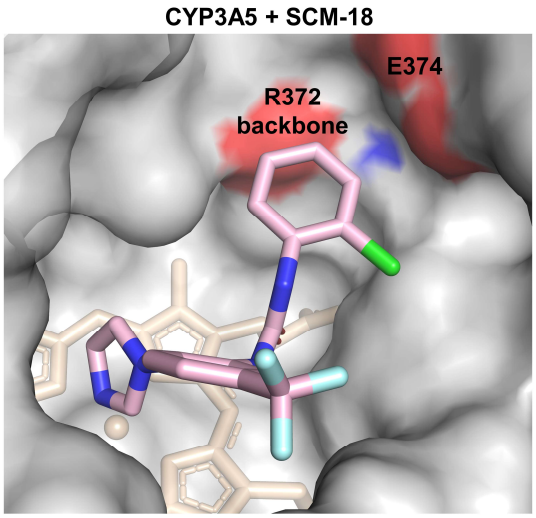
Supplementary Fig. 8 | X-ray structures of CYP3A4 bound to various SCM-1 analogs. Crystal structure models (sticks) and electron density maps (meshes) of the heme group and selective inhibitors (a) SCM-08, (b) SCM-18, (c) SCM-24, (d) SCM-25, (e) SCM-26, (f) SCM-27 in CYP3A4 and (g) SCM-27 in CYP3A5. Ambiguous electron density for unknown molecules near SCM-27 in CYP3A5 is not modeled. Final figure-of-merit–weighted $2F_o–F_c$ maps (blue) are contoured at 1.0 standard deviation. The $F_o–F_c$ omit maps of the heme group and selective inhibitors are shown in green at 2.6-2.9 standard deviations.



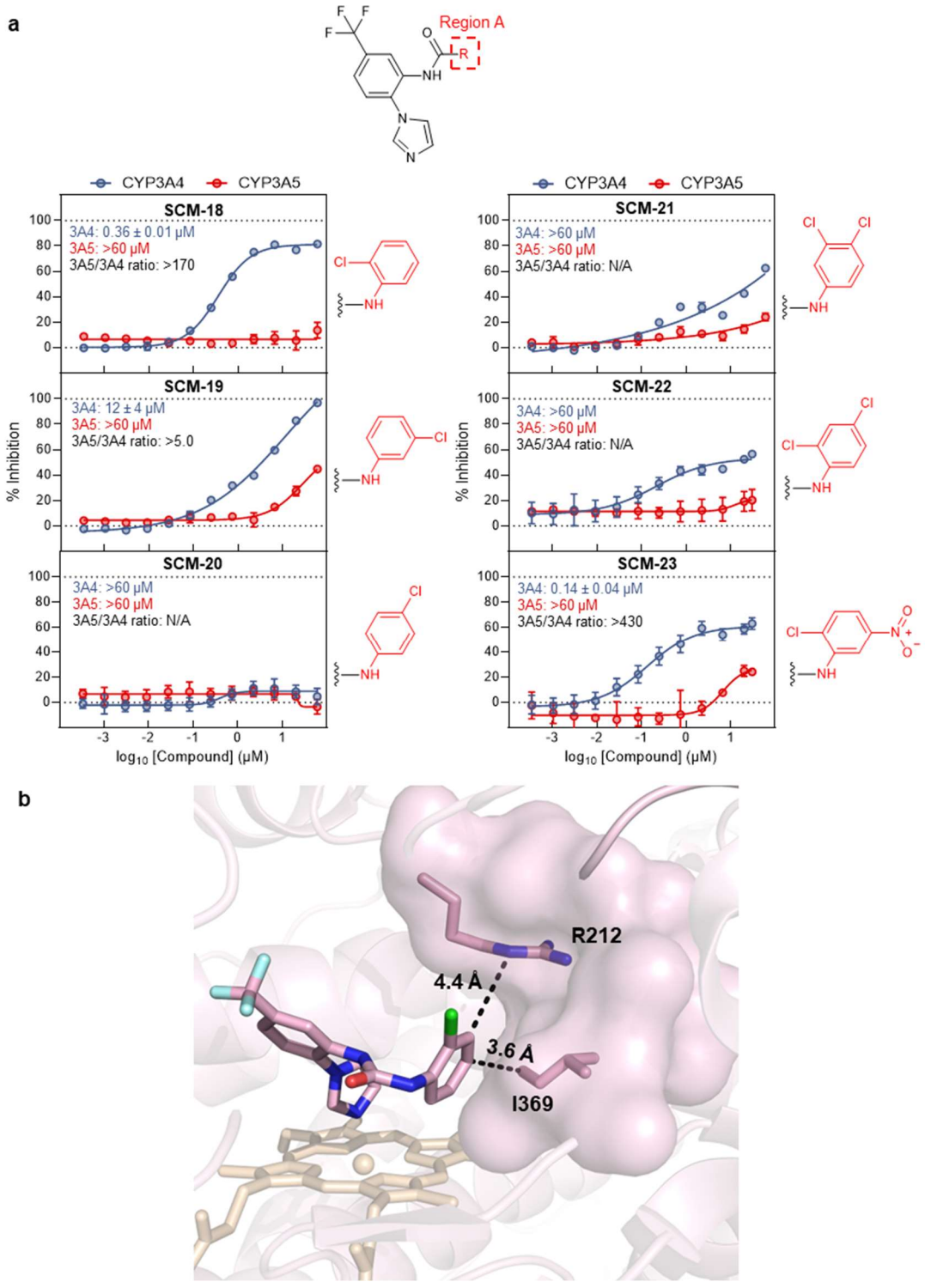
Supplementary Fig. 9 | Most of SCM-01 analogs are non-suicide CYP3A4/5 inhibitors. Dose–response curves showing time-dependent inhibition of CYP3A4/5 by SCM-01 analogs. The chemical scaffold for SCM-01 analogs is shown on top, and the structure of the region A group for each compound is shown in the inset. Percentage inhibition data were normalized against DMSO controls (as 0% inhibition) and 30 μM ketoconazole controls (as 100% inhibition). The IC_{50} values calculated from triplicate experiments (n = 3) are reported in Supplementary Table 5. Source data are provided as a Source Data file.



Supplementary Fig. 10 | Two surfaces in the ligand binding site with distinct chemical environment are responsible for selective CYP3A4 inhibition. (a) Overlay of docking results (blue and green) and the CYP3A4–SCM-01 crystal structure (gray) showing that docking pose 1 overlaps with the conformation in the crystal structure. (b) The CYP3A4–SCM-01 docking pose 1 showing that the region A group points towards the mostly hydrophobic surface 1. (c) Overlay of the CYP3A4–SCM-01 docking pose 1 and CYP3A5-apo crystal structure showing that SCM-01 would clash with CYP3A5 if bound in pose 1. (d) The CYP3A4–SCM-01 docking pose 2 showing that the region A group points towards the highly polar surface 2. (e) CYP3A5–SCM-01 pose 2 docking result showing that SCM-01 binds to CYP3A5 in pose 2, and surface 2 is mostly conserved between CYP3A4 and CYP3A5. For panels b-e, compound poses 1 and 2 are both shown as yellow stick representations, while surfaces 1 and 2 are shown as green and blue surfaces, respectively.

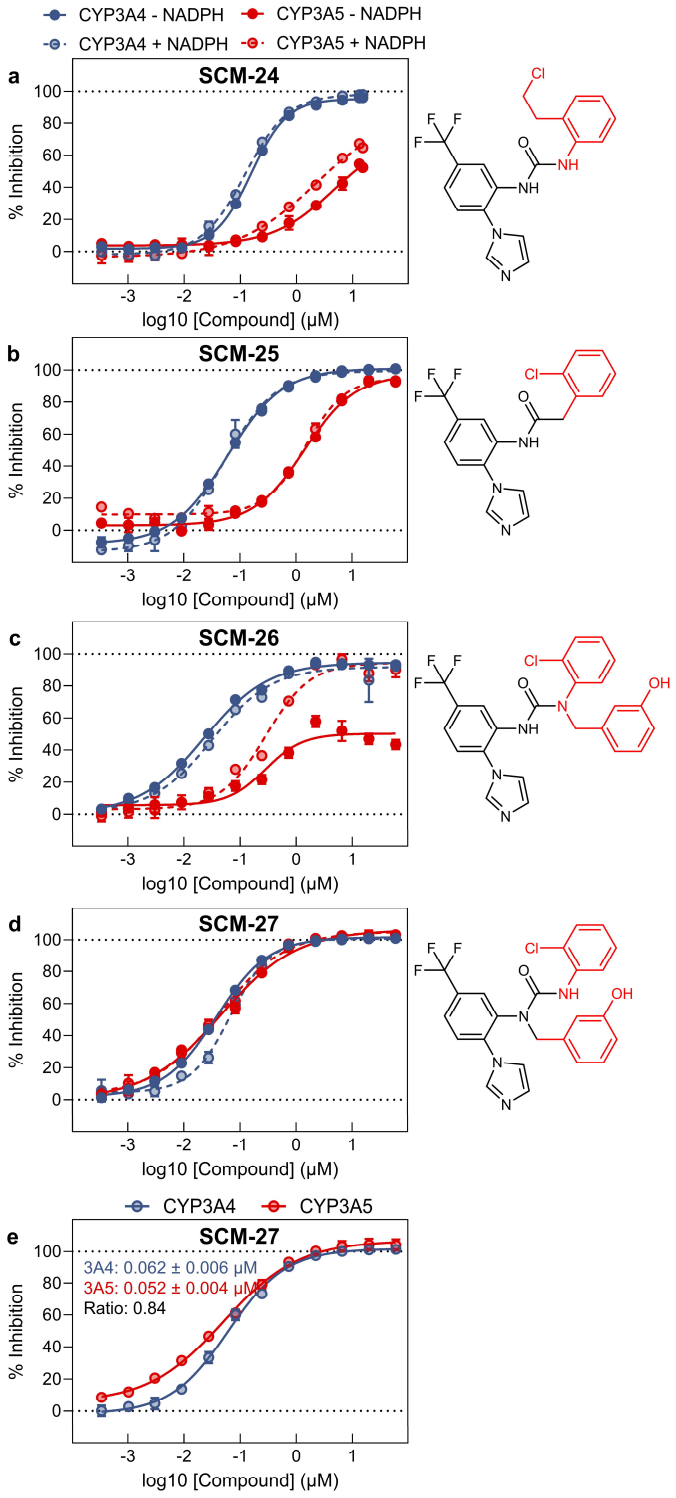


Supplementary Fig. 11 | Docking model explains the loss of CYP3A5 inhibition by SCM-18. Hypothetical SCM-18 pose 2 (pink, stick representation) binding model to CYP3A5 showing that the hydrophobic chlorophenyl group is near the unfavorable polar environment (red and blue, surface representation) on surface 2 formed by residues E374 and R372.



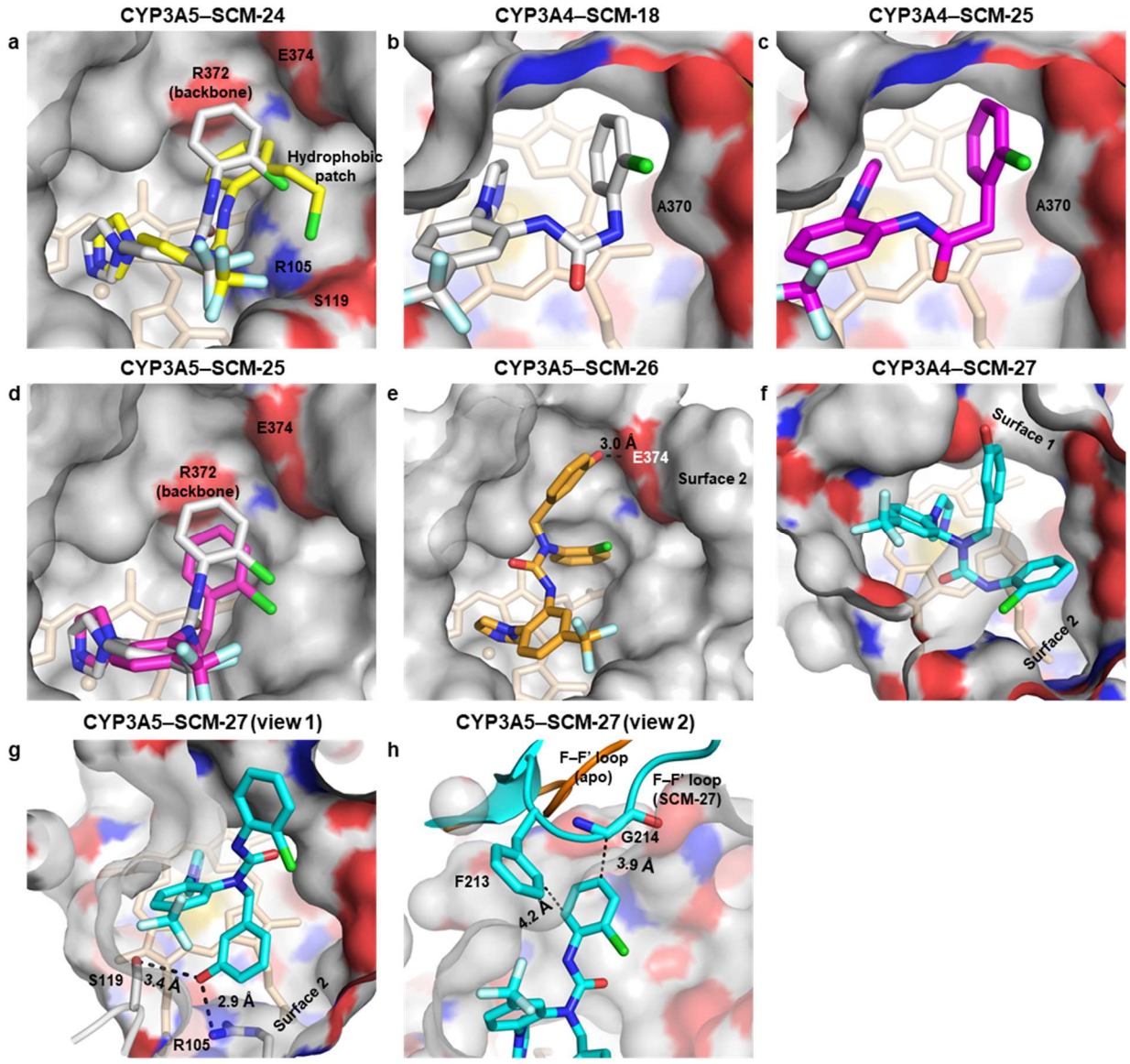
Supplementary Fig. 12 | Meta- and para-substituted benzene derivatives are unfavorable for CYP3A4 inhibition. (a) Dose-response curves showing concentration-dependent inhibition of CYP3A4 and CYP3A5. The chemical scaffold of SCM-01 analogs is shown on top, and the structure of the region A group for each compound is shown in red. Percentage inhibition data were normalized against their DMSO controls (as 0% inhibition) and against 30 μM ketoconazole controls (as 100% inhibition). The reported

numerical values are the means and standard deviations of the IC_{50} values derived from triplicate experiments (n = 3). (b) The crystal structure of CYP3A4 in complex with SCM-18 showing that the chlorophenyl group (stick representation) is close to surface 1 (surface representation), and further extension may cause clash with residues R212 and I369. Source data for (a) are provided as a Source Data file.



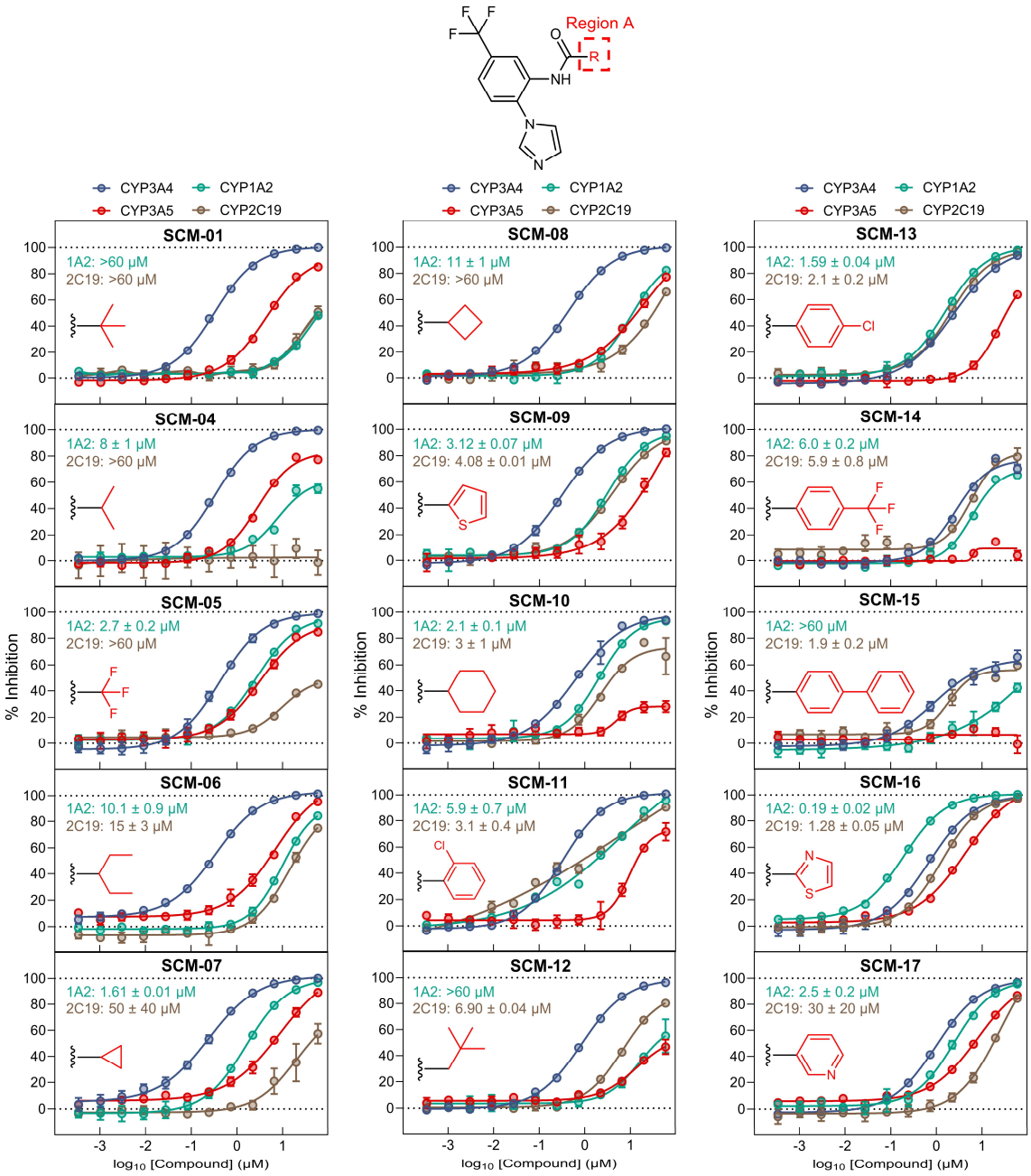
Supplementary Fig. 13 | Increasing in CYP3A4 inhibitory potency resulted in loss of CYP3A4 selectivity. (a–d) Dose–response curves showing time-dependent inhibition of CYP3A4/5 by (a) SCM-24, (b) SCM-25, (c) SCM-26, and (d) SCM-27. Percentage inhibition data were normalized against DMSO controls (as 0% inhibition) and 30 μM ketoconazole controls (as 100% inhibition). The IC_{50} values

calculated from triplicate experiments (n = 3) are reported in Supplementary Table 5. Chemical structures of SCM-24, SCM-25, SCM-26, and SCM-27 are shown on the right. (e) Dose–response curves showing concentration-dependent inhibition of CYP3A4/5 by SCM-27. Percentage inhibition data were normalized against DMSO controls (as 0% inhibition) and 30 μM ketoconazole controls (as 100% inhibition). The reported numerical values are means and standard deviations of IC_{50} values derived from triplicate experiments (n = 3). Source data are provided as a Source Data file.

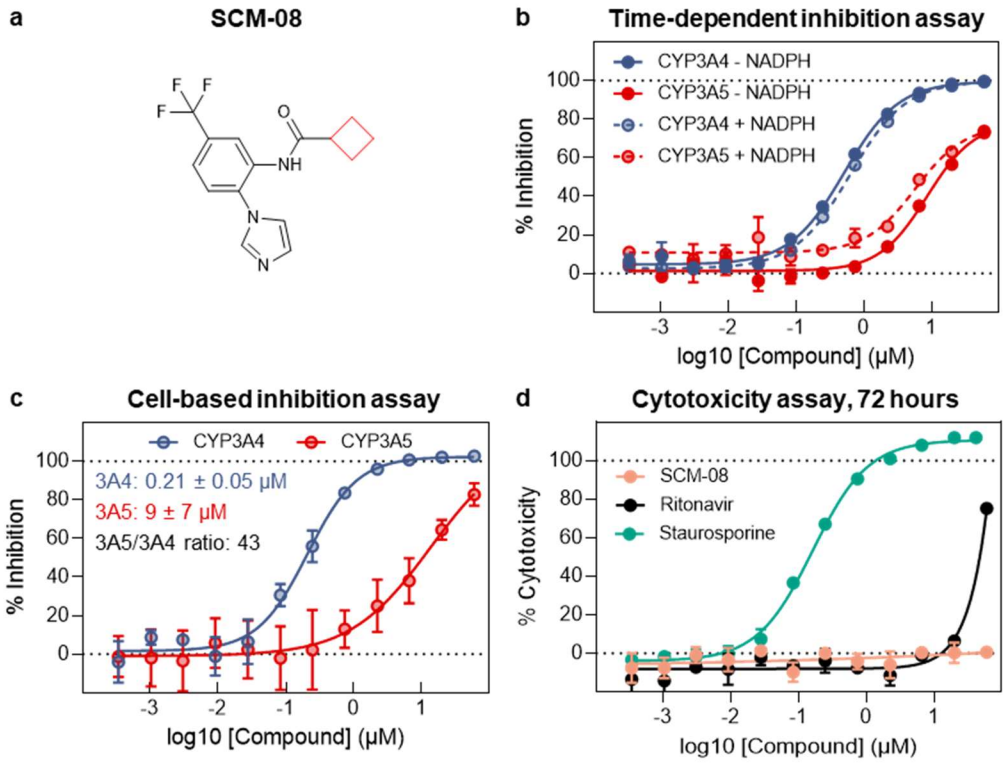


Supplementary Fig. 14 | Structural studies explain the observed inhibitory profile. (a) The CYP3A5–SCM-24 docking result showing that the hydrophobic benzene ring of SCM-24 (yellow, stick representation) is positioned farther away from the unfavorable polar environment formed by E374 and R372 as compared to that of SCM-18 (white, stick representation). Additionally, the ethyl chloride group is seen favorably interacting with a hydrophobic patch, but the chloride end is seen close to the polar surface formed by S119 and R105. (b–c) Crystal structures of CYP3A4 in complex with (b) SCM-18 (white, stick representation) and (c) SCM-25 (magenta, stick representation) showing that the nitrogen of the SCM-18 urea linker is near the hydrophobic residue A370, whereas a more favorable hydrophobic interaction is observed between the carbon of the SCM-25 methyl amide and A370, thus explaining the higher potency of SCM-25. (d) The CYP3A5–SCM-25 docking result showing that the hydrophobic chlorophenyl group of SCM-25 (magenta, stick representation) is positioned farther away from the unfavorable polar environment formed by E374 and R372 as compared to that of SCM-18 (white, stick representation). (e) The CYP3A5–SCM-26 docking result showing that the phenol group of SCM-26 (orange carbon, stick representation) has a potential hydrogen bond with E374, but the hydrophobic ring occupies an unfavorable polar space due to the oxygen

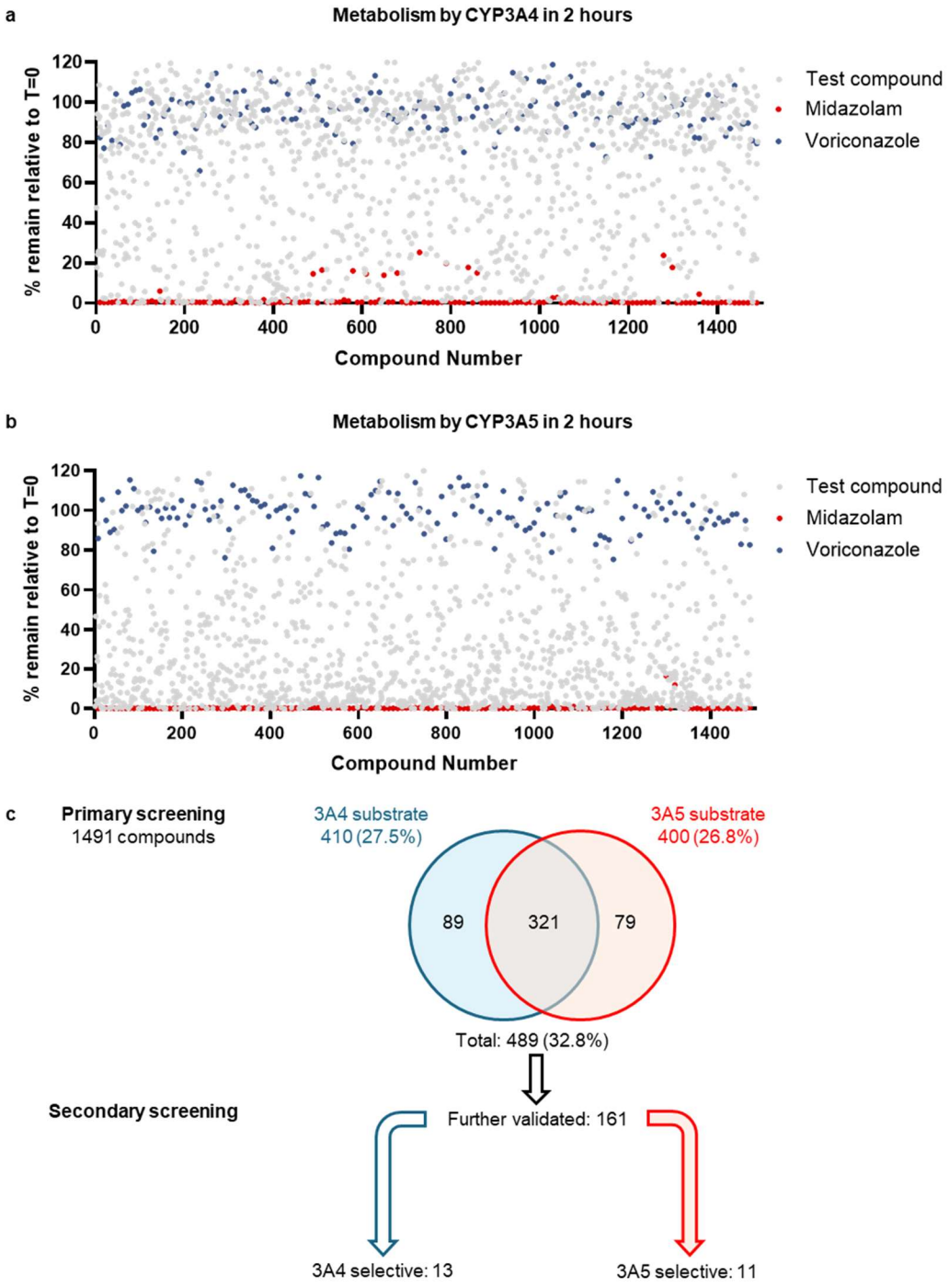
backbone of G480. The chlorophenyl ring resides in a neutral space. (f) The CYP3A4–SCM-27 crystal structure showing the two branched aromatic groups of SCM-27 (cyan carbon, stick representation) facing towards surfaces 1 and 2. (g-h) The crystal structure of CYP3A5 in complex with SCM-27 (cyan carbon, stick representation) showing that (g) its phenol group is positioned towards surface 2, forming H-bonds with R105 and S119, and (h) its chlorophenyl moiety resides in an opening surface formed by the of the rearranged F–F' loop (cyan, cartoon representation), interacting with F213 and G214. The F–F' loop of the CYP3A5-apo crystal structure is shown as orange cartoon representation for comparison.



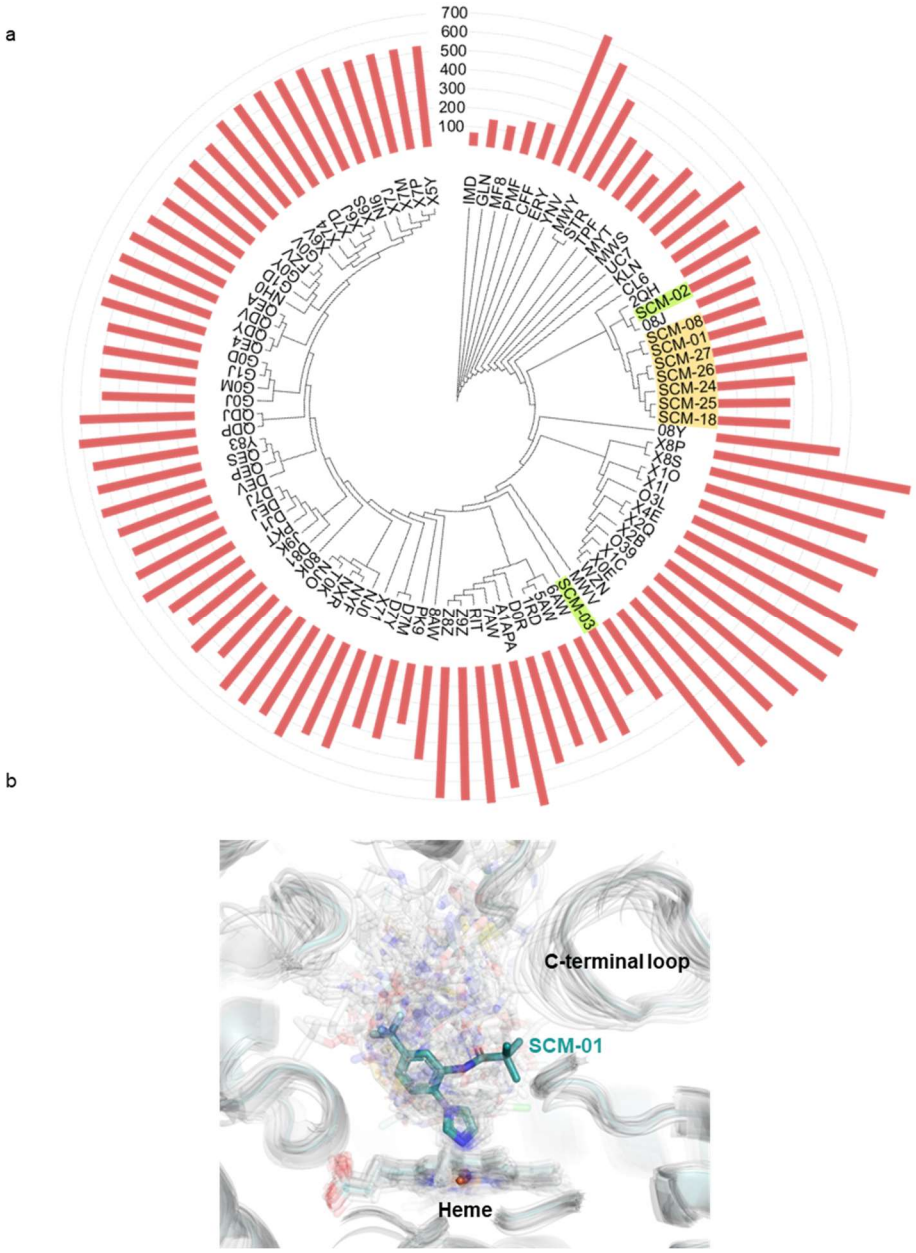
Supplementary Fig. 15 | Structure-activity relationship analysis of SCM-01 analogs indicates that larger A groups tend to have more potent inhibition of CYP1A2 and CYP2C19. Dose–response curves showing concentration-dependent inhibition of CYP1A2, CYP2C19, CYP3A4, and CYP3A5 by SCM-01 analogs. The inhibitory potencies of CYP3A4/5 were determined using the P450-Glo biochemical assay, and the inhibitory potencies of CYP1A2 and CYP2C19 were measured using the Vivid P450 biochemical assay. The chemical scaffold for SCM-01 analogs is shown on top, and the structure of the region A group for each compound is shown in the inset. Percentage inhibition data were normalized against their DMSO controls (as 0% inhibition) and 30 μM ketoconazole controls (as 100% inhibition). The reported numerical values are the means and standard deviations of the IC_{50} values derived from triplicate experiments ($n = 3$). Source data are provided as a Source Data file.



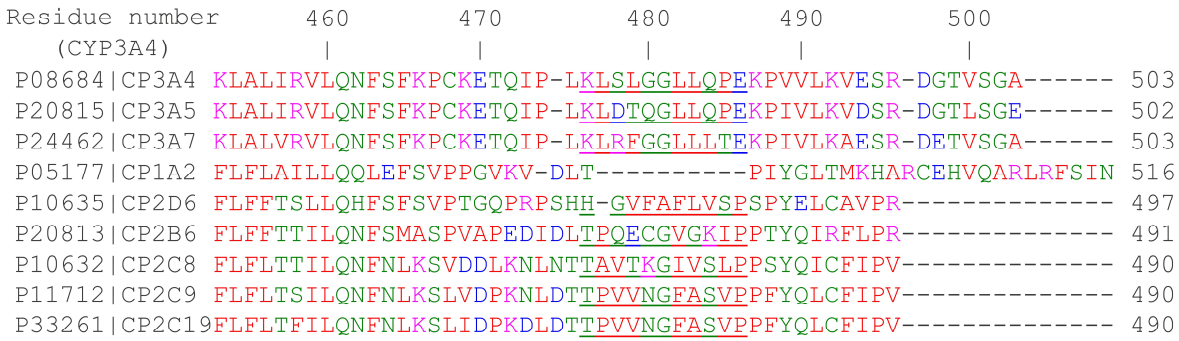
Supplementary Fig. 16 | SCM-08 is a non-suicide CYP3A4/5 inhibitor that selectively inhibits CYP3A4 in the cellular environment. (a) Chemical structure of SCM-08. The region A group is colored in red. (b) Dose–response curves showing time-dependent CYP3A4/5 inhibition by SCM-08 as determined using the biochemical P450-Glo assay. (c) Dose–response curves showing concentration-dependent inhibition of CYP3A4/5 by SCM-08 as determined using the cell-based P450-Glo assay. Percentage inhibition data were normalized against DMSO controls (as 0% inhibition) and 30 μM ketoconazole controls (as 100% inhibition). The reported numerical values are the means and standard deviations of the IC_{50} values calculated from triplicate experiments (n = 3). (d) Dose-response curves showing SCM-08 is not cytotoxic to 293T/17 cells. Cells were treated with up to 60 μM of SCM-08, ritonavir, or staurosporine (positive reference) for 72 hours, and cell viability was assessed with the CellTiter-Glo Luminescent Cell Viability Assay. Data were normalized from using DMSO (as 0% toxicity) and media only (as 100% toxicity). Source data for (b-d) are provided as a Source Data file.



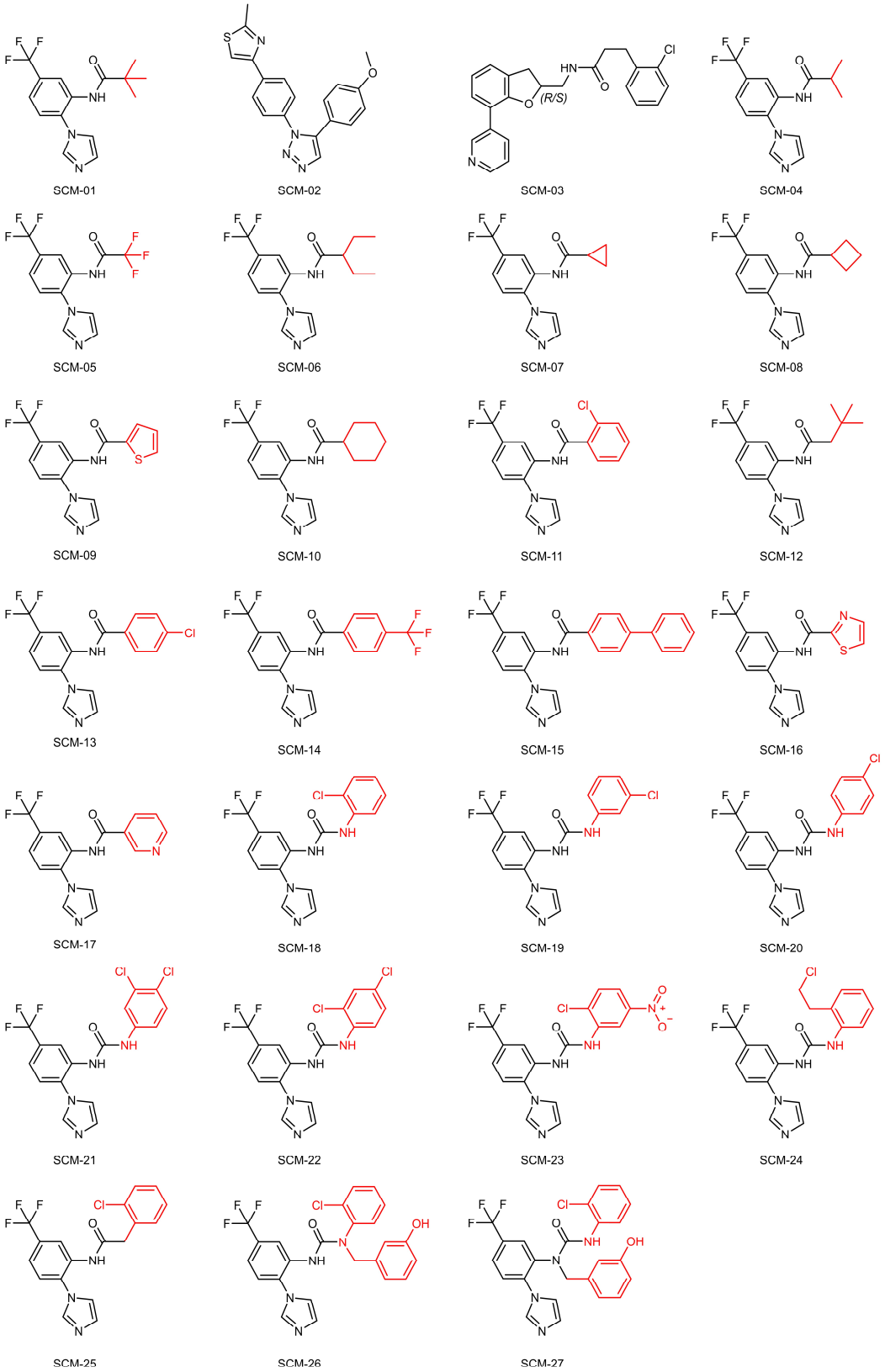
Supplementary Fig. 17 | Screening of FDA-approved drugs identified many selective CYP3A4 or CYP3A5 substrates. (a-b) Primary screening results showing the percentage of compound remaining (gray spots) after 2 hours of metabolism by (a) CYP3A4 or (b) CYP3A5. A CYP3A4/5 substrate, midazolam (red spots), and a CYP3A4/5 inhibitor, voriconazole (blue spots) were used as reference compounds. The values of plotted data points are means of triplicate experiment (n = 3). (c) Venn diagram showing the number of CYP3A4 and CYP3A5 substrates (based on a cutoff of >50% metabolism in 2 hours) found in primary screening and selective CYP3A4 and CYP3A5 substrates identified in the secondary screening. Source data for (a-b) are provided as a Source Data file.



Supplementary Fig. 18 | Distinctiveness of SCM-01 analogs. (a) Clustering of reported ligands co-crystallized with CYP3A4 by their structural similarity. Height of red bars indicates molecular weights. SCM-01 and its analogs are highlighted in yellow, while SCM-02 and SCM-03 are highlighted in green. (b) Overlay of CYP3A4 crystal structures in complex with all reported ligands. The heme group and ligands are shown as sticks. SCM-01 and its CYP3A4 backbone (cartoon representation) are colored deep teal.



Supplementary Fig. 19 | The C-terminal loop region is not conserved among major human CYPs. Sequence alignment of the C-terminal loop of major human CYPs. Residue numbers correspond to CYP3A4, and C-terminal loop residues (476-486) are underlined. The alignment was carried out using Clustal Omega.[1]



Supplementary Fig. 20 | Chemical structures of compounds SCM-01 to SCM-27. The region A groups of SCM-01 analogs are color in red.

Supplementary Table 1. Selective CYP3A4 inhibitor screening data

Category	Parameter	Description
Assay	Type of Assay	*In vitro* biochemical assay
	Target	CYP3A4 (UniProt ID P08684) and CYP3A5 (UniProt ID P20815)
	Primary measurement	Detection of luminescence signal
	Key reagents	P450-Glo CYP3A4 Assay and Screening System (Promega)
	Assay protocol	Please see Materials and Methods section "P450-Glo biochemical inhibition assay"
	Additional comments	
Library	Library size	9299 compounds
	Library composition	Drug-like library
	Source	Multiple vendors compiled by St. Jude Children's Research Hospital[2]
	Additional comments	
Screen	Format	384-well plate
	Concentrations tested	Primary screen: 10 μM Secondary screen: 0.00017—60 μM
	Plate controls	Primary screen: 15 μM ritonavir; Secondary Screen: 30 μM ketoconazole
	Reagent/compound dispensing system	Echo 650 (compound) and Multidrop Combi (reagent)
	Detection instrument and software	EnVision Multimode Plate Reader
	Assay validation/QC	Average Z'=0.85
	Correction factors	
	Normalization	DMSO as 0% inhibition, 15 μM ritonavir (primary screen) or 30 μM ketoconazole (secondary screen) as 100% inhibition
	Additional comments	
Post-HTS analysis	Hit criteria	Primary screen: >80% CYP34 inhibition Secondary screen: CYP3A4 IC_{50}<0.1 μM and max inhibition >50%, CYP3A5/CYP3A4 IC_{50} ratio>100
	Hit rate	Primary screen: 10.3% (956/9299); Secondary screen: 4.3% (41/956)
	Additional assays	
	Confirmation of hit purity and structure	Compounds were repurchased and re-tested using the same P450-Glo assay (Supplementary Table 2). Purchased compounds were verified to have the corrected mass and >95% purity using high resolution mass spectrometry and HPLC.
	Additional comments	

Supplementary Table 2. Validation of commercially available selective CYP3A4/5 inhibitors identified in the HTS

No.	Library number	Alternative name	CYP3A4 IC_{50} (μM)	CYP3A5 IC_{50} (μM)	IC_{50} ratio CYP3A5/CYP3A4
1	SJ000132055	ChemBridge 7669009	0.44 ± 0.04	1.7 ± 0.1	3.9
2	SJ000305877	ChemBridge 16833787	0.107 ± 0.006	0.201 ± 0.001	1.9
3	SJ000310315	ChemBridge 15009711	0.048 ± 0.004	0.30 ± 0.04	6.3
4	SJ000137498	ChemBridge 7921636	0.076 ± 0.002	0.82 ± 0.09	11
5	SJ000113446	ChemBridge 6058429	0.12 ± 0.02	0.58 ± 0.03	4.8
6	SJ000129663	ChemBridge 6905860	0.19 ± 0.02	1.44 ± 0.07	7.6
7	SJ000293582	ChemBridge 6004532	0.121 ± 0.008	1.01 ± 0.07	8.3
8	SJ000310522	ChemBridge 28889850	0.082 ± 0.004	0.11 ± 0.01	1.3
9	SJ000174031	ChemBridge 6858700	0.46 ± 0.01	0.94 ± 0.03	2.0
10	SJ000131514	ChemBridge 7632365	0.118 ± 0.003	1.5 ± 0.1	13
11	SJ000064999	ChemBridge 7906779	0.606 ± 0.007	2.6 ± 0.2	4.3
12	SJ000310519	ChemBridge 48875881	0.201 ± 0.005	2.40 ± 0.03	12
13	SJ000007224	ChemBridge 6061756	0.5 ± 0.1	3.2 ± 0.5	6.4
14	SJ000303133	ChemBridge 67692263	0.110 ± 0.001	2.3 ± 0.4	21
15	SJ000340912	ChemBridge 9102543	0.07 ± 0.05	>60[a]	>860
16	SJ000139218	ChemBridge 7957511	0.43 ± 0.04	6 ± 1	14
17	SJ000212946	ChemBridge 9054357	0.51 ± 0.07	0.76 ± 0.03	1.5
18	SJ000176651	ChemBridge 6987665	0.61 ± 0.08	3.2 ± 0.3	5.2
19	SJ000136749	ChemBridge 7910146	0.51 ± 0.02	6.1 ± 0.1	12
20	SJ000189244	ChemBridge 7651664	1.14 ± 0.04	14 ± 2	12
21	SJ000143899	ChemBridge 5270555	0.37 ± 0.01	1.57 ± 0.01	4.2
22	SJ000300221	ChemBridge 6074427	0.30 ± 0.03	1.03 ± 0.07	3.4
23	SJ000307960	ChemBridge 19459521	0.48 ± 0.07	2.2 ± 0.2	4.6
24	SJ000301921	ChemBridge 31063884	0.15 ± 0.02	1.6 ± 0.2	11
25	SJ000138907	ChemBridge 7950679	0.15 ± 0.03	3.3 ± 0.8	22
26	SJ000475206	ChemBridge 9272018	1.0 ± 0.4	5.4 ± 0.3	5.4
27	SJ000137306	ChemBridge 7917759	0.28 ± 0.03	1.8 ± 0.2	6.4
28	SJ000096334	ChemDiv E005-0732	0.071 ± 0.004	0.8 ± 0.2	11
29	SJ000055399	ChemDiv 8015-3739	0.13 ± 0.02	18 ± 1	140
30	SJ000116554	ChemDiv C696-1151	0.081 ± 0.002	0.65 ± 0.05	8.0
31	SJ000440778	Enamine Z162479870	0.141 ± 0.003	0.23 ± 0.01	1.6
32	SJ000408377	Enamine Z16306263	0.91 ± 0.09	0.8 ± 0.2	0.88
33	SJ000388260	Enamine Z94599677	0.057 ± 0.002	0.39 ± 0.07	6.8
34	SJ000362065	Enamine Z56792718	0.32 ± 0.03	4.33 ± 0.09	14
35	SJ000273271	Life Chemicals F2725-1203	0.29 ± 0.02	2.8 ± 0.2	9.7
36	SJ000233786	Life Chemicals F0528-0892	0.46 ± 0.04	>60[a]	>130
37	SJ000796016	MedChem Express HY-12273	0.084 ± 0.005	>60[a]	>720
38	SJ000984157	Molport 000-464-739	9 ± 1	>60[a]	>6.7
39	SJ000484828	Molport 005-913-862	1.24 ± 0.05	5.5 ± 0.4	4.4
40	SJ000983500	Sigma-Aldrich R660817	0.20 ± 0.02	22 ± 25	110
41	SJ000060458	Vitasmlab STK228064	0.135 ± 0.008	>60[a]	>440

All data were obtained using the P450-Glo biochemical inhibition assay. The IC_{50} values were generated by fitting dose–response data to Equation 1, and the reported values are means and standard deviations of triplicate experiments (n = 3). Source data are provided as a Source Data file.

[a]For weak inhibitors for which IC_{50} values could not be determined, their IC_{50} values are reported as greater than the highest compound concentrations tested.

Supplementary Table 3. Results of CYP3A4/5 biochemical inhibition assay

Compound	CYP3A4 IC_{50} (μM)	CYP3A5 IC_{50} (μM)	Selectivity 3A5/3A4 IC_{50} ratio	Alternative name
Ketoconazole	0.030 ± 0.004	0.225 ± 0.009	7.5	-
SCM-01	0.32 ± 0.03	4.33 ± 0.09	14	SJ000362065 Enamine Z56792718
SCM-02	0.057 ± 0.002	0.39 ± 0.07	6.8	SJ000388260 Enamine Z94599677
SCM-03	0.048 ± 0.004	0.30 ± 0.04	6.3	SJ000310315 ChemBridge 15009711
SCM-04	0.33 ± 0.02	2.9 ± 0.2	8.8	Enamine Z56794030
SCM-05	0.43 ± 0.04	3.22 ± 0.02	7.5	Enamine Z56795105
SCM-06	0.34 ± 0.03	7 ± 1	21	SJYHJ-120
SCM-07	0.240 ± 0.009	8.9 ± 0.4	37	SJYHJ-113
SCM-08	0.43 ± 0.02	20 ± 3	47	SJYHJ-114
SCM-09	0.31 ± 0.04	19 ± 2	61	SJYHJ-116
SCM-10	0.7 ± 0.2	>60[a]	>86	SJYHJ-115
SCM-11	0.33 ± 0.01	10 ± 2	30	SJYHJ-079
SCM-12	0.87 ± 0.07	>60[a]	>69	SJYHJ-119
SCM-13	2.3 ± 0.1	26 ± 8	11	Enamine Z56787794
SCM-14	2.7 ± 0.1	>60[a]	>22	Enamine Z56912610
SCM-15	0.9 ± 0.2	>60[a]	>67	Enamine Z56795104
SCM-16	0.68 ± 0.07	4.4 ± 0.3	6.5	SJYHJ-117
SCM-17	1.02 ± 0.03	8.2 ± 0.6	8.0	SJYHJ-118
SCM-18	0.36 ± 0.01	>60[a]	>170	Enamine Z56791366
SCM-19	12 ± 4	>60[a]	>5.0	Enamine Z56789847
SCM-20	>60[a]	>60[a]	N/A[b]	Enamine Z56787891
SCM-21	>60[a]	>60[a]	N/A[b]	Enamine Z56789845
SCM-22	>60[a]	>60[a]	N/A[b]	Enamine Z56791367
SCM-23	0.14 ± 0.04	>60[a]	>430	Enamine Z56791329
SCM-24	0.146 ± 0.006	3.19 ± 0.03	22	SJYHJ-106
SCM-25	0.027 ± 0.004	1.5 ± 0.1	56	SJYHJ-075
SCM-26	0.067 ± 0.004	1.65 ± 0.03	25	SJYHJ-110
SCM-27	0.062 ± 0.006	0.052 ± 0.004	0.84	SJYHJ-111
Ritonavir	0.045 ± 0.001	0.03 ± 0.01	0.67	-

All data were obtained using the P450-Glo biochemical inhibition assay. The IC_{50} values were generated by fitting dose–response data to Equation 1, and the reported values are means and standard deviations of triplicate experiments (n = 3). Source data are provided as a Source Data file.

[a]For weak inhibitors for which IC_{50} values could not be determined, their IC_{50} values are reported as greater than the highest compound concentrations tested.

[b]N/A: not applicable

Supplementary Table 4. Results of CYP3A4/5 UV-vis binding measurements

Compound	CYP3A4			CYP3A5			K_s ratio 3A5/3A4	Alternative name
	K_s (μM)	ΔA_{max}	Type	K_s (μM)	ΔA_{max}	Type		
Ketoconazole	0.77 ± 0.02	0.497 ± 0.007	II	2.98 ± 0.04	0.443 ± 0.006	II	3.9	-
SCM-01	1.17 ± 0.02	0.364 ± 0.005	II	51 ± 2	0.361 ± 0.003	II	44	SJ000362065 Enamine Z56792718
SCM-02	5.0 ± 0.8	0.326 ± 0.006	II	ND[a]	ND[a]	II	N/A[b]	SJ000388260 Enamine Z94599677
SCM-03	0.018 ± 0.006	0.255 ± 0.009	II	2.2 ± 0.2	0.17 ± 0.01	I	120	SJ000310315 ChemBridge 15009711
SCM-18	3.6 ± 0.5	0.277 ± 0.007	II	ND[a]	ND[a]	ND[a]	N/A[b]	Enamine Z56791366

All data were determined using UV-vis measurements. The K_s and ΔA_{max} values were generated by fitting concentration vs ΔA plot to Equation 2, and the reported numerical values are the means and standard deviations of triplicate experiments (n = 3). Source data are provided as a Source Data file.

[a]ND: not determined because the binding was too weak to determine its binding type or fit for K_s and ΔA_{max} values.

[b]N/A: not applicable.

Supplementary Table 5. Results of CYP3A4/5 time-dependent IC_{50} shift assay

Compound	CYP3A4			CYP3A5			Alternative name
	IC_{50} (μM) pre-incubated without NADPH	IC_{50} (μM) pre-incubated with NADPH	IC_{50} fold change	IC_{50} (μM) pre-incubated without NADPH	IC_{50} (μM) pre-incubated with NADPH	IC_{50} fold change	
Ketoconazole	0.021 ± 0.002	0.023 ± 0.003	0.91	0.16 ± 0.02	0.15 ± 0.02	1.1	-
CYP3cide	0.20 ± 0.02	0.0111 ± 0.0004	18	>60[a]	7 ± 2	>8.6	-
SCM-01	0.31 ± 0.06	0.42 ± 0.05	0.74	5.3 ± 0.3	6 ± 1	0.88	SJ000362065 Enamine Z56792718
SCM-02	0.054 ± 0.001	0.073 ± 0.008	0.74	0.37 ± 0.05	0.21 ± 0.02	1.8	SJ000388260 Enamine Z94599677
SCM-03	0.042 ± 0.001	0.10 ± 0.02	0.42	0.43 ± 0.03	0.4 ± 0.1	1.1	SJ000310315 ChemBridge 15009711
SCM-04	0.24 ± 0.02	0.35 ± 0.02	0.69	1.46 ± 0.09	1.17 ± 0.08	1.2	Enamine Z56794030
SCM-05	0.58 ± 0.03	0.72 ± 0.03	0.81	4.3 ± 0.2	3.4 ± 0.3	1.3	Enamine Z56795105
SCM-06	0.29 ± 0.03	0.48 ± 0.04	0.6	5.6 ± 0.3	6.8 ± 0.6	0.82	SJYHJ-120
SCM-07	0.40 ± 0.02	0.51 ± 0.03	0.78	6 ± 1	6 ± 3	1.0	SJYHJ-113
SCM-08	0.51 ± 0.02	0.63 ± 0.03	0.81	9 ± 2	5.8 ± 0.9	1.6	SJYHJ-114
SCM-09	0.45 ± 0.02	0.045 ± 0.005	10	15.4 ± 0.7	2 ± 1	7.7	SJYHJ-116
SCM-10	0.59 ± 0.02	0.64 ± 0.03	0.92	2.5 ± 0.4	0.75 ± 0.04	3.3	SJYHJ-115
SCM-11	0.32 ± 0.02	0.302 ± 0.003	1.1	16 ± 1	10.7 ± 0.8	1.5	SJYHJ-079
SCM-12	1.2 ± 0.2	1.10 ± 0.09	1.1	11 ± 3	8 ± 2	1.4	SJYHJ-119
SCM-13	2.9 ± 0.3	2.7 ± 0.2	1.1	23.0 ± 0.2	25 ± 5	0.92	Enamine Z56787794
SCM-14	3 ± 1	1.1 ± 0.3	2.7	>60[a]	>60[a]	N/A[b]	Enamine Z56912610
SCM-15	>60[a]	>60[a]	N/A[b]	>60[a]	>60[a]	N/A[b]	Enamine Z56795104
SCM-16	0.78 ± 0.07	0.97 ± 0.09	0.8	4.2 ± 0.4	4 ± 1	1.1	SJYHJ-117
SCM-17	1.6 ± 0.2	1.8 ± 0.1	0.89	8 ± 1	14 ± 6	0.57	SJYHJ-118
SCM-18	0.42 ± 0.03	0.43 ± 0.08	0.98	>60[a]	>60[a]	N/A[b]	Enamine Z56791366
SCM-24	0.156 ± 0.006	0.122 ± 0.003	1.3	5 ± 2	3 ± 2	1.7	SJYHJ-106
SCM-25	0.060 ± 0.001	0.053 ± 0.009	1.1	1.4 ± 0.1	1.5 ± 0.1	0.93	SJYHJ-075
SCM-26	0.023 ± 0.001	0.032 ± 0.005	0.72	0.29 ± 0.07	0.29 ± 0.04	1.0	SJYHJ-110
SCM-27	0.038 ± 0.005	0.068 ± 0.003	0.56	0.047 ± 0.006	0.044 ± 0.001	1.1	SJYHJ-111

All data were obtained using the P450-Glo time-dependent inhibition assay. The IC_{50} values were generated by fitting dose–response data to Equation 1, and the reported numerical values are the means and standard deviations of triplicate experiments (n = 3). Source data are provided as a Source Data file.

[a]For weak inhibitors for which IC_{50} values could not be determined, the IC_{50} values are reported as greater than the highest compound concentrations tested.

[b]N/A: not applicable

Supplementary Table 6. Data collection and refinement statistics for CYP3A4 in complex with SCM-01, SCM-02, SCM-03, and SCM-08

	CYP3A4–SCM-01	CYP3A4–SCM-02	CYP3A4–SCM-03	CYP3A4–SCM-08
Data collection				
Wavelength	1.000	0.979	0.9200	0.979
Beamline	SER-CAT-22-ID	FMX-17-ID-2	FMX-17-ID-2	FMX-17-ID-2
Resolution range (Å)	49.2 – 2.71 (2.84 – 2.71)	43.18 – 3.10 (3.32 – 3.10)	44.18 – 3.21 (3.43 – 3.21)	44.85 – 3.00 (3.18 – 3.00)
Space group	*I* 2 2 2	*I* 2 2 2	*I* 2 2 2	*I* 2 2 2
Unit cell: *a*, *b*, *c* (Å)	76.36 98.39 132.26 90	75.88 100.69 123.09	76.83 101.94 127.35	77.24 100.81 131.56
α, β, γ (˚)	90 90	90 90 90	90 90 90	90 90 90
Mosaicity (˚)	0.23	0.31	0.46	0.17
Total reflections	185545	96568	62068	110215
Unique reflections	13859 (1833)	8850 (1575)	8457 (1481)	10614 (1698)
Multiplicity	13.4 (13.6)	10.9 (11.2)	7.3 (7.4)	10.4 (10.0)
Completeness (%)	99.7 (99.9)	99.9 (99.4)	99.9 (99.8)	100.0 (99.9)
Mean $I/\sigma(I)$	20.0 (2.4)	15.2 (2.6)	10.4 (2.5)	9.8 (2.6)
Wilson B-factor (Å^2)	74.8	106.4	102.2	81.6
R_{sym}	0.09 (1.10)	0.10 (0.91)	0.12 (0.77)	0.16 (1.18)
$CC_{1/2}$ (%)	100.0 (83.0)	99.5 (83.7)	99.8 (79.8)	99.5 (75.6)
Refinement statistics				
Resolution range (Å)	49.2 – 2.71 (2.807 – 2.71)	38.97 – 3.10 (3.21 – 3.10)	39.19 – 3.21 (3.33 –3.21)	40.19 – 3.00 (3.11 – 3.00)
Reflections used in refinement	13816 (1343)	8842 (859)	8447 (810)	10602 (1043)
Reflections used for R_{free}	691 (67)	442 (40)	422 (41)	530 (52)
R_{work}	0.224 (0.367)	0.246 (0.362)	0.235 (0.322)	0.233 (0.394)
R_{free}	0.245 (0.501)	0.268 (0.422)	0.256 (0.361)	0.261 (0.386)
No. of non-hydrogen atoms				
Protein	3679	3452	3497	3622
Ligand	22	25	28	22
Heme	43	43	43	43
Water	13	1	1	0
Protein residues	470	456	464	464
RMS (bonds)	0.003	0.003	0.002	0.003
RMS (angles)	0.52	0.56	0.52	0.58
Ramachandran favored (%)	97.22	97.54	96.52	97.39
Ramachandran allowed (%)	2.78	2.46	3.48	2.61
Ramachandran outliers (%)	0	0	0	0
Rotamer outliers (%)	0.2	0	0	0
Clashscore	4.45	5.40	5.22	4.13
Average B-factor (Å^2)	70.84	98.86	93.99	76.25
Protein	71.00	99.28	94.30	76.56
Ligand	63.57	92.93	81.51	63.49
Heme	60.65	72.73	76.31	56.30
Water	64.63	79.65	85.76	-
PDB ID	9BV5	9BV6	9BV7	9BV8

Values in parentheses for the highest resolution shell

Supplementary Table 7. Data collection and refinement statistics for CYP3A4 in complex with SCM-18, SCM-24, SCM-25, and SCM-26

	CYP3A4–SCM-18	CYP3A4–SCM-24	CYP3A4–SCM-25	CYP3A4–SCM-26
Data collection				
Wavelength	0.979	0.979	0.920	0. 920
Beamline	FMX-17-ID-2	FMX-17-ID-2	AMX-17-ID-1	AMX-17-ID-1
Resolution range (Å)	79.29 – 2.95 (3.13 – 2.95)	65.52 – 3.02 (3.20 – 3.02)	33.24 – 3.00 (3.18 – 3.00)	34.55 – 2.80 (2.95 – 2.80)
Space group	*I* 2 2 2	*I* 2 2 2	*I* 2 2 2	*I* 2 2 2
Unit cell: *a*, *b*, *c* (Å)	77.04 100.90 128.19	76.78 101.10 125.64	77.50 100.53 129.33	76.74 101.71 127.32
α, β, γ (˚)	90 90 90	90 90 90	90 90 90	90 90 90
Mosaicity (˚)	0.21	0.15	0.39	0.09
Total reflections	144830	132350	124921	169102
Unique reflections	10774 (1704)	9846 (1584)	10437 (1645)	12624 (1810)
Multiplicity	13.4 (13.3)	13.4 (13.5)	12.0 (11.8)	13.4 (14.0)
Completeness (%)	99.5 (99.2)	99.3 (99.7)	99.9 (100.0)	99.9 (100.0)
Mean $I/\sigma(I)$	15.0 (1.5)	12.6 (1.3)	11.8 (1.6)	16.1 (1.4)
Wilson B-factor (Å^2)	96.1	104.6	102.7	104.4
R_{sym}	0.11 (1.82)	0.15 (2.29)	0.12 (1.73)	0.08 (2.10)
$CC_{1/2}$ (%)	99.9 (56.9)	99.9 (50.0)	99.9 (60.7)	99.9 (57.1)
Refinement statistics				
Resolution range (Å)	50.45 – 2.95 (3.06 – 2.95)	65.52 – 3.02 (3.13 – 3.02)	33.24 – 3.00 (3.11 – 3.00)	32.86 – 2.80 (2.90 – 2.80)
Reflections used in refinement	10769 (1036)	9841 (970)	10433 (1014)	12618 (1248)
Reflections used for R_{free}	539 (52)	489 (48)	521 (51)	631 (62)
R_{work}	0.265 (0.417)	0.260 (0.387)	0.250 (0.401)	0.252 (0.468)
R_{free}	0.284 (0.511)	0.274 (0.381)	0.277 (0.452)	0.270 (0.452)
No. of non-hydrogen atoms				
Protein	3471	3471	3419	3398
Ligand	26	28	26	34
Heme	43	43	43	43
Water	0	0	0	2
Protein residues	462	462	461	460
RMS (bonds)	0.002	0.002	0.002	0.003
RMS (angles)	0.55	0.52	0.53	0.59
Ramachandran favored (%)	96.49	96.49	97.36	96.04
Ramachandran allowed (%)	3.51	3.51	2.64	3.96
Ramachandran outliers (%)	0	0	0	0
Rotamer outliers (%)	0	0	0	0.3
Clashscore	5.56	5.42	4.35	4.39
Average B-factor (Å^2)	89.86	101.04	95.49	101.16
Protein	90.19	101.52	95.89	101.56
Ligand	79.18	85.47	81.87	89.67
Heme	69.64	72.56	71.42	78.50
Water	-	-	-	96.69
PDB ID	9BV9	9BVA	9BVB	9BVC

Values in parentheses for the highest resolution shell

Supplementary Table 8. Data collection and refinement statistics for CYP3A4 and CYP3A5 in complex with SCM-27

	CYP3A4–SCM-27	CYP3A5–SCM-27
Data collection		
Wavelength	0.9201	0.9793
Beamline	BNL/AMX-17-ID-1	BNL/FMX-17-ID-2
Resolution range (Å)	30.27 – 3.40 (3.67 – 3.40)[a]	34.47 – 2.25 (2.32 – 2.25)[a]
Space group	*I* 2 2 2	*C* 2 2 2_1
Unit cell: *a*, *b*, *c* (Å)	75.77 100.65 121.13	65.09 210.69 153.99
α, β, γ (˚)	90 90 90	90 90 90
Mosaicity (˚)	0.11	0.15
Total reflections	37592	306203
Unique reflections	6641 (1348)	50634 (4596)
Multiplicity	5.7 (5.6)	6.0 (5.9)
Completeness (%)	99.8 (99.9)	99.9 (100.0)
Mean $I/\sigma(I)$	6.4 (1.5)	10.1 (1.8)
Wilson B-factor (Å^2)	103.1	33.2
R_{merge}[b]	0.16 (1.56)	0.14 (0.10)
$CC_{1/2}$ (%)	99.7 (65.5)	99.6 (50.7)
Refinement statistics		
Resolution range (Å)	30.27 – 3.40 (3.52 – 3.40)	31.95 – 2.25 (2.33 – 2.25)
Reflections used in refinement	6640 (651)	50601 (4982)
Reflections used for R_{free}	334 (40)	2623 (263)
R_{work}	0.284 (0.373)	0.198 (0.285)
R_{free}	0.297 (0.481)	0.239 (0.337)
No. of non-hydrogen atoms		
Protein	3086	7175
Ligand	34	34
Heme	43	43
Water	0	327
Protein residues	453	922
RMS (bonds)	0.004	0.004
RMS (angles)	0.69	0.71
Ramachandran favored (%)	93.45	96.26
Ramachandran allowed (%)	6.55	3.74
Ramachandran outliers (%)	0	0
Rotamer outliers (%)	0.4	0.3
Clashscore	5.21	3.76
Average B-factor (Å^2)	101.92	39.75
Protein	102.32	39.77
Ligand	99.59	42.48
Heme	74.40	26.47
Water	-	41.04
PDB ID	9MS1	9MS2

Values in parentheses for the highest resolution shell

Supplementary Table 9. Inhibitory potencies of test compounds against major human CYPs

Compound	IC_{50} (μM)									3A5/3A4 IC_{50} ratio	Alternative name
	CYP1A2	CYP2B6	CYP2C8	CYP2C9	CYP2C19	CYP2D6	CYP3A7	CYP3A4	CYP3A5		
SCM-01	>60[a]	>60[a]	>60[a]	>60[a]	>60[a]	>60[a]	>60[a]	0.32 ± 0.03	4.33 ± 0.09	14	SJ000362065 Enamine Z56792718
SCM-04	8 ± 1	-	-	-	>60[a]	-	-	0.33 ± 0.02	2.9 ± 0.2	8.8	Enamine Z56794030
SCM-05	2.7 ± 0.2	-	-	-	>60[a]	-	-	0.43 ± 0.04	3.22 ± 0.02	7.5	Enamine Z56795105
SCM-06	10.1 ± 0.9	-	-	-	15 ± 3	-	40 ± 10	0.34 ± 0.03	7 ± 1	21	SJYHJ-120
SCM-07	1.61 ± 0.01	-	-	-	50 ± 40	-	>60[a]	0.240 ± 0.009	8.9 ± 0.4	37	SJYHJ-113
SCM-08	11 ± 1	>60[a]	>60[a]	>60[a]	>60[b]	>60[a]	>60[a]	0.43 ± 0.02	20 ± 3	47	SJYHJ-114
SCM-09	3.12 ± 0.07	-	-	-	4.08 ± 0.01	-	>60[a]	0.31 ± 0.04	19 ± 2	61	SJYHJ-116
SCM-10	2.1 ± 0.1	-	-	-	3 ± 1	-	>60[a]	0.7 ± 0.2	>60	>86	SJYHJ-115
SCM-11	5.9 ± 0.7	-	-	-	3.1 ± 0.4	-	-	0.33 ± 0.01	10 ± 2	30	SJYHJ-079
SCM-12	>60	-	-	-	6.90 ± 0.04	-	>60[a]	0.87 ± 0.07	>60	>69	SJYHJ-119
SCM-13	1.59 ± 0.04	-	-	-	2.1 ± 0.2	-	-	2.3 ± 0.1	26 ± 8	11	Enamine Z56787794
SCM-14	6.0 ± 0.2	-	-	-	5.9 ± 0.8	-	-	2.7 ± 0.1	>60	>22	Enamine Z56912610
SCM-15	>60[a]	-	-	-	1.9 ± 0.2	-	-	0.9 ± 0.2	>60	>67	Enamine Z56795104
SCM-16	0.19 ± 0.02	-	-	-	1.28 ± 0.05	-	>60[a]	0.68 ± 0.07	4.4 ± 0.3	6.5	SJYHJ-117
SCM-17	2.5 ± 0.2	-	-	-	30 ± 20	-	>60[a]	1.02 ± 0.03	8.2 ± 0.6	8.0	SJYHJ-118
SCM-18	0.8 ± 0.4	8 ± 1	>60[a]	>60[a]	1.0 ± 0.3	>60[a]	>60[a]	0.36 ± 0.01	>60	>170	Enamine Z56791366
SCM-25	22 ± 2	2.5 ± 0.4	>60[a]	>60[a]	>60[a]	>60[a]	9 ± 7	0.027 ± 0.004	1.5 ± 0.1	56	SJYHJ-075
Ritonavir	>60[a]	11 ± 1	12 ± 1	1.2 ± 0.1	1.58 ± 0.09	14 ± 2	0.109 ± 0.001	0.045 ± 0.001	0.03 ± 0.01	0.67	-

The inhibitory potency data for CYP3A4, 3A5, and 3A7 were determined using P450-Glo luminescence-based inhibition assays, whereas the inhibitory potency data for CYP1A2, 2B6, 2C8, 2C9, 2C19, 2D6 were determined using Vivid P450 fluorescence-based inhibition assays. The IC_{50} values were generated by fitting dose–response data to Equation 1, and the reported numerical values are the means and standard deviations of triplicate experiments (n = 3). Source data are provided as a Source Data file.

[a]For weak inhibitors for which IC_{50} values could not be determined, the IC_{50} values are reported as greater than the highest compound concentrations tested.

[b]Due to the incomplete dose–response curve the reported IC_{50} value of SCM-08 is an estimation. If data were fitted using equation 1 with top constraint of 100%, the fitted IC_{50} value is 28 ± 3 μM.

Supplementary Table 10. Metabolic stability of SCM-08 and ritonavir in human liver microsomes

Compound	Concentration (μM)	$T_{1/2}$ (hour)	Cl_{int} (mL/Min/Kg)
Verapamil	1	0.231±0.007	90
	5	0.938±0.001	2.5
SCM-08	1	0.99 ± 0.05	21
	5	>2[a]	N/A[b]
Ritonavir	1	0.8±0.1	26
	5	>2[a]	N/A[b]

All data were obtained using the metabolic stability assay. The half-life ($T_{1/2}$) values were calculated by the linear fit of Ln percentage remaining *vs* incubation time,[3] and intrinsic clearance (Cl_{int}) was calculated according to the equation published previously.[4] The reported numerical values are means and standard deviations of triplicate experiments (n = 3). Source data are provided as a Source Data file.

[a]For any compounds with fitted $T_{1/2}$ > 2 hours or have >50% remain at 2 hours, the $T_{1/2}$ is reported as > 2 hours, and Cl_{int} is not calculated

[b]N/A: not applicable

Supplementary Table 11. Selective CYP3A4 and CYP3A5 substrates

No.	Compound name	CYP3A4		CYP3A5		Comment[b]
		$T_{1/2}$ (min)[a]	%Remain	$T_{1/2}$ (min)[a]	%Remain[a]	
1	CH5424802	29 ± 2	7 ± 1	>120	63 ± 4	CYP3A4 selective
2	Loteprednol etabonate	25 ± 1	3.6 ± 0.4	>120	89 ± 7	
3	Regorafenib	21 ± 2	1.6 ± 0.4	109 ± 20	39 ± 6	
4	Pranlukast	23 ± 10	3 ± 5	>120	68 ± 2	
5	Sorafenib Tosylate	21 ± 1	1.6 ± 0.3	>120	53 ± 5	
6	Regorafenib monohydrate	20 ± 4	1 ± 1	>120	71 ± 8	
7	LY2835219 free base	12 ± 1	0.16 ± 0.03	74 ± 13	36 ± 6	
8	Medroxyprogesterone	18 ± 2	0.6 ± 0.2	>120	59 ± 2	
9	Mometasone furoate	17.9 ± 0.4	1.3 ± 0.2	>120	71 ± 4	
10	Sorafenib	15.9 ± 0.4	0.56 ± 0.05	>120	74 ± 8	
11	Megestrol Acetate	13 ± 1	0.3 ± 0.1	103 ± 34	47 ± 8	
12	Bosutinib (SKI-606)	14 ± 1	0.4 ± 0.1	>120	61 ± 6	
13	Medroxyprogesterone acetate	12 ± 1	0.1 ± 0.04	>120	78 ± 2	
14	Darunavir	73 ± 2	33 ± 2	16.5 ± 0.5	0.62 ± 0.02	CYP3A5 selective
15	Darunavir Ethanolate	>120	53 ± 4	27 ± 1	4.9 ± 0.2	
16	Glimepiride	>120	51 ± 4	19 ± 1	0.7 ± 0.1	
17	Indinavir sulfate	110 ± 20	50 ± 3	21 ± 1	2.9 ± 0.4	
18	Lapatinib	>120	51 ± 3	21 ± 1	1.4 ± 0.3	
19	Lapatinib Ditosylate	67 ± 8	24 ± 2	13 ± 1	0.2 ± 0.1	
20	Metronidazole Benzoate	>120	90 ± 20	24 ± 3	3 ± 1	
21	Raloxifene HCl	>120	71 ± 6	13 ± 2	0.1 ± 0.1	
22	Roflumilast	>120	49 ± 2	20 ± 20	1 ± 5	
23	Saikosaponin A	>120	100 ± 10	25 ± 1	4 ± 1	
24	Tamibarotene	>120	53 ± 4	22 ± 1	3 ± 1	

All data were determined using LC-MS-based metabolic assay. The half-life ($T_{1/2}$) was calculated from the linear fit of Ln percentage remaining *vs* incubation time.[3] The %Remain is the percentage parent compound remaining calculated from the fit at 120 minutes. The reported numerical values are means and standard deviations of triplicate experiments (n = 3). Source data are provided as a Source Data file.

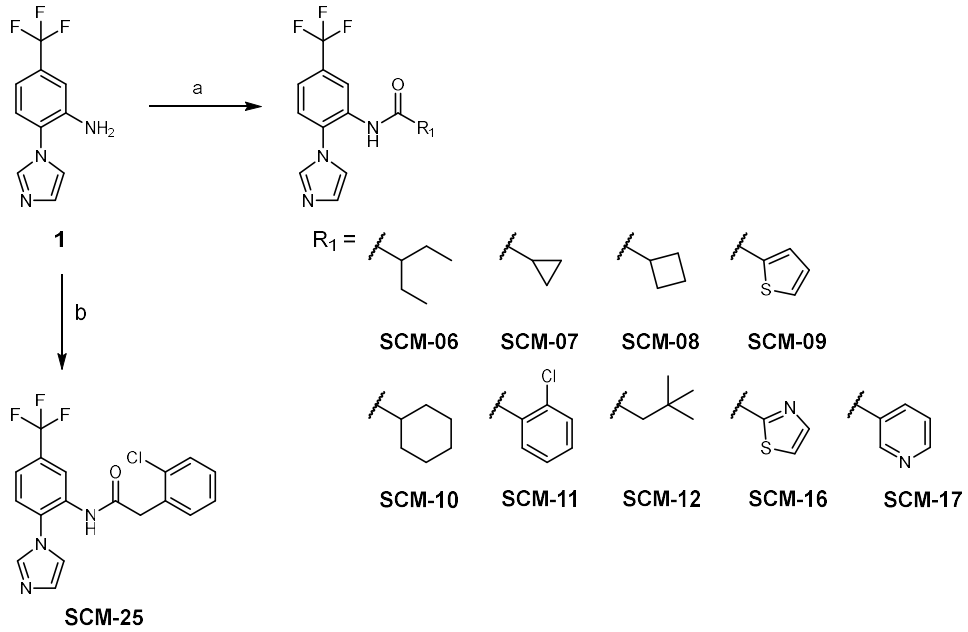
[a]For compounds with fitted $T_{1/2}$ > 120 minutes or have >50% remain, the $T_{1/2}$ is reported as > 120 minutes

[b]Selective substrates are defined as compounds with at least 4-fold difference in $T_{1/2}$ values

Supplementary Methods

Chemical synthesis

All reagents and solvents were purchased from Sigma-Aldrich (St. Louis, MO) or Enamine, Ltd. (Monmouth Junction, NJ) unless otherwise noted and were used without further purification. All NMR spectra were recorded on a Bruker 400-MHz or 500-MHz spectrometer in the solvents indicated, and spectra were processed using MestReNova (14.1.1). Flash column chromatography was performed using Biotage Isolera Flash systems with Biotage Sfär Silica or Biotage Sfär C18 columns. All compounds used for biological assays had >95% purity as determined with a Waters Acquity UPLC MS system with a C18 column and a 2-minute gradient (H_2O + 0.1% formic acid (FA) → acetonitrile (ACN) + 0.1% formic acid), an evaporative light scattering detector (ELSD), and an Acquity SQD ESI-positive mass spectrometer (Waters Corporation, Milford, MA). High-resolution mass spectra were determined by using a Waters Acquity UPLC system with a C18 column (H_2O + 0.1% FA → ACN + 0.1% FA gradient over 2.5 minutes) and a Xevo G2Q-TOF ESI-positive mass spectrometer in resolution mode. Compounds were internally normalized to leucine−enkephalin lock-mass solution, with a calculated error of <3 ppm.



Supplementary Fig. 21 | Synthesis of SCM-06 to SCM-12, SCM-16, SCM-17, and SCM-25. Reagents and conditions: (a) acid chloride, DMF, 0°C to room temperature, 16 hours, N_2 atmosphere, 32%–53%; (b) 2-chlorophenylacetic acid, HATU, DIPEA, DMF, room temperature, 16 hours, 78%.

General procedure A: To a solution of 2-(1*H*-imidazol-1-yl)-5-(trifluoromethyl)aniline (**1**, 1.0 eq) in anhydrous DMF was added an acid chloride (3.0 eq) by dropwise addition at 0 °C under a N_2 atmosphere, and then this reaction mixture was stirred at room temperature for 16 hours. The reaction mixture was partitioned with ethyl acetate and water, and the aqueous layer was extracted with ethyl acetate. The combined organic layer was washed with brine, dried with Na_2SO_4, filtered, and evaporated under reduced pressure. The reaction mixture was concentrated under reduced pressure. The residue was purified by

reversed-phase flash chromatography (running a gradient of 0%-100% acetonitrile in water over 16 minutes) to yield the product.

N-(2-(1*H*-imidazol-1-yl)-5-(trifluoromethyl)phenyl)-2-ethylbutanamide (**SCM-06**). Compound **SCM-06** (91.0 mg, 49%) was synthesized in accordance with general procedure A: ^{1}H NMR (500 MHz, DMSO-d_6) δ 7.96 (s, 1H), 7.90 (s, 1H), 7.71 (d, J = 8.40 Hz, 1H), 7.63 (d, J = 8.40 Hz, 1H), 7.40 (s, 1H), 7.12 (s, 1H), 2.21–2.16 (m, 1H), 1.54–1.45 (m, 2H), 1.43–1.34 (m, 2H), 0.79 (t, J = 7.45 Hz, 6H); ^{13}C NMR (126 MHz, DMSO) δ 175.28, 135.40, 133.40, 129.56, 129.15, 128.90, 128.64, 128.23, 125.16, 124.47, 123.58, 123.00, 120.72, 49.45, 25.36, 12.22; ESI-TOF HRMS: m/z 326.1488 ($C_{16}H_{19}F_3N_3O$ + H^+ requires 326.1480).

N-(2-(1*H*-imidazol-1-yl)-5-(trifluoromethyl)phenyl)cyclopropanecarboxamide (**SCM-07**). Compound **SCM-07** (56.0 mg, 43%) was synthesized in accordance with general procedure A: ^{1}H NMR (500 MHz, $CDCl_3$) δ 8.65 (s, 1H), 7.48 (s, 1H), 7.44–7.42 (m, 1H), 7.31 (d, J = 8.20 Hz, 1H), 7.15 (s, 1H), 7.11 (s, 1H), 1.71–1.66 (m, 1H), 1.10–1.07 (m, 2H), 0.87–0.83 (m, 2H); ^{13}C NMR (126 MHz, $CDCl_3$) δ 173.28, 134.62, 132.50, 132.23, 131.97, 131.71, 130.73, 127.46, 124.56, 122.39, 121.28, 120.11, 15.31, 8.72; ESI-TOF HRMS: m/z 296.1024 ($C_{14}H_{13}F_3N_3O$ + H^+ requires 296.1010).

N-(2-(1*H*-imidazol-1-yl)-5-(trifluoromethyl)phenyl)cyclobutanecarboxamide (**SCM-08**). Compound **SCM-08** (58.0 mg, 40%) was synthesized in accordance with general procedure A: ^{1}H NMR (500 MHz, $CDCl_3$) δ 7.67 (s, 1H), 7.48–7.46 (m, 1H), 7.37 (d, J = 8.20 Hz, 1H), 7.32 (s, 1H), 7.17 (s, 1H), 7.12 (s, 1H), 3.10–3.03 (m, 1H), 2.31–2.23 (m, 2H), 2.18–2.12 (m, 2H), 2.01–1.84 (m, 2H); ^{13}C NMR (126 MHz, $CDCl_3$) δ 173.79, 134.35, 132.81, 132.55, 132.28, 132.02, 131.03, 129.68, 124.54, 122.37, 121.43, 120.08, 40.73, 25.26, 18.14; ESI-TOF HRMS: m/z 310.1173 ($C_{15}H_{15}F_3N_3O$ + H^+ requires 310.1167).

N-(2-(1*H*-imidazol-1-yl)-5-(trifluoromethyl)phenyl)thiophene-2-carboxamide (**SCM-09**). Compound **SCM-09** (70.0 mg, 47%) was synthesized in accordance with general procedure A: ^{1}H NMR (500 MHz, $CDCl_3$) δ 7.71 (s, 1H), 7.60 (s, 1H), 7.57 (d, J = 4.95 Hz, 1H), 7.51 (d, J = 8.15 Hz, 1H), 7.46 (d, J = 8.25 Hz, 1H), 7.40 (s, 1H), 7.28 (d, J = 3.50 Hz, 1H), 7.20 (s, 1H), 7.08 (t, J = 4.05 Hz, 1H); ^{13}C NMR (126 MHz, $CDCl_3$) δ 159.88, 137.95, 134.19, 132.72, 132.39, 131.70, 129.16, 128.36, 127.41, 126.82, 124.52, 122.35, 121.59, 120.03, 119.44; ESI-TOF HRMS: m/z 338.0590 ($C_{15}H_{11}F_3N_3OS$ + H^+ requires 338.0575).

N-(2-(1*H*-imidazol-1-yl)-5-(trifluoromethyl)phenyl)cyclohexanecarboxamide (**SCM-10**). Compound **SCM-10** (60.0 mg, 35%) was synthesized in accordance with general procedure A: ^{1}H NMR (500 MHz, $CDCl_3$) δ 7.65 (s, 1H), 7.47–7.45 (m, 1H), 7.38–7.30 (m, 3H), 7.14 (s, 1H), 2.19–2.13 (m, 1H), 1.85–1.76 (m, 4H), 1.68–1.65 (m, 1H), 1.44–1.36 (m, 2H), 1.29–1.17 (m, 3H); ^{13}C NMR (126 MHz, $CDCl_3$) δ 174.81, 134.42, 132.76, 132.49, 132.23, 131.97, 131.34, 129.79, 127.41, 124.54, 122.37, 121.39, 120.16, 46.19, 29.47, 25.62, 25.56; ESI-TOF HRMS: m/z 338.1487 ($C_{17}H_{19}F_3N_3O$ + H^+ requires 338.1480).

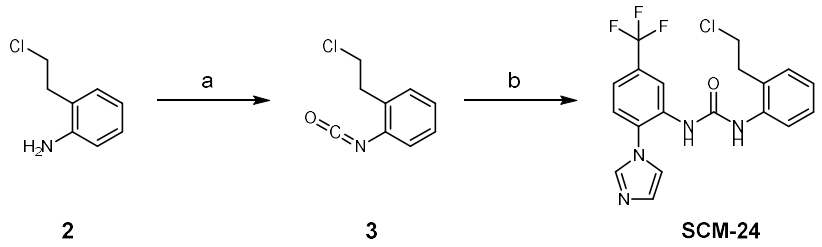
N-(2-(1*H*-imidazol-1-yl)-5-(trifluoromethyl)phenyl)-2-chlorobenzamide (**SCM-11**). Compound **SCM-11** (25.0 mg, 52%) was synthesized in accordance with general procedure A: ^{1}H NMR (500 MHz, MeOD) δ 8.10 (s, 1H), 7.97 (s, 1H), 7.78 (d, J = 8.40 Hz, 1H), 7.69 (d, J = 8.25 Hz, 1H), 7.50–7.37 (m, 5H), 7.19 (s, 1H); ^{13}C NMR (126 MHz, MeOD) δ 167.38, 135.62, 135.17, 132.64, 131.37, 131.05, 130.78, 130.62, 129.77, 128.69, 127.77, 126.81, 124.48, 124.45, 124.23, 124.20; ESI-TOF HRMS: m/z 366.0633 ($C_{17}H_{12}ClF_3N_3O$ + H^+ requires 366.0621).

N-(2-(1*H*-imidazol-1-yl)-5-(trifluoromethyl)phenyl)-3,3-dimethylbutanamide (**SCM-12**). Compound **SCM-12** (87.0 mg, 53%) was synthesized in accordance with general procedure A: ^{1}H NMR (500 MHz, DMSO-d_6) δ 8.01 (s, 1H), 7.89 (s, 1H), 7.69 (dd, J = 2.30 and 8.25 Hz, 1H), 7.61 (d, J = 8.25 Hz, 1H), 7.40 (s, 1H), 7.11 (s, 1H), 2.15 (s, 2H), 0.95 (s, 9H); ^{13}C NMR (126 MHz, DMSO) δ 170.79, 137.96, 134.55, 133.02, 129.21, 128.63, 128.37, 127.74, 124.73, 123.69, 122.85, 122.56, 120.23, 48.52, 30.78, 29.56; ESI-TOF HRMS: m/z 326.1491 ($C_{16}H_{19}F_3N_3O$ + H^+ requires 326.1480).

N-(2-(1*H*-imidazol-1-yl)-5-(trifluoromethyl)phenyl)thiazole-2-carboxamide (**SCM-16**). Compound **SCM-16** (77.0 mg, 48%) was synthesized in accordance with general procedure A: ^{1}H NMR (500 MHz, $CDCl_3$) δ 7.77 (d, J = 2.10 Hz, 1H), 7.68 (s, 1H), 7.57 (d, J = 2.05 Hz, 1H), 7.45 (d, J = 8.10 Hz, 1H), 7.39–7.34 (m, 3H), 7.18–7.16 (m, 1H); ^{13}C NMR (126 MHz, $CDCl_3$) δ 162.18, 157.68, 144.19, 133.37, 132.73, 132.47, 132.20, 131.94, 130.00, 127.62, 126.19, 124.52, 121.91, 119.07; ESI-TOF HRMS: m/z 339.0540 ($C_{14}H_{10}F_3N_4OS$ + H^+ requires 339.0527).

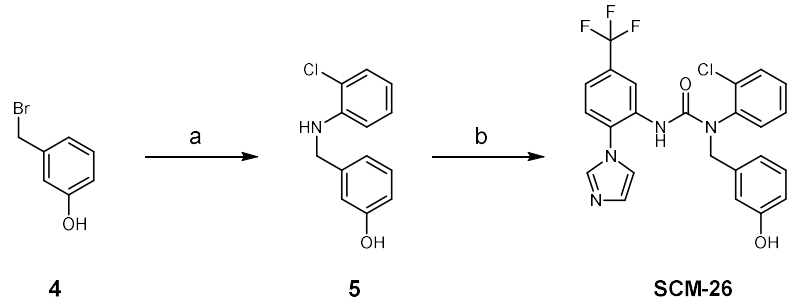
N-(2-(1*H*-imidazol-1-yl)-5-(trifluoromethyl)phenyl)nicotinamide (**SCM-17**). Compound **SCM-17** (56.0 mg, 32%) was synthesized in accordance with general procedure A: ^{1}H NMR (500 MHz, $CDCl_3$) δ 8.75 (s, 1H), 8.71 (s, 1H), 8.56 (s, 1H), 8.07 (d, J = 8.00 Hz, 1H), 7.81 (s, 1H), 7.60 (dd, J = 2.00 and 8.30 Hz, 1H), 7.48 (d, J = 8.20 Hz, 1H), 7.43–7.40 (m, 1H), 7.30 (s, 1H), 7.21 (s, 1H); ^{13}C NMR (126 MHz, $CDCl_3$) δ 164.12, 152.97, 148.08, 135.49, 133.61, 132.90, 132.64, 132.37, 132.11, 130.98, 129.30, 127.38, 124.29, 123.86, 122.73, 121.56; ESI-TOF HRMS: m/z 333.0974 ($C_{16}H_{12}F_3N_4O$ + H^+ requires 333.0963).

N-(2-(1*H*-imidazol-1-yl)-5-(trifluoromethyl)phenyl)-2-(2-chlorophenyl)acetamide (**SCM-25**). To a solution of 2-chlorophenylacetic acid (30.0 mg, 0.176 mmol) in DMF (2.0 mL) were added 2-(1*H*-imidazol-1-yl)-5-(trifluoromethyl)aniline (**1**, 60.0 mg, 0.264 mmol), HATU (100.0 mg, 0.264 mmol), and *N*,*N*-diisopropylethylamine (46.0 µL, 0.264 mmol). This reaction mixture was then stirred at room temperature for 16 hours. The reaction mixture was partitioned with ethyl acetate (10 mL) and water (10 mL), and the aqueous layer was extracted with ethyl acetate (5 mL × 2). The combined organic layer was washed with brine (3 mL), dried with Na_2SO_4, filtered, and evaporated to dryness under reduced pressure. The residue was purified by flash chromatography (running a gradient of 0%–100% ethyl acetate in hexane over 16 minutes) to yield compound **SCM-25** (52.0 mg, 78%) as a white solid; ^{1}H NMR (500 MHz, MeOD) δ 8.08 (s, 1H), 7.86 (s, 1H), 7.69 (d, J = 8.10 Hz, 1H), 7.61 (d, J = 8.30 Hz, 1H), 7.41 – 7.39 (m, 1H), 7.32–7.27 (m, 4H), 7.13 (s, 1H), 3.82 (s, 2H); ^{13}C NMR (126 MHz, DMSO) δ 169.48, 137.82, 134.10, 133.90, 133.08, 132.73, 129.85, 129.47, 129.18, 129.02, 128.76, 127.99, 127.54, 125.17, 123.01, 120.56, 38.72; ESI-TOF HRMS: m/z 380.0783 ($C_{18}H_{14}ClF_3N_3O$ + H^+ requires 380.0777).



Supplementary Fig. 22 | Synthesis of SCM-24. Reagents and conditions: (a) triphosgene, TEA, DCM, 0°C to room temperature, 0.5 hour, N_2 atmosphere; (b) **1**, DCM, room temperature, 16 hours, N_2 atmosphere, 43%.

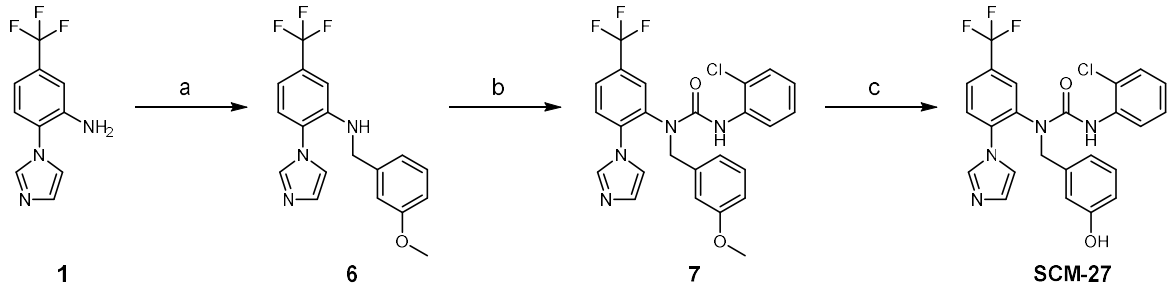
1-(2-(1*H*-imidazol-1-yl)-5-(trifluoromethyl)phenyl)-3-(2-(2-chloroethyl)phenyl)urea (**SCM-24**). To a solution of triphosgene (38.0 mg, 0.129 mmol) in DCM (3.0 mL) was added **2** (20.0 mg, 0.129 mmol) in DCM (3.0 mL) by dropwise addition at 0°C under an N_2 atmosphere, then triethylamine (53.7 µL, 0.386 mmol) in DCM (3.0 mL) was added dropwise to the reaction mixture. After the mixture had been stirred at room temperature for 0.5 hour, the solvent was removed on a rotary evaporator. The residue was dissolved in DCM (5.0 mL), and 2-(1*H*-imidazol-1-yl)-5-(trifluoromethyl)aniline (**1**, 23.4 mg, 0.129 mmol) in THF (3.0 mL) was added. The reaction mixture was stirred for 16 hours at room temperature under an N_2 atmosphere and then concentrated under reduced pressure. The residue was purified by reversed-phase flash chromatography (running a gradient of 0%–100% acetonitrile in water over 16 minutes) to yield compound **SCM-24** (23.0 mg, 43%) as a white solid; ^{1}H NMR (400 MHz, MeOD) δ 8.42 (s, 1H), 7.98 (broad s, 1H), 7.55 (s, 2H), 7.45 (dd, J = 1.40 and 7.96 Hz, 2H), 7.32–7.24 (m, 3H), 7.21–7.17 (m, 1H), 3.73 (t, J = 7.40 Hz, 2H), 3.05 (t, J = 7.40 Hz, 2H); ^{13}C NMR (126 MHz, MeOD) δ 155.49, 137.25, 136.54, 136.20, 133.41, 132.82, 132.56, 131.21, 128.99, 128.53, 126.95, 126.90, 126.87, 126.51, 125.79, 123.63, 121.76, 44.50, 35.50; ESI-TOF HRMS: m/z 409.1058 ($C_{19}H_{17}ClF_3N_4O + H^+$ requires 409.1043).



Supplementary Fig. 23 | Synthesis of SCM-26. Reagents and conditions: (a) 2-chloroaniline, DIPEA, DMF, 50°C, 16 hours, N_2 atmosphere, 47%; (b) (i) triphosgene, **1**, TEA, ACN, 0°C to room temperature, 0.5 hour, N_2 atmosphere, (ii) **5**, ACN, room temperature, 16 hours, N_2 atmosphere, 22%.

3-(((2-chlorophenyl)amino)methyl)phenol (**5**). To a solution of 2-chloroaniline (243.0 mg, 1.902 mmol) in DMF (5.0 mL) were added 3-(bromomethyl)phenol (**4**, 356.0 mg, 1.902 mmol) and *N*,*N*-diisopropylethylamine (497.0 µL, 2.850 mmol) under an N_2 atmosphere. This reaction mixture was stirred at 50°C for 16 hours and then concentrated under reduced pressure. The residue was purified by reversed-phase flash chromatography (running a gradient of 0%–100% acetonitrile in water over 16 minutes) to yield compound **5** (210.0 mg, 47%) as a white solid; ^{1}H NMR (500 MHz, DMSO-d_6) δ 7.23 (dd, J = 1.50 and 7.85 Hz, 1H), 7.09 (t, J = 7.75 Hz, 1H), 7.03–6.99 (m, 1H), 6.75–6.72 (m, 2H), 6.59 (dd, J = 1.60 and 8.20 Hz, 1H), 6.54–6.49 (m, 2H), 4.31 (d, 2H); ^{13}C NMR (126 MHz, DMSO) δ 157.95, 144.41, 141.76, 129.79, 129.37, 128.28, 118.19, 117.80, 116.83, 114.10, 113.84, 112.09, 46.40; LCMS: m/z = 232.16 $[M–H]^-$.

3-(2-(1*H*-imidazol-1-yl)-5-(trifluoromethyl)phenyl)-1-(2-chlorophenyl)-1-(3-hydroxybenzyl)urea (**SCM-26**). To a solution of triphosgene (54.4 mg, 0.183 mmol) in ACN (3.0 mL) was added 2-(1*H*-imidazol-1-yl)-5-(trifluoromethyl)aniline (**1**) (50.0 mg, 0.220 mmol) in ACN (1.0 mL) by dropwise addition at 0°C under an N_2 atmosphere, then triethylamine (102.0 µL, 0.734 mmol) in ACN (1.0 mL) was added dropwise to the reaction mixture. After the mixture had been stirred at room temperature for 0.5 hour, 3-(((2-chlorophenyl)amino)methyl)phenol (**5**) (42.9 mg, 0.183 mmol) in ACN (1.0 mL) was added. The reaction mixture was stirred for 16 hours at room temperature under an N_2 atmosphere and then concentrated under reduced pressure. The residue was purified by reversed-phase flash chromatography (running a gradient of 0%–65% acetonitrile in water over 16 minutes) to yield compound **SCM-26** (20.0 mg, 22%). ^{1}H NMR (500 MHz, DMSO-d_6) δ 9.33 (s, 1H), 8.19 (s, 1H), 7.82 (s, 1H), 7.62 (dd, J = 8.3, 2.1 Hz, 1H), 7.58 (d, J = 8.2 Hz, 1H), 7.55 (dd, J = 8.1, 1.4 Hz, 1H), 7.37 (td, J = 7.7, 1.6 Hz, 1H), 7.27 (td, J = 7.7, 1.4 Hz, 1H), 7.26 – 7.22 (m, 2H), 7.05 (t, J = 7.7 Hz, 1H), 7.02 (dd, J = 7.8, 1.6 Hz, 1H), 7.01 – 6.96 (m, 1H), 6.64 – 6.58 (m, 2H), 6.55 (d, J = 7.5 Hz, 1H), 5.13 (br s, 1H), 4.12 (br s, 1H). ^{19}F NMR (471 MHz, DMSO-d_6) δ -61.24. ^{13}C NMR (126 MHz, DMSO-d_6) δ 157.21, 153.64, 138.57, 137.34, 136.81, 134.71, 133.47, 132.56, 131.42, 130.77, 130.16, 129.22, 128.91 (q, J = 32.2 Hz), 128.50, 127.66, 123.70 (q, J = 272.5 Hz), 121.57, 121.33, 119.69, 118.86, 115.08, 114.28, 51.40. ESI-TOF HRMS: m/z 487.1159 ($C_{24}H_{19}ClF_3N_4O_2$ + H^+ requires 487.1148).



Supplementary Fig. 24 | Synthesis of SCM-27. Reagents and conditions: (a) (i) 3-methoxybenzaldehyde, AcOH, MeOH, rt, 18 hours, (ii) $NaBH_4$, rt, 10 minutes, 23%; (b) 2-chlorobenzoic acid, DPPA, Et_3N, toluene, 100°C, 30 minutes, 35%; (c) BBr_3, DCM, -78°C-rt, 7 hours, 78%.

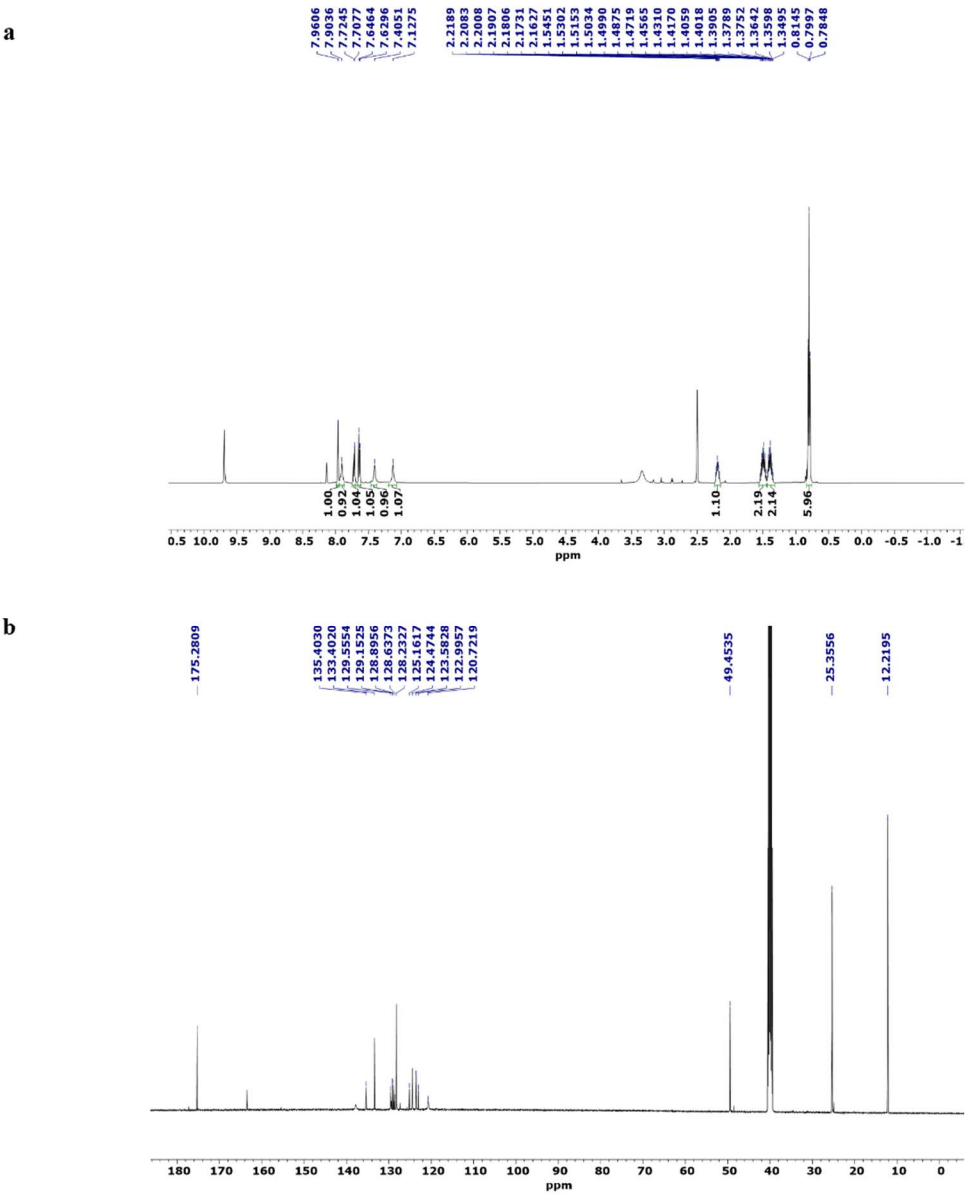
2-(1*H*-imidazol-1-yl)-*N*-(3-methoxybenzyl)-5-(trifluoromethyl)aniline (**6**). To a solution of 2-(1*H*-imidazol-1-yl)-5-(trifluoromethyl)aniline (**1**) (300 mg, 1.32 mmol, 1.0 eq) and 3-methoxybenzaldehyde (180 mg, 1.32 mmol, 1.0 eq) in anhydrous MeOH (4.4 mL) was added two drops of AcOH. The reaction mixture was stirred at rt for 18 hours, then $NaBH_4$ (150 mg, 3.96 mmol, 3.0 eq) was carefully added to the reaction mixture, and the reaction mixture was stirred for 10 minutes, then concentrated in vacuo and partitioned between EtOAc (10 mL) and water (10 mL). The aqueous layer was extracted with EtOAc (10 mL × 3), washed with brine, dried over $MgSO_4$, filtered, concentrated in vacuo, and then purified by reverse-phase flash chromatography (10–80% MeCN in H_2O) to yield compound **6** (105 mg, 23% yield) as an off-white solid. ^{1}H NMR (500 MHz, DMSO-d_6) δ 7.88 (d, J = 1.2 Hz, 1H), 7.42 (t, J = 1.3 Hz, 1H), 7.27 (d, J = 8.0 Hz, 1H), 7.23 (t, J = 8.0 Hz, 1H), 7.18 (s, 1H), 6.95 (dd, J = 8.1, 1.9 Hz, 1H), 6.93 – 6.90 (m, 2H), 6.85 (d, J = 2.0 Hz, 1H), 6.79 (dd, J = 8.0, 2.5 Hz, 1H), 6.03 (t, J = 6.0 Hz, 1H), 4.32 (d, J = 6.0 Hz, 2H), 3.72 (s, 3H). ^{19}F NMR (471 MHz, DMSO-d_6) δ -61.49. ^{13}C NMR (126 MHz, DMSO-d_6) δ 159.40, 143.75, 140.73, 137.64, 129.85 (q, J = 31.4 Hz), 129.48, 128.13, 126.05, 124.02 (q, J = 272.5 Hz), 120.47, 119.09, 112.57, 112.25, 112.08 (q, J = 4.0 Hz), 108.00 (q, J = 3.8 Hz), 54.92, 45.84. LCMS: m/z = 348 $[M+H]^+$.

1-(2-(1*H*-imidazol-1-yl)-5-(trifluoromethyl)phenyl)-3-(2-chlorophenyl)-1-(3-methoxybenzyl)urea 2,2,2-trifluoroacetate (**7**). To a solution of 2-(1*H*-imidazol-1-yl)-*N*-(3-methoxybenzyl)-5-(trifluoromethyl)aniline (**6**) (49 mg, 0.14 mmol, 1.0 eq), 2-chlorobenzoic acid (67 mg, 0.43 mmol, 3.0 eq), triethylamine (79 µL, 57 mg, 0.57 mmol, 4.0 eq), in toluene (1 mL) was added DPPA (91 µL, 117 mg, 0.43 mmol, 3.0 eq). The reaction mixture was stirred at 100°C for 10 minutes, then cooled to rt. To improve conversion, an additional solution of 2-chlorobenzoic acid (67 mg, 0.43 mmol, 3.0 eq), triethylamine (79 µL, 57 mg, 0.57 mmol, 4.0 eq), and DPPA (91 µL, 117 mg, 0.43 mmol, 3.0 eq) in toluene (0.5 mL) was next added, and the reaction mixture was stirred at 100°C for 10 minutes, then cooled to rt. A solution of 2-chlorobenzoic acid (67 mg, 0.43 mmol, 3.0 eq), triethylamine (79 µL, 57 mg, 0.57 mmol, 4.0 eq), and DPPA (91 µL, 117 mg, 0.43 mmol, 3.0 eq) in toluene (0.5 mL) was again added, and the reaction mixture was stirred at 100°C for 10 minutes, then cooled to rt and diluted with EtOAc (10 mL) and water (10 mL). The aqueous layer was extracted with EtOAc (10 mL × 3). The combined organic layers were washed with brine, dried over $MgSO_4$, filtered, concentrated in vacuo, and purified by reverse-phase flash chromatography (30–100% MeCN in H_2O, then 10–60% MeCN in H_2O with 0.05% TFA) to yield **7** (31 mg, 35% yield) as a white solid. ^{1}H NMR (500 MHz, DMSO-d_6) δ 8.64 (s, 1H), 8.40 (s, 1H), 7.96 (dd, J = 8.3, 2.0 Hz, 1H), 7.88 (d, J = 8.3 Hz, 1H), 7.63 (d, J = 2.4 Hz, 2H), 7.58 (s, 1H), 7.47 (dd, J = 8.0, 1.5 Hz, 1H), 7.42 (dd, J = 8.1, 1.6 Hz, 1H), 7.32 (td, J = 7.7, 1.5 Hz, 1H), 7.24 – 7.17 (m, 2H), 6.82 (dd, J = 8.3, 2.4 Hz, 1H), 6.72 – 6.68 (m, 2H), 4.88 (br s, 2H), 3.68 (s, 3H). ^{19}F NMR (471 MHz, DMSO-d_6) δ -61.45, -

73.99. ^{13}C NMR (126 MHz, DMSO-d_6) δ 159.28, 157.86 (q, J = 33.6, 33.1 Hz), 154.42, 138.32, 137.45, 136.87, 136.61, 135.49, 130.23 (q, J = 31.4 Hz), 129.52, 129.35, 129.28, 128.59, 128.27, 128.19, 127.39, 126.93, 126.02 (q, J = 3.4 Hz), 124.80, 123.17 (q, J = 272.8 Hz), 121.40, 120.26, 116.64 (q, J = 297.5 Hz), 113.53, 113.17, 54.97, 51.64. LCMS: m/z = 501 $[M+H]^+$.

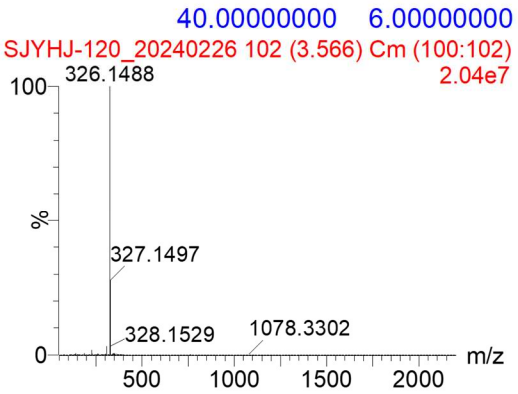
1-(2-(1*H*-imidazol-1-yl)-5-(trifluoromethyl)phenyl)-3-(2-chlorophenyl)-1-(3-hydroxybenzyl)urea (**SCM-27**). To a solution of 1-(2-(1*H*-imidazol-1-yl)-5-(trifluoromethyl)phenyl)-3-(2-chlorophenyl)-1-(3-methoxybenzyl)urea 2,2,2-trifluoroacetate (**7**) in DCM (0.45 mL) in a N_2 atmosphere cooled to -78°C was added BBr_3 (1 M in DCM, 41 µL, 41 mmol, 2.5 eq) dropwise. The reaction was slowly warmed to rt and then stirred at rt for 5 hours. The reaction mixture was cooled to 0°C, additional BBr_3 (1 M in DCM, 41 µL, 41 mmol, 2.5 eq) was added, then the reaction was warmed to rt and stirred at rt for 2 hours, then cooled to 0°C, and quenched with dropwise addition of water (120 µL) and saturated aqueous $NaHCO_3$ solution (240 µL). The solvent was removed in vacuo, and the crude product was purified by reverse-phase flash chromatography (10–60% MeCN in H_2O) to yield **SCM-27** (6.4 mg, 78% yield) as a white solid. ^{1}H NMR (500 MHz, DMSO-d_6) δ 9.35 (s, 1H), 8.24 (s, 1H), 7.93 (d, J = 1.1 Hz, 1H), 7.85 (dd, J = 8.5, 2.1 Hz, 1H), 7.78 (d, J = 8.3 Hz, 1H), 7.50 (d, J = 2.1 Hz, 1H), 7.46 (d, J = 1.5 Hz, 1H), 7.45 (t, J = 1.3 Hz, 2H), 7.31 (td, J = 7.6, 1.5 Hz, 1H), 7.23 – 7.15 (m, 2H), 7.07 – 7.00 (m, 1H), 6.64 – 6.58 (m, 2H), 6.50 (d, J = 7.5 Hz, 1H), 5.07 (br s, 1H), 3.51 (br s, 1H). ^{19}F NMR (471 MHz, DMSO-d_6) δ -61.29. ^{13}C NMR (126 MHz, DMSO-d_6) δ 157.41, 154.31, 138.41, 138.19, 137.15, 135.65, 135.44, 129.71, 129.31, 129.24, 128.90, 128.80 (q, J = 32.6 Hz), 128.59 (q, J = 3.7 Hz), 127.92, 127.82, 127.33, 126.57, 125.85 (q, J = 3.3 Hz), 123.32 (q, J = 272.5 Hz), 119.90, 118.66, 114.96, 114.41, 50.70. LCMS: m/z = 487 $[M+H]^+$. ESI-TOF HRMS: m/z 487.1133 ($C_{24}H_{19}ClF_3N_4O_2$ + H^+ requires 487.1143).

Evaluation of synthesized compound identity and purity

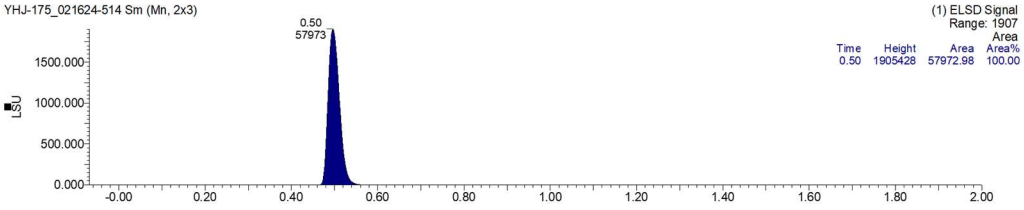


Supplementary Fig. 25 | (a) ^{1}H NMR and (b) ^{13}C NMR of **SCM-06**

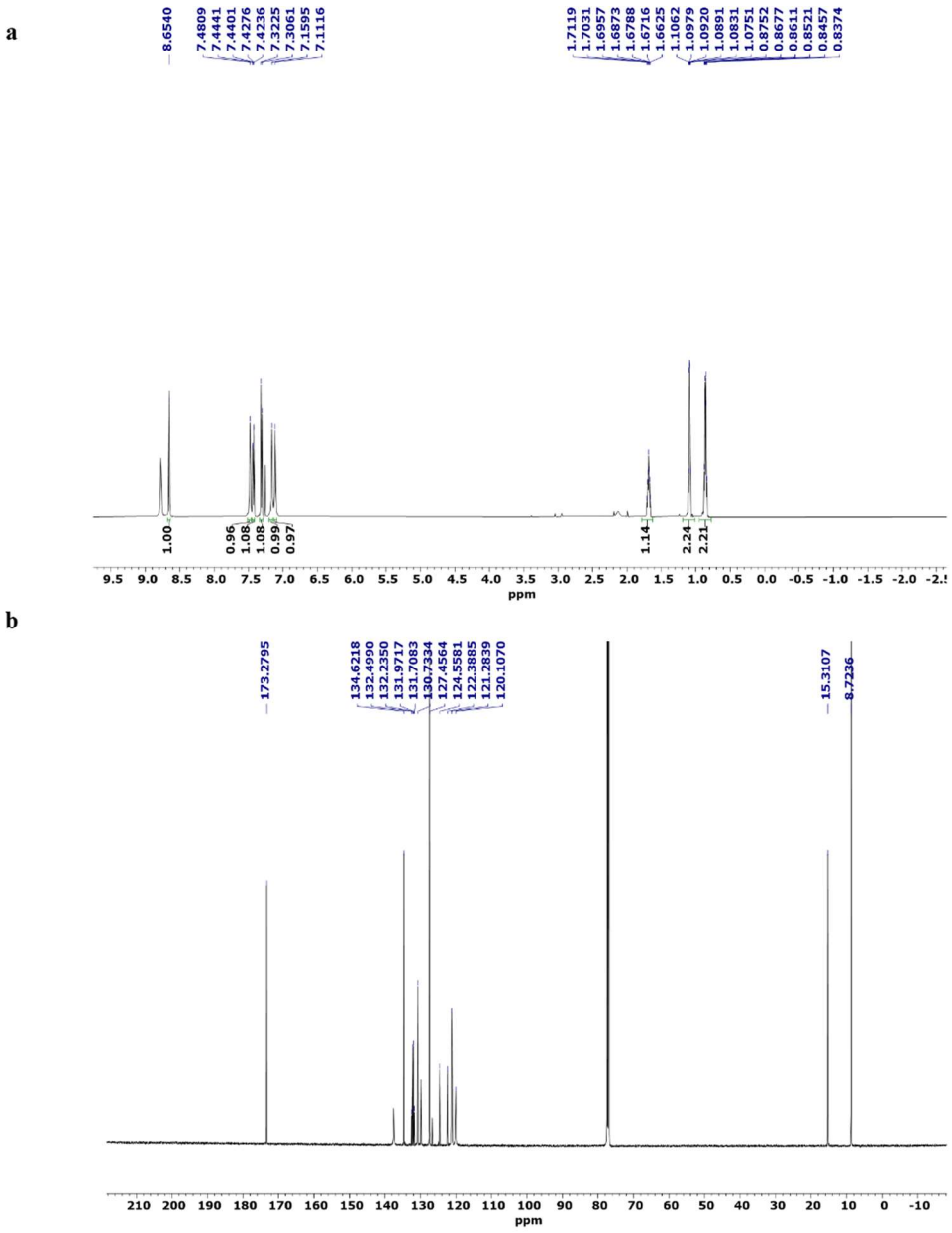
a



b

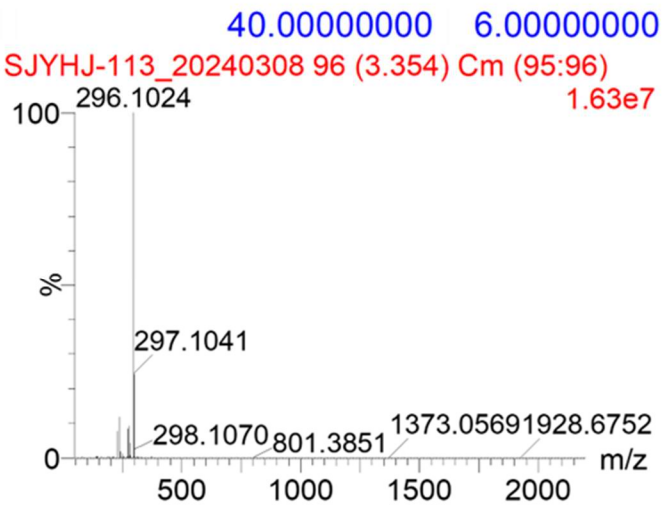


Supplementary Fig. 26 | (a) HRMS and (b) HPLC of **SCM-06**

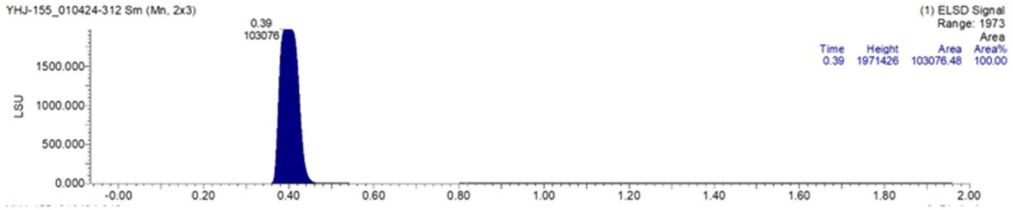


Supplementary Fig. 27 | (a) ^{1}H NMR and (b) ^{13}C NMR of **SCM-07**

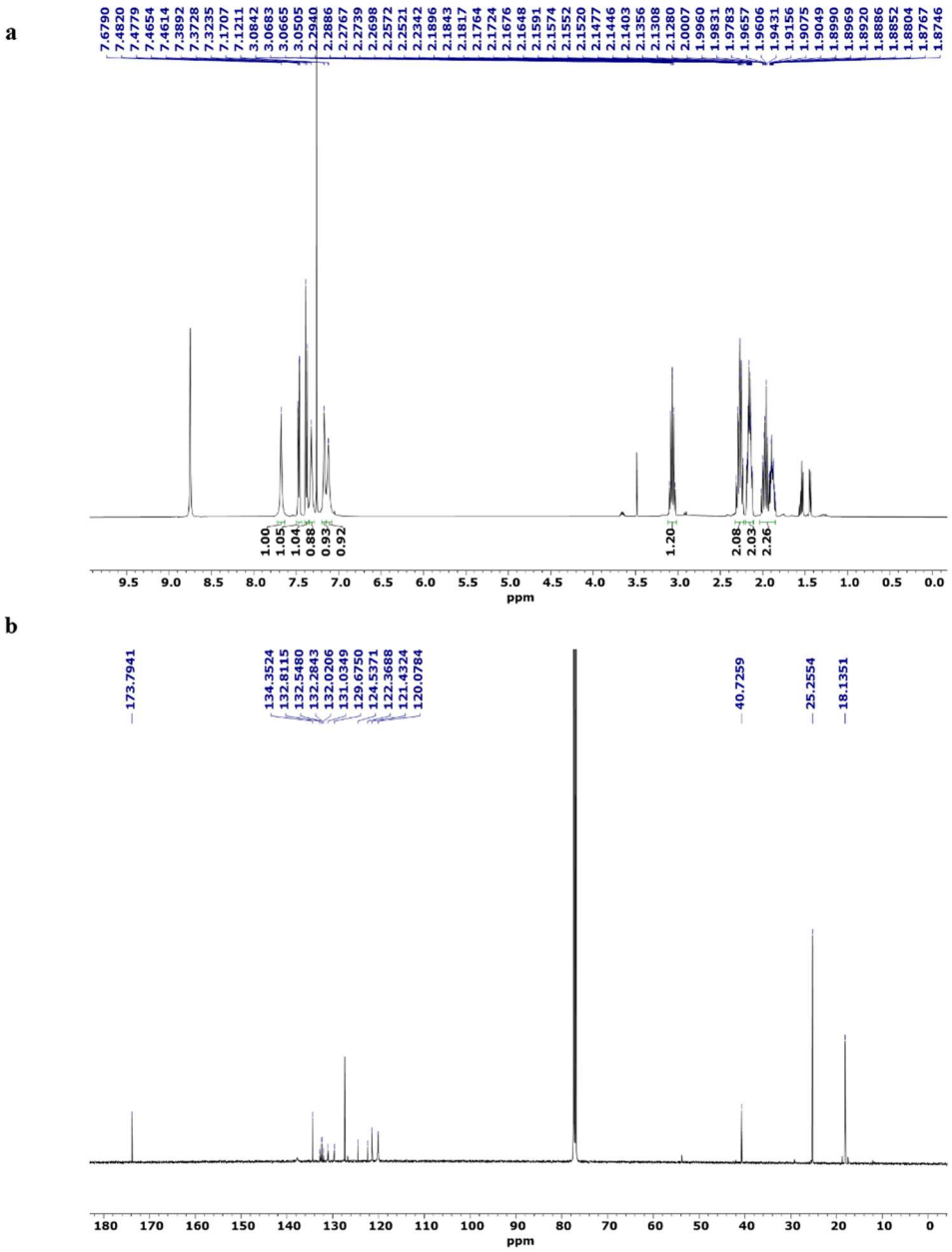
a



b

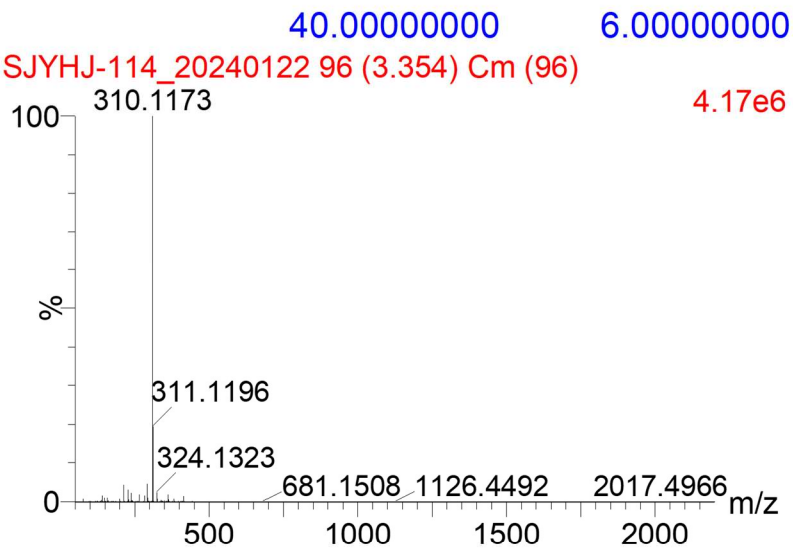


Supplementary Fig. 28 | (a) HRMS and (b) HPLC of **SCM-07**

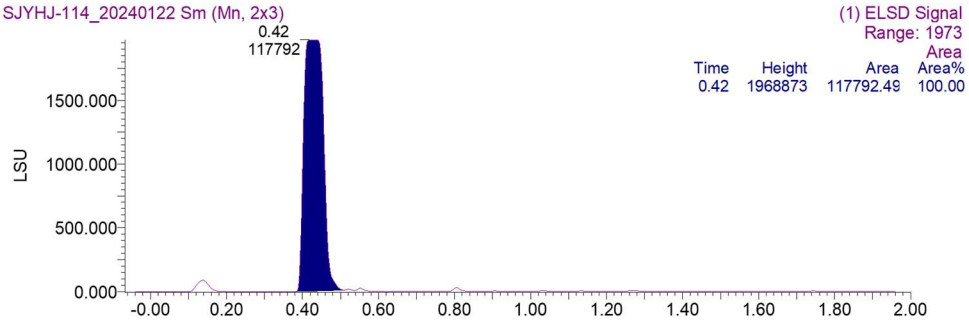


Supplementary Fig. 29 | (a) ^{1}H NMR and (b) ^{13}C NMR of **SCM-08**

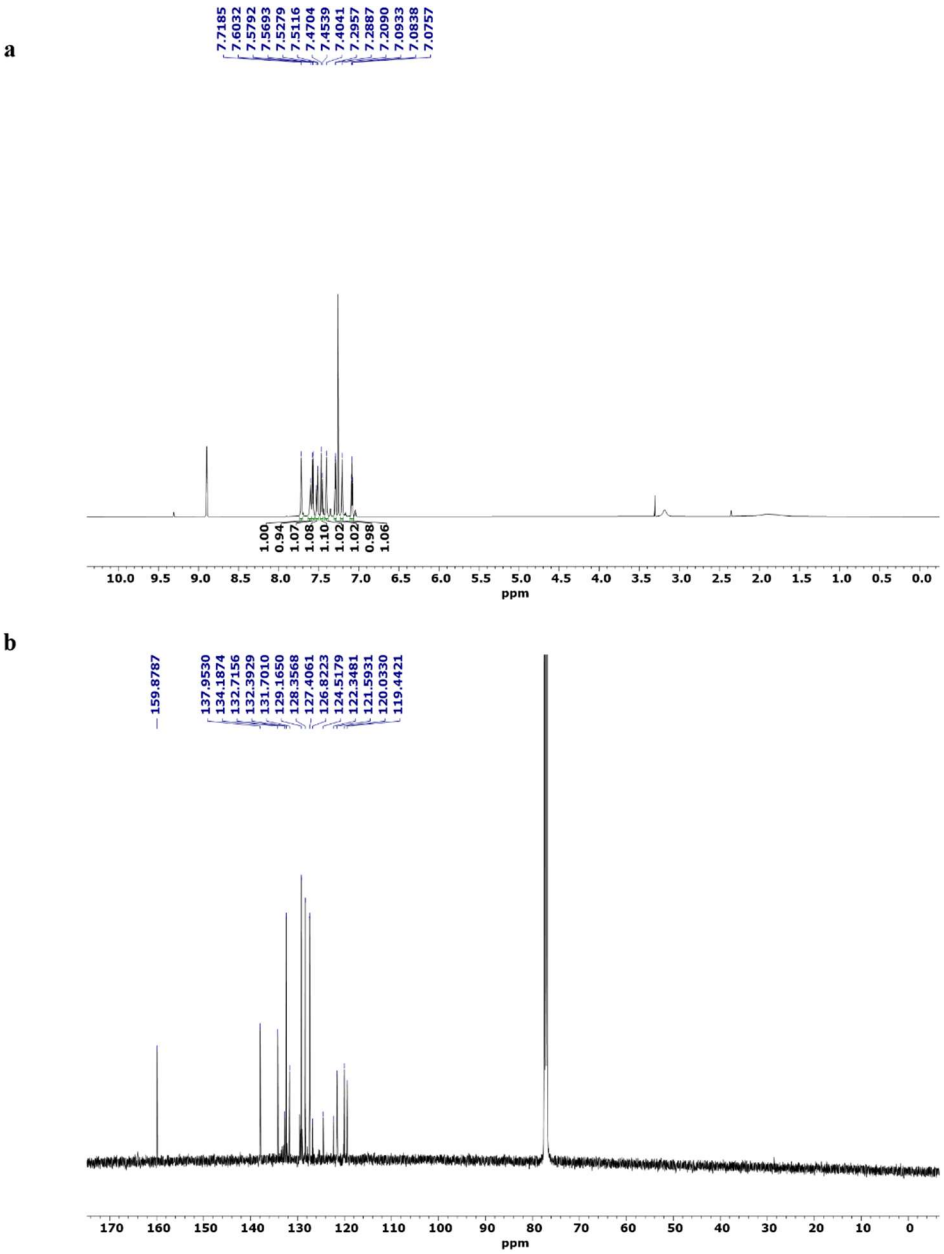
a



b

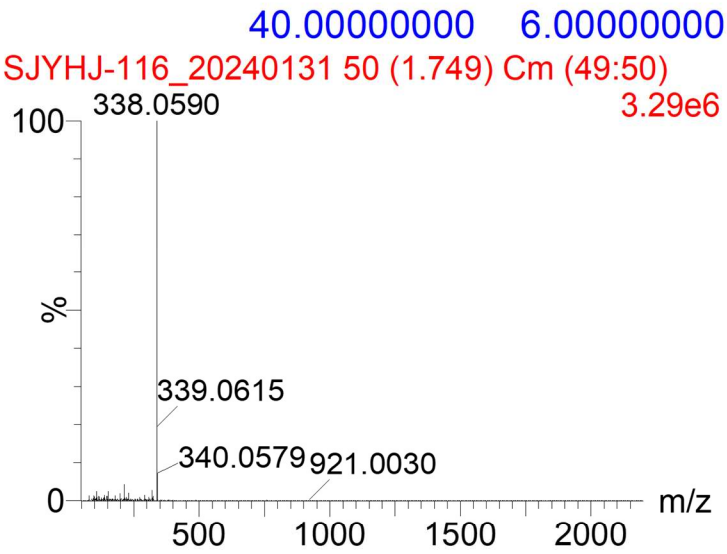


Supplementary Fig. 30 | (a) HRMS and (b) HPLC of **SCM-08**

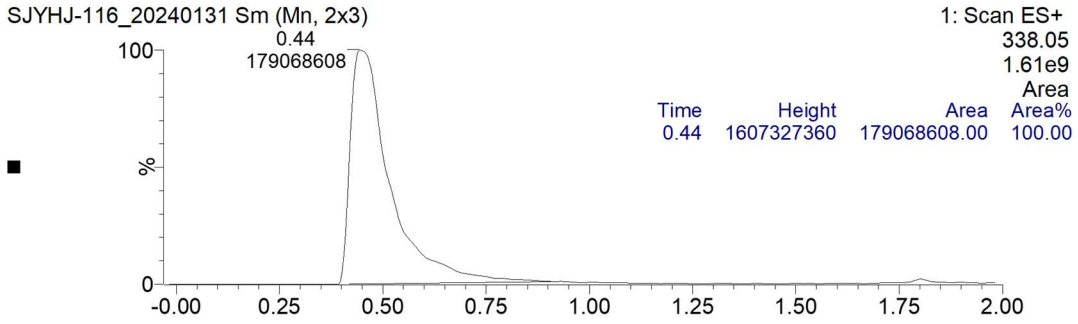


Supplementary Fig. 31 | (a) ^{1}H NMR and (b) ^{13}C NMR of **SCM-09**

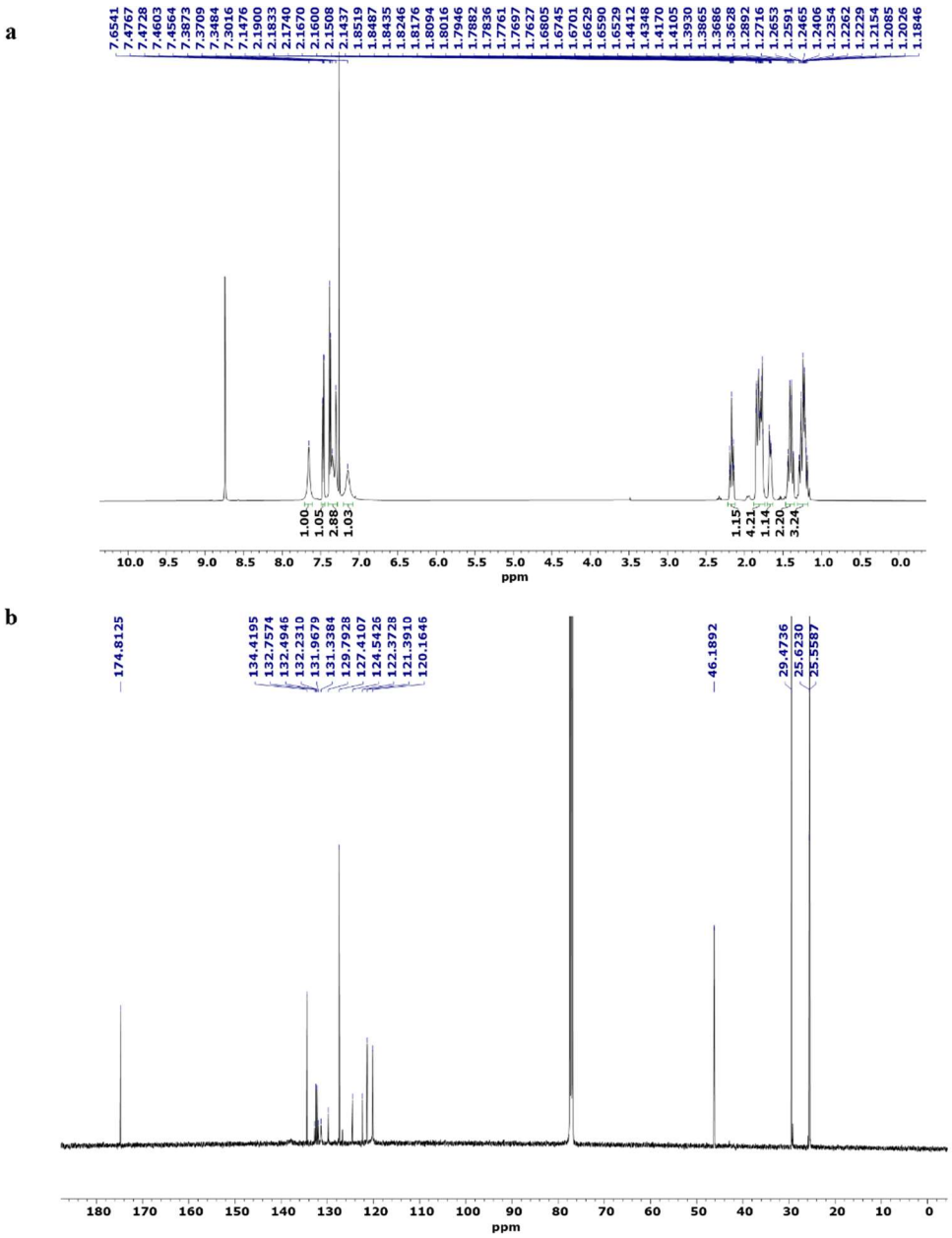
a



b

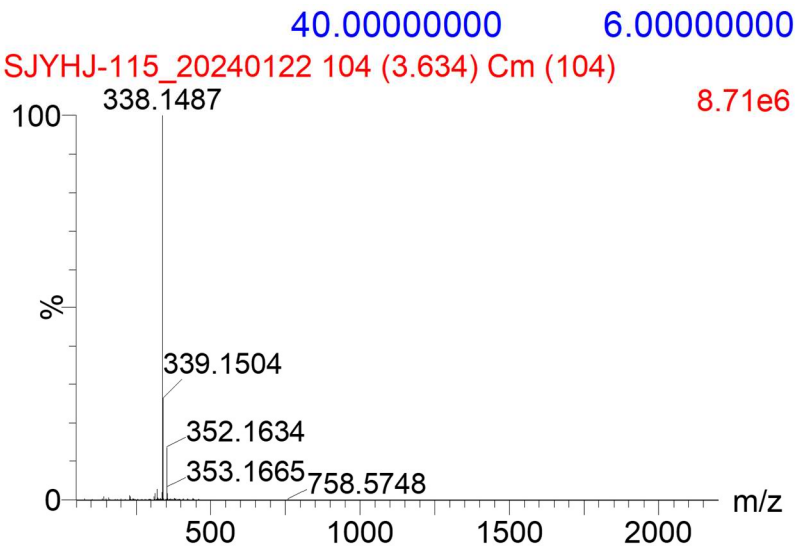


Supplementary Fig. 32 | (a) HRMS and (b) HPLC of **SCM-09**

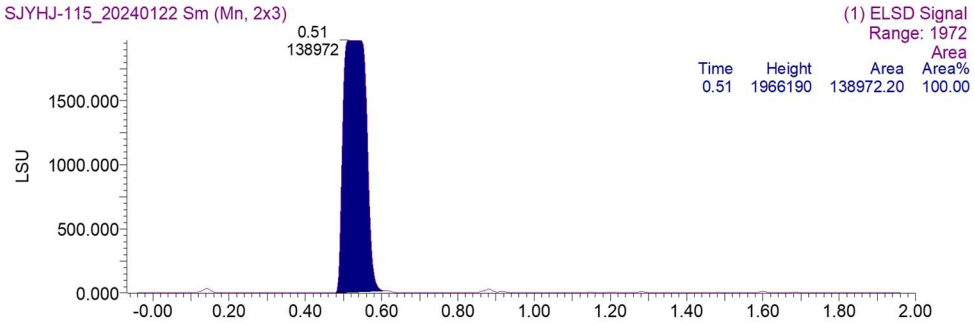


Supplementary Fig. 33 | (a) ^{1}H NMR and (b) ^{13}C NMR of **SCM-10**

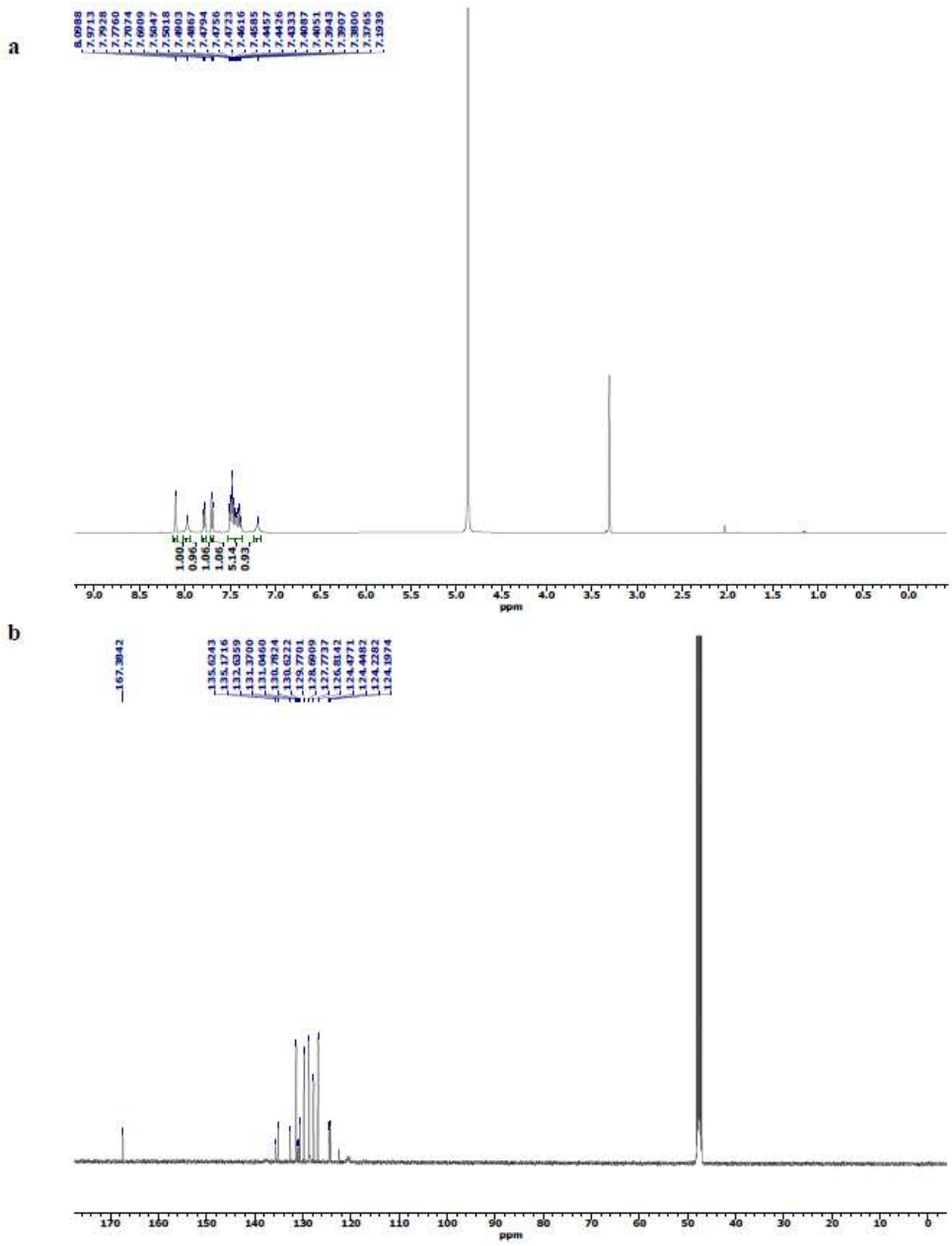
a



b

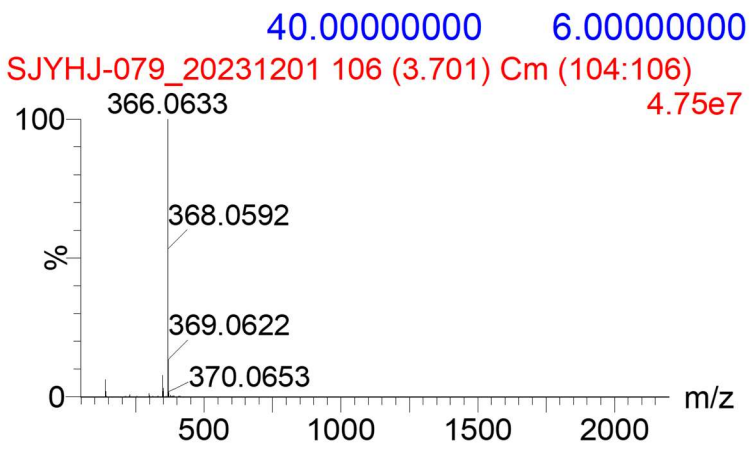


Supplementary Fig. 34 | (a) HRMS and (b) HPLC of **SCM-10**

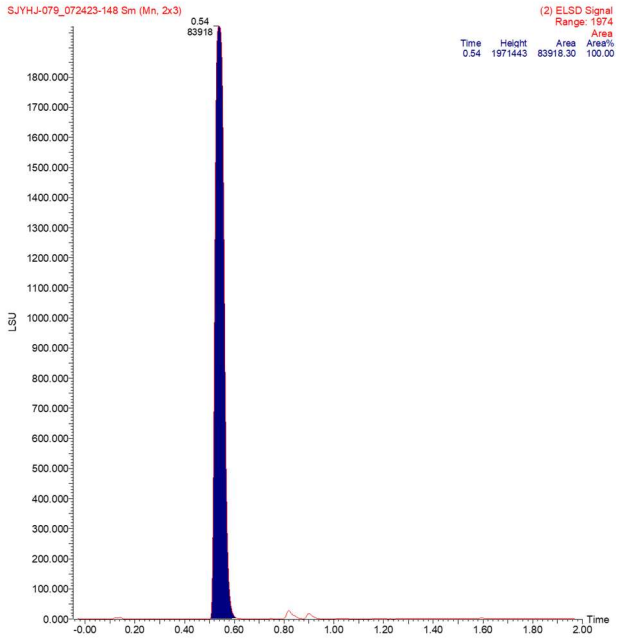


Supplementary Fig. 35 | (a) ^{1}H NMR and (b) ^{13}C NMR of **SCM-11**

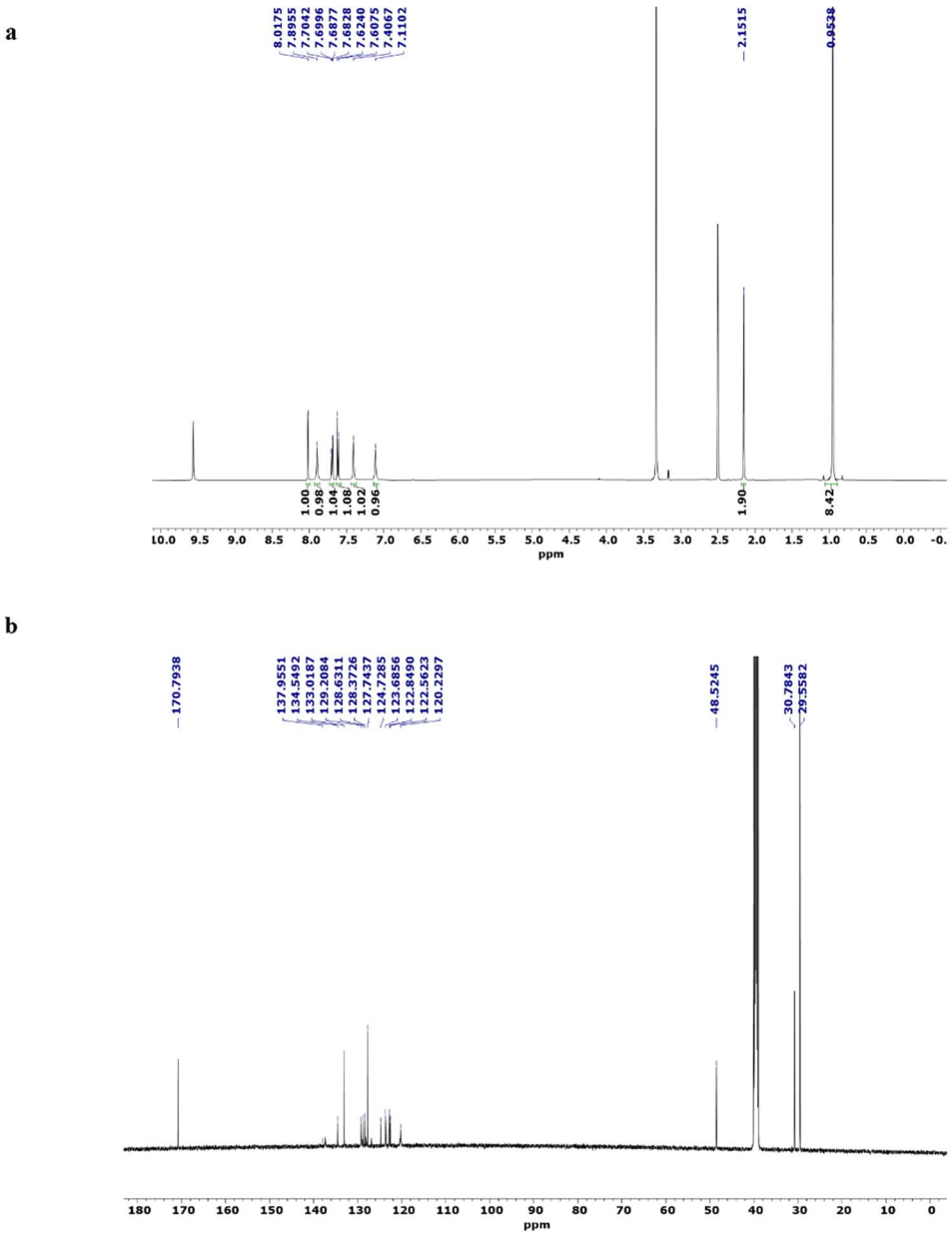
a



b

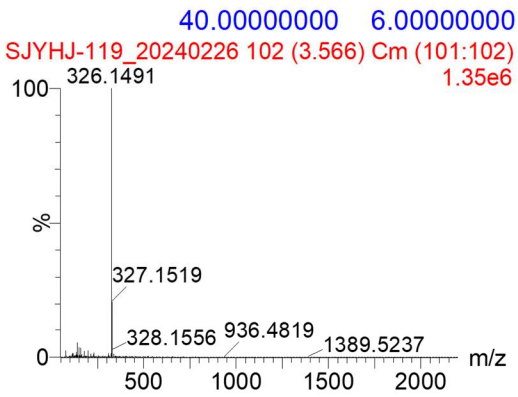


Supplementary Fig. 36 | (a) HRMS and (b) HPLC of **SCM-11**

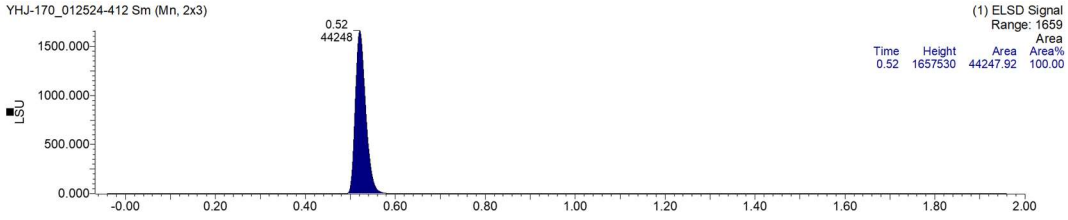


Supplementary Fig. 37 | (a) ^{1}H NMR and (b) ^{13}C NMR of **SCM-12**

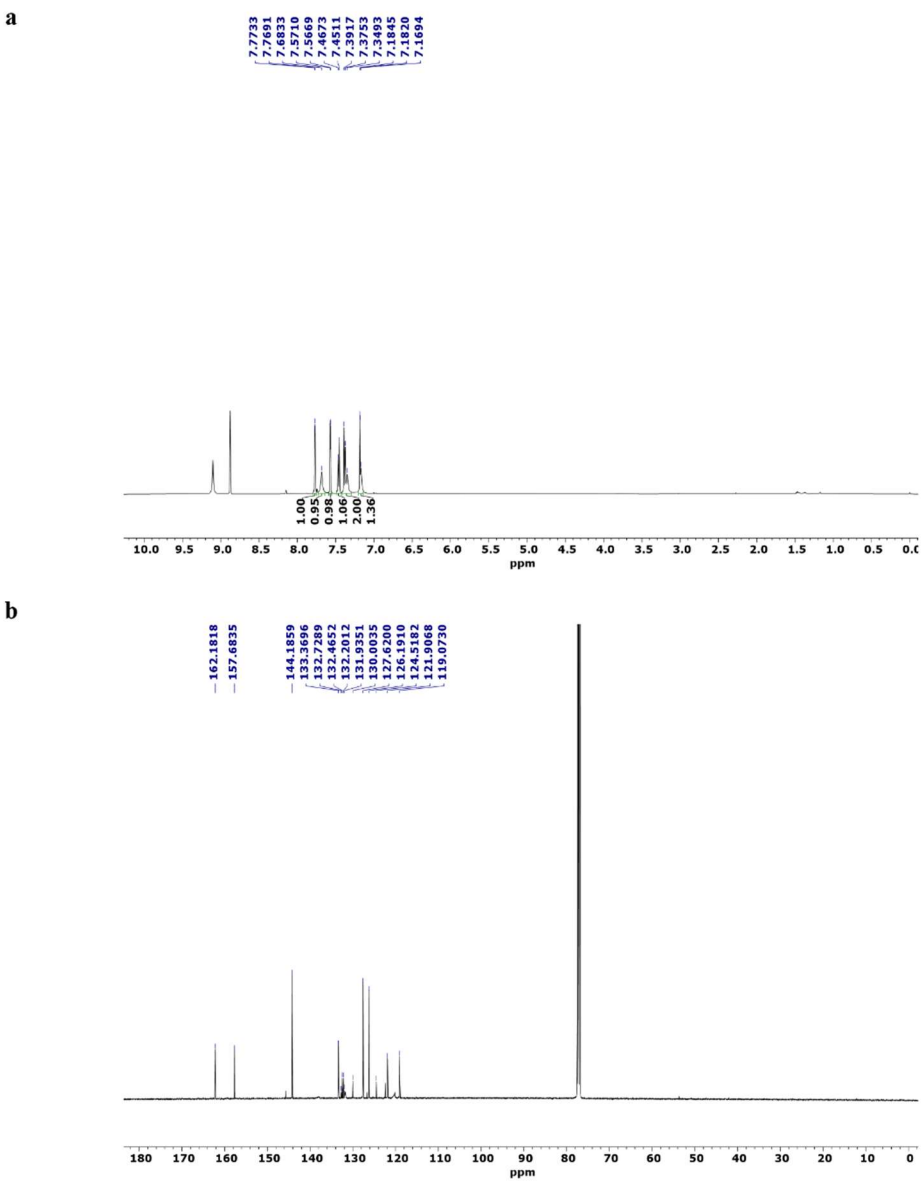
a



b

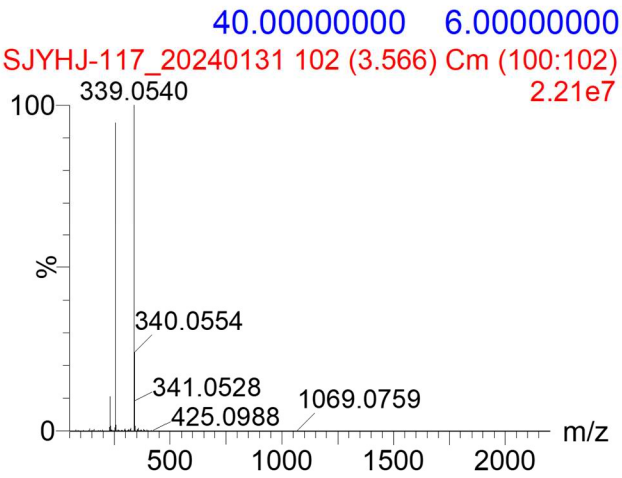


Supplementary Fig. 38 | (a) HRMS and (b) HPLC of **SCM-12**

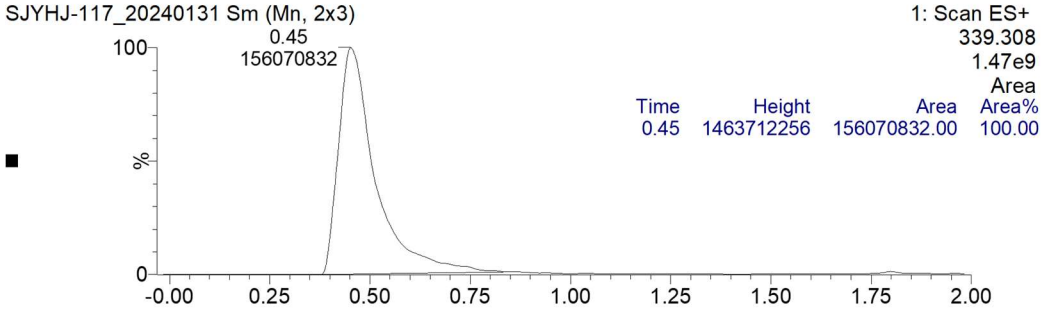


Supplementary Fig. 39 | (a) ^{1}H NMR and (b) ^{13}C NMR of **SCM-16**

a

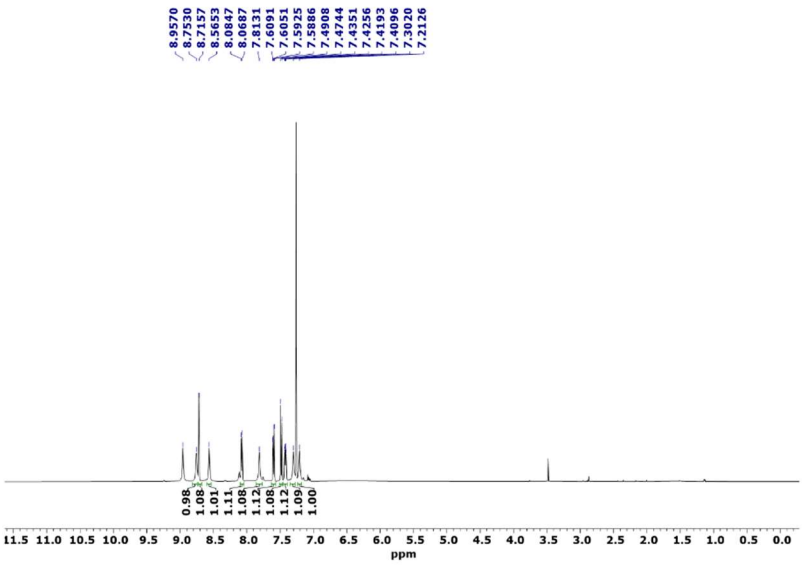


b

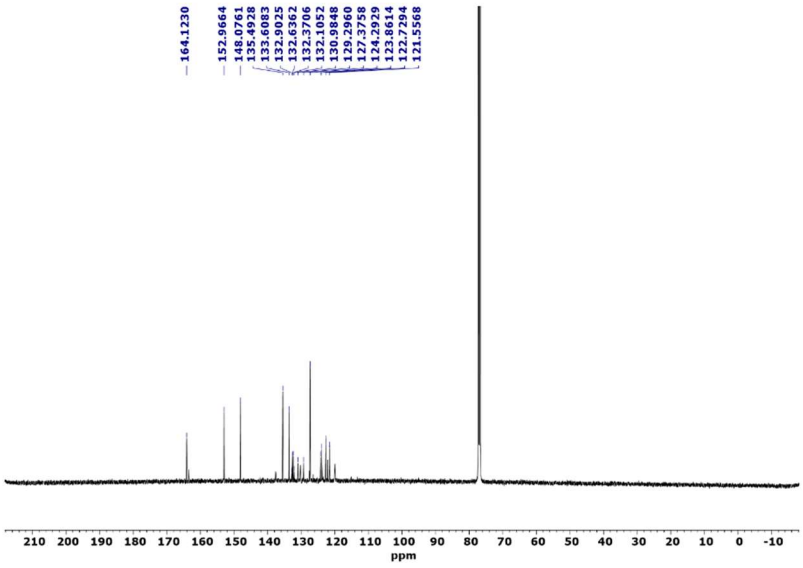


Supplementary Fig. 40 | (a) HRMS and (b) HPLC of **SCM-16**

a

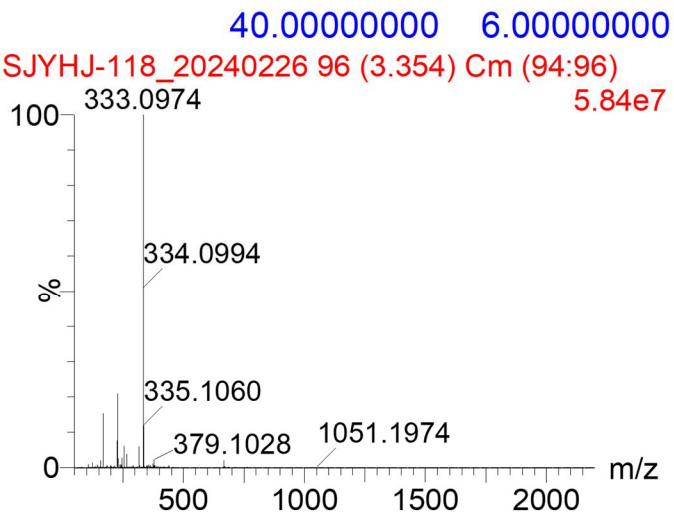


b

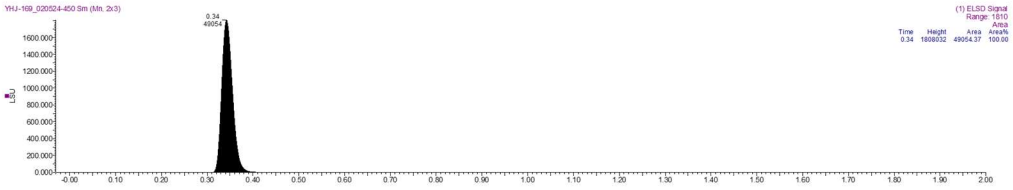


Supplementary Fig. 41 | (a) ^{1}H NMR and (b) ^{13}C NMR of **SCM-17**

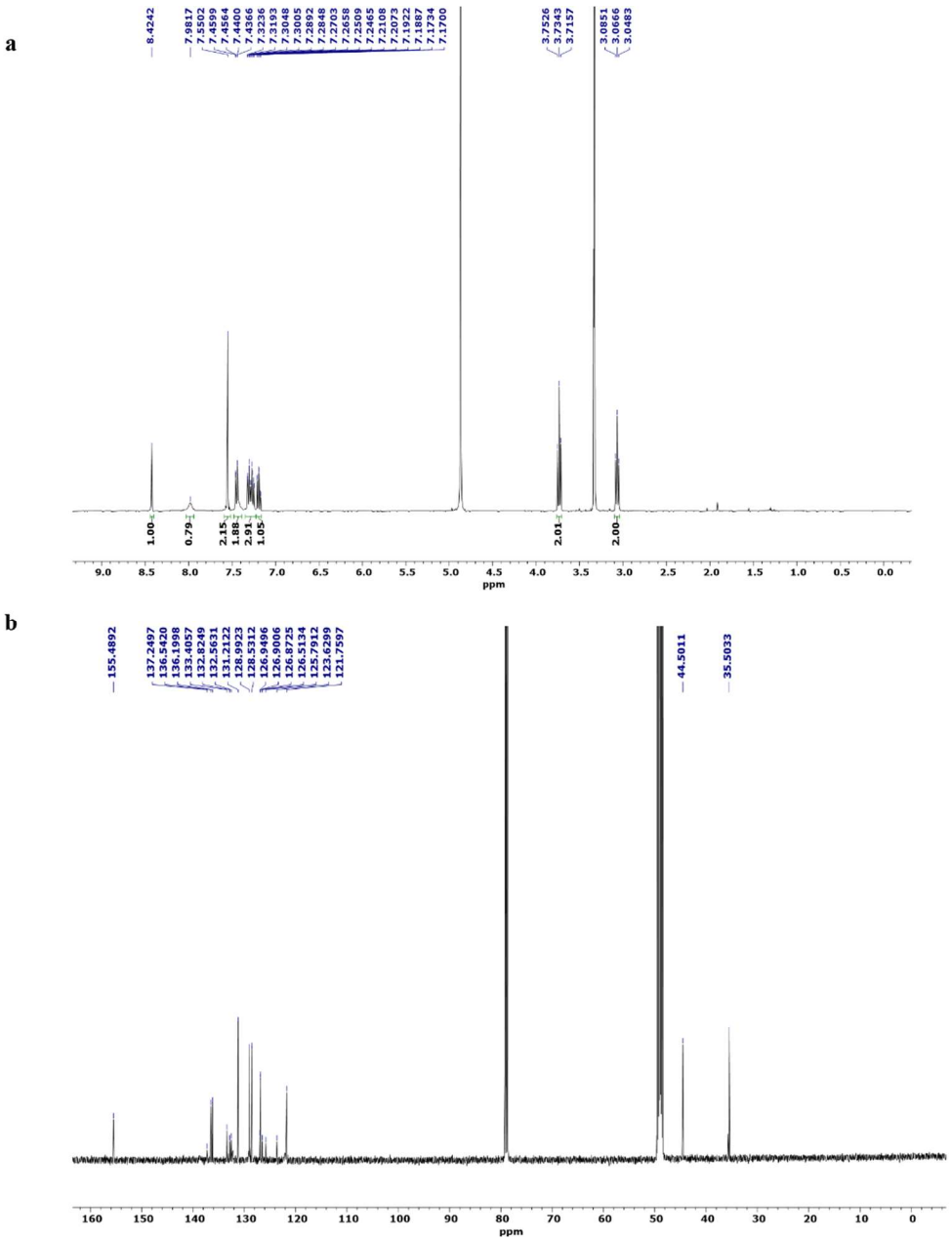
a



b

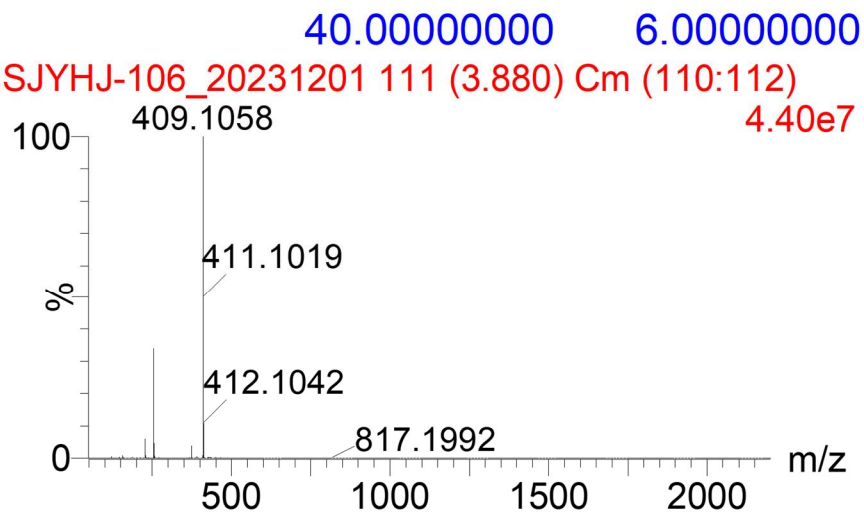


Supplementary Fig. 42 | (a) HRMS and (b) HPLC of **SCM-17**

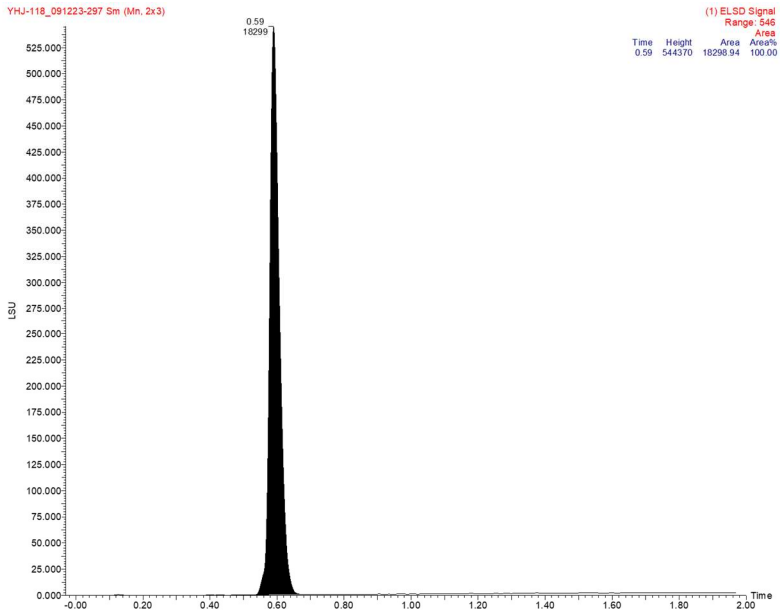


Supplementary Fig. 43 | (a) ^{1}H NMR and (b) ^{13}C NMR of **SCM-24**

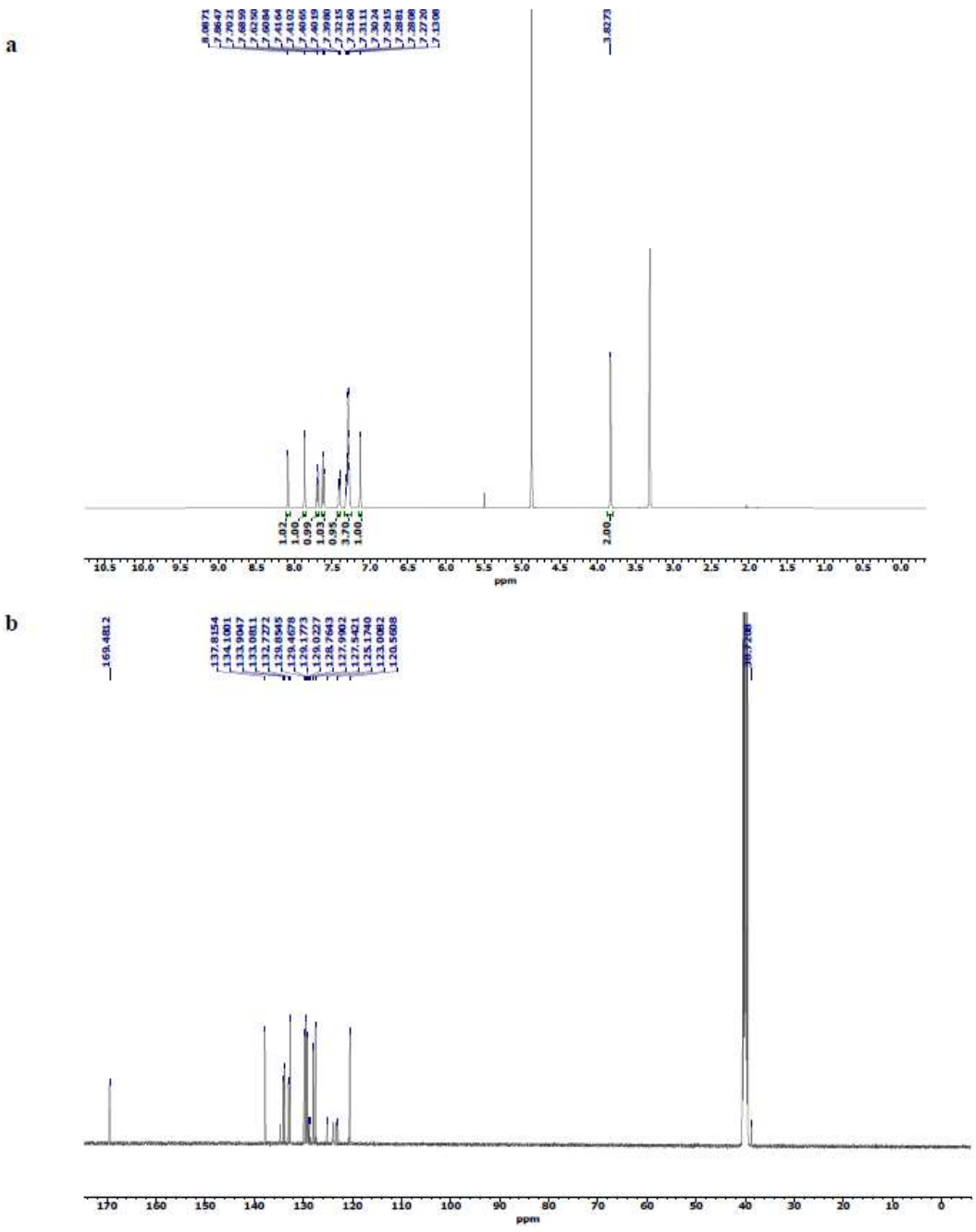
a



b

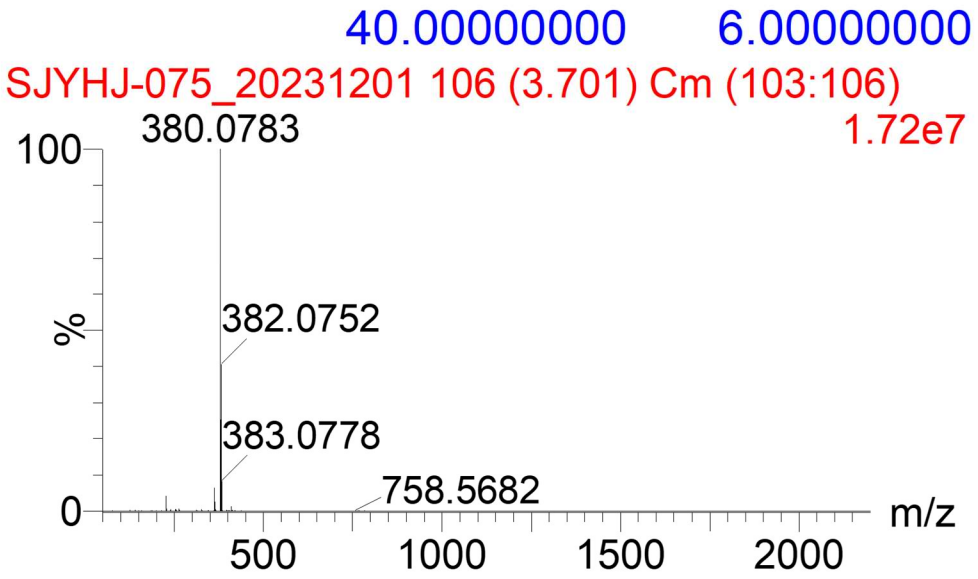


Supplementary Fig. 44 | (a) HRMS and (b) HPLC of **SCM-24**

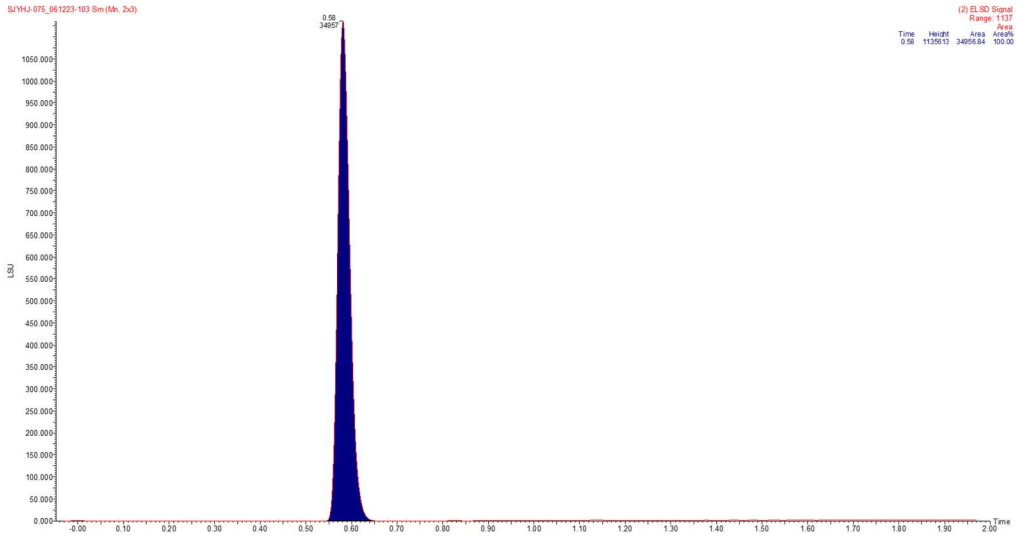


Supplementary Fig. 45 | (a) ^{1}H NMR and (b) ^{13}C NMR of **SCM-25**

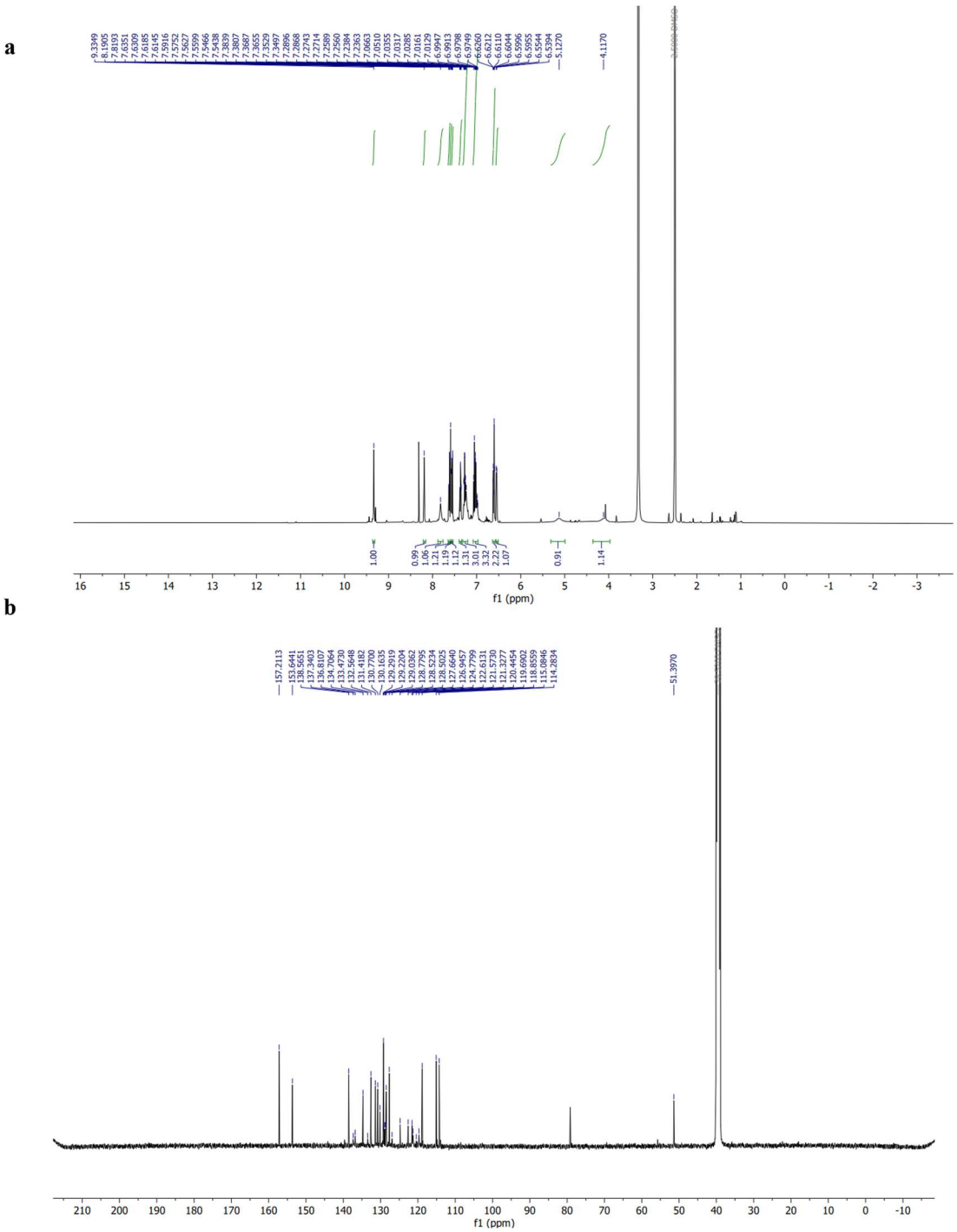
a



b

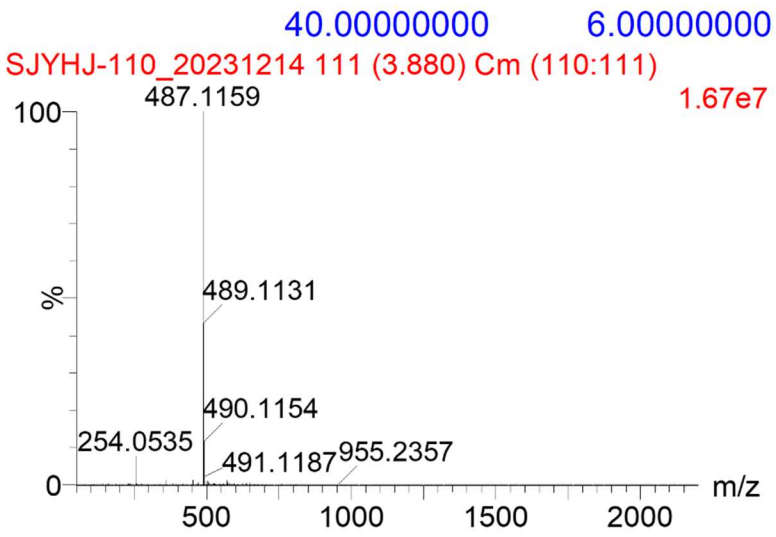


Supplementary Fig. 46 | (a) HRMS and (b) HPLC of **SCM-25**

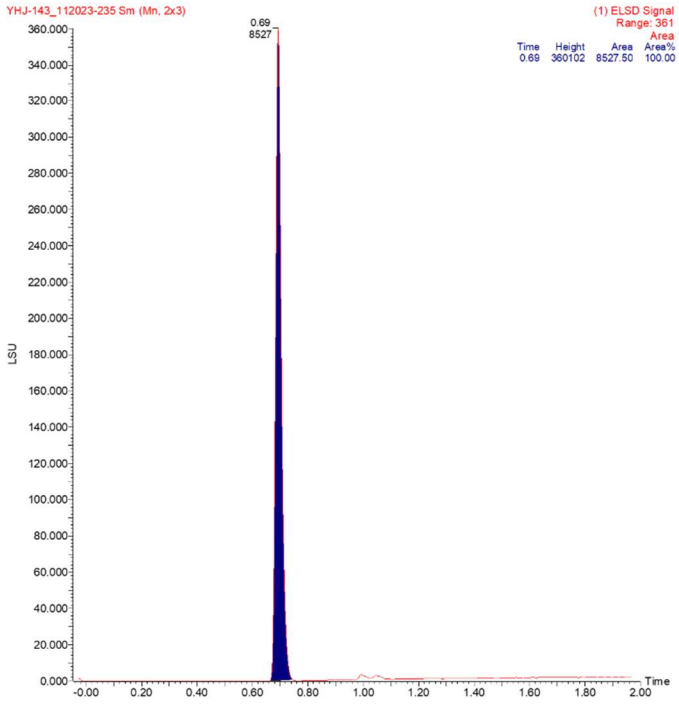


Supplementary Fig. 47 | (a) ^{1}H NMR and (b) ^{13}C NMR of **SCM-26**

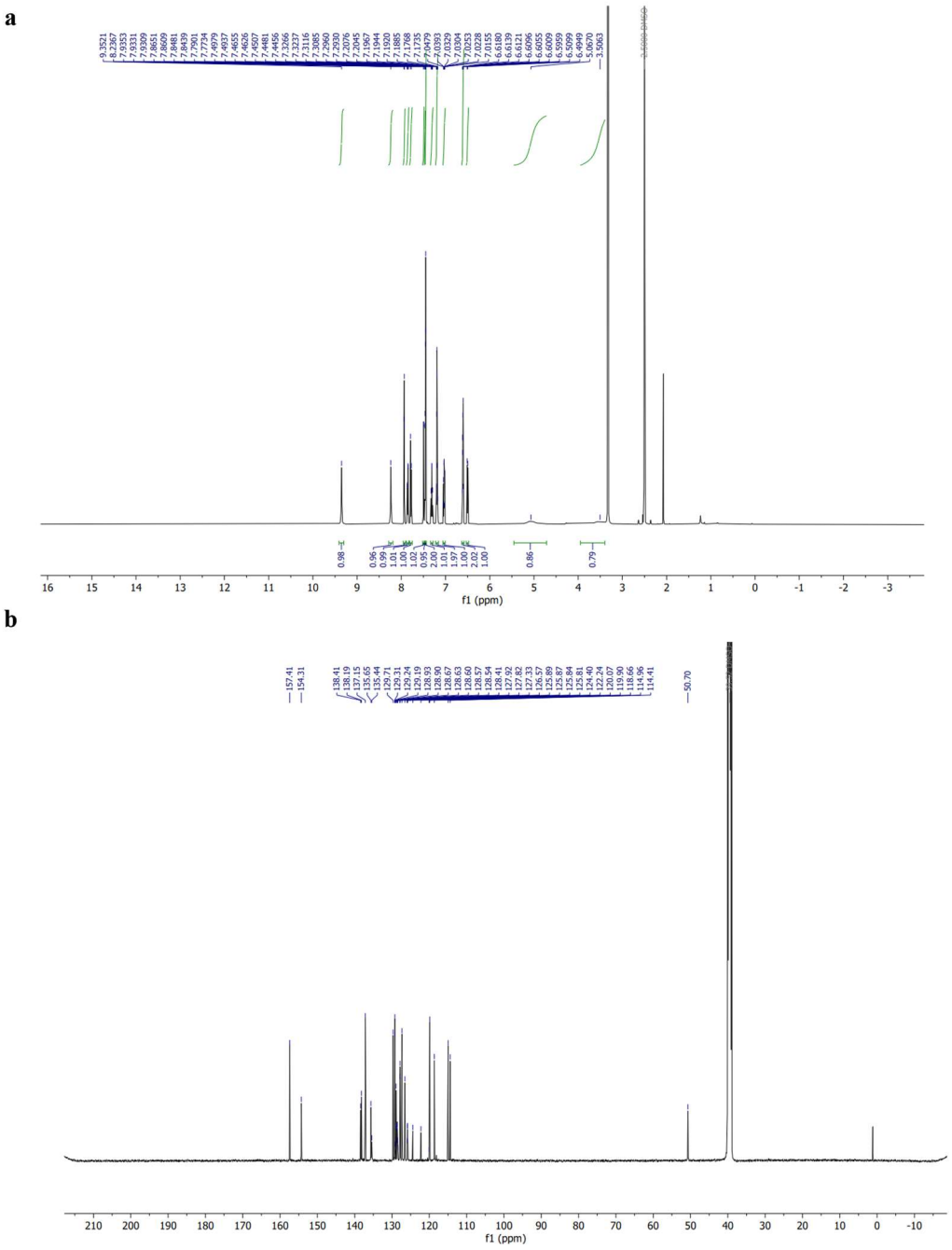
a



b

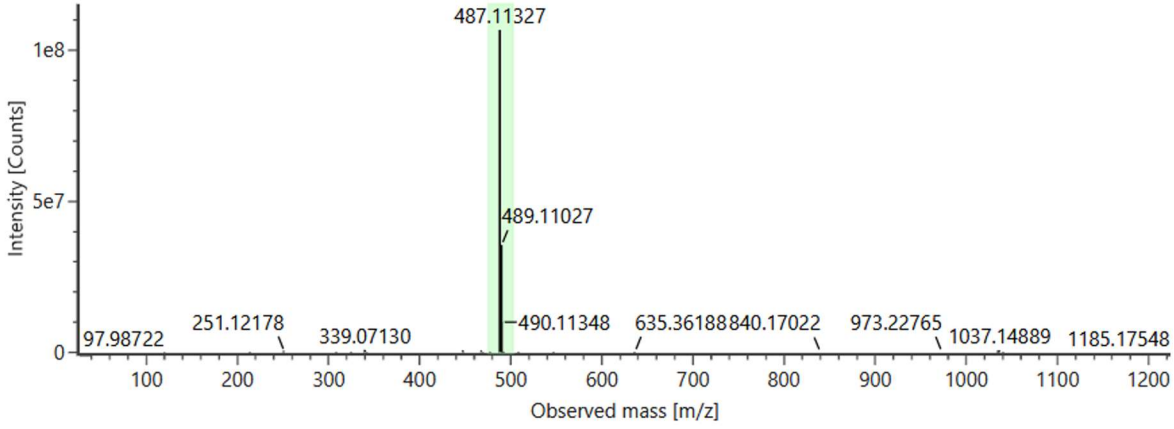


Supplementary Fig. 48 | (a) HRMS and (b) HPLC of **SCM-26**

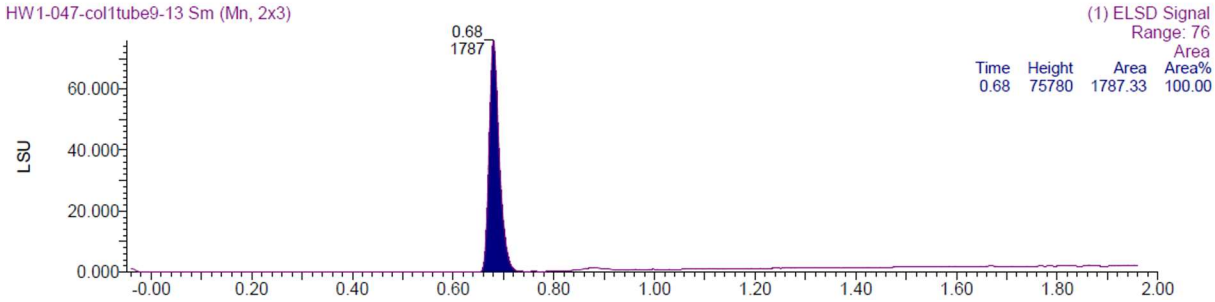


Supplementary Fig. 49 | (a) ^{1}H NMR and (b) ^{13}C NMR of **SCM-27**

a



b



Supplementary Fig. 50 | (a) HRMS and (b) HPLC of **SCM-27**

References

1 Madeira, F. *et al.* Search and sequence analysis tools services from EMBL-EBI in 2022. *Nucleic Acids Res* **50**, W276-W279 (2022). https://doi.org/10.1093/nar/gkac240

2 Nishiguchi, G. *et al.* Evaluating and evolving a screening library in academia: the St Jude approach. *Drug Discov Today* **26**, 1060-1069 (2021). https://doi.org/10.1016/j.drudis.2021.01.005

3 Shah, P. *et al.* An Automated High-Throughput Metabolic Stability Assay Using an Integrated High-Resolution Accurate Mass Method and Automated Data Analysis Software. *Drug Metab Dispos* **44**, 1653-1661 (2016). https://doi.org/10.1124/dmd.116.072017

4 Obach, R. S. Prediction of human clearance of twenty-nine drugs from hepatic microsomal intrinsic clearance data: an examination of in vitro half-life approach and nonspecific binding to microsomes. *Drug Metabolism and Disposition* **27**, 1350-1359 (1999).